FROESE MECHANISMS OF TGFβ ACTIVATION IN LUNG FIBROSIS PHD

MECHANISMS OF TGFβ ACTIVATION IN LUNG FIBROSIS

By: Aaron R. Froese, B.Sc.

A Thesis Submitted to the School of Graduate Studies in Partial Fulfillment of the Requirements for the Degree of Doctor of Philosophy

McMaster University DOCTOR OF PHILOSOPHY (2012) Hamilton, Ontario (Medical Sciences)
TITLE: MECHANISMS OF TGFβ ACTIVATION IN LUNG FIBROSIS
AUTHOR: Aaron R. Froese, B.Sc. (McMaster University)
SUPERVISOR: Martin R.J. Kolb, Associate Professor
NUMBER OF PAGES: xii, 150

Abstract

This PhD thesis focuses on the mechanical activation of TGFβ in the context of pulmonary fibrosis. Mechanical TGFβ activation occurs by physical force of breathing and signals to the nucleus via phospho-Smad2. This activation occurs in presence of strong pan-serine protease and matrix metalloproteinase inhibition. The augmented expression of latent TGFβ in lung tissue also lead to TGFβ activity following tissue stretch. Tissue biopsies from pulmonary fibrosis patients exhibited the same mechanical TGFβ activation and subsequent accumulation of phospho-Smad2 as was seen in animal models. In rodent models and human control tissue, TGFβ was not released in detectable quantities, nor was there any significant upregulation of phospho-Smad2. These data show that mechanical TGFβ activation is a relevant and limited to the context of a fibrotic disease process.

Non-invasive investigation of lung fibrosis was evaluated for correlation to classical assessments. We found that non-invasive lung function parameters measured by a rodent ventilator, and small animal CT imaging correlated significantly with histomorphometic Ashcroft scoring. Exercise testing and quantification of the maximal oxygen consumption rate was a valuable indicator of overall rodent lung health but did not correlated significantly with Ashcroft scoring. Non-invasive investigation tools evaluated here represent important advances in the quality of interpretation of pre-clinical lung fibrosis trials.

Finally, collagen turnover was investigated by measurement of pyridinolines and serum collagen metabolic peptides. A novel method was developed and tested to detect pyridinolines in facile procedure. We found that deoxypyridinolines, but not pyridinolines, were significantly increased in the serum of lung fibrosis patients with respect to healthy controls. Furthermore, collagen type 1 telopeptide, a collagen breakdown product, was significantly increased in lung fibrosis patient serum. These data intriguingly indicate that under stable lung fibrosis conditions, more collagen appears to be breaking down into the serum then is synthesized.

Acknowledgments

I would like to thank Melanie Froese her constant love and support over the years. I couldn't have done it without you. I'd like to thank Bethany and Joel for being such wonderful children and supporting me with your love. I'd like to thank my parents who modeled a sense of determined discipline for me. I'd like to thank my small group including Edu Pallek, Micah Fuller, Bruce Landman, and Rob McElravy whose encouragement never failed. I'd like to acknowledge Royal Pizza on James Street for feeding me over the years. I would like to thank my supervisors Jack and Martin for all their advice and confidence in my work.

Most of all, I'd like to thank God for helping me. You carried me through the first two difficult years.

Table of Contents

List of Figures and Tables

List of Abbreviations

ACE	Angiotensin Converting Enzyme
Ad	Adenovirus
αSMA	alpha Smooth Muscle Actin
AT-2	Angiotensin-2
BALF	Bronchoalveolar Lavage Fluid
BSA	Bovine Serum Albumin
COX-2	Cyclooxygenase-2
DHLNL	Dihydroxylysinenorleucine
DL_{CO}	Diffusion Capacity for Carbon Monoxide
Dyd	Deoxypyridinoline
FDG	18-Fluorine Deoxyglucose
ECM	Extracellular Matrix
EMT	Epithelial to Mesenchymal Cellular Transition
ET-1	Endothelin-1
FEV_1	Forced Expiratory Volume in One Second
FVC	Forced Vital Capacity
GARP	Glycoprotein-A Repetitions Predominant Protein
HGF	Hepatocyte Growth Factor
HLNL	Hydroxylysinenorleucine
HPLC	High Pressure Liquid Chromatography
HRCT	High Resolution Computed Tomography
HU	Hounsfield Units
ILD	Interstitial Lung Disease
IPF	Idiopathic Pulmonary Fibrosis

IT	Intratracheal
LacZ	Beta-Galactosidase
LAP	(TGFβ) Latency Associated Peptide
LPA	Lysophosphatidic Acid
LTBP	Latent TGFβ Binding Protein
MRI	Magnetic Resonance Imaging
MMP	Matrix Metalloproteinases
NAC	N-Acetyl Cysteine
PAI1	Plasminogen Activator Inhibitor 1
PAR	Protease Activated Receptor
PAO_2	Partial Alveolar Pressure of Oxygen
PDGF	Platelet Derived Growth Factor
PET	Positron Emission Tomography
PIIINP	N-Terminal Propeptide Fragment of Collagen III
pSmad2	Phosphorylated Smad2
Pyd	Pyridinoline
SBE	Smad DNA Binding Elements
SIK	Salt Inducible Kinase
SP-A	Surfactant Protein A
SP-D	Surfactant Protein D
TGFβ	Transforming Growth Factor Beta
TLC	Total Lung Capacity
TRE	TGFβ Responsive Elements
TRPM7	Transient Receptor Potential

	Melastatin7
TSP-1	Thrombospondin-1
UIP	Usual Interstitial Pneumonia
Voxel	Volume Pixel (used in 3D imaging)
VO_2max	Maximal rate of oxygen consumption

Declaration of Academic Achievement

This thesis contributes to the field of lung fibrosis research through the elucidation of mechanical TGFβ activation. All of the work on TGFβ activation presented was all produced by Aaron Froese. This thesis also analyzes non-invasive evaluations of lung fibrosis models by lung function, exercise testing, and small animal CT imaging analysis. Non-invasive evaluation work was primary done by Kjetil Ask with heavy involvement and co-authorship by Aaron Froese. Finally, this thesis includes novel methods and evaluations of collagen turnover products called pyridinolines. The methods development and subsequent lung fibrosis patient sample analysis was all done by Aaron Froese.

1.0 General Introduction

Fibrosis is an abnormal wound healing process which can affect any organ or tissue of the body. Fibrosis and scarring are often synonymous with fibrogenesis implying an active or ongoing wound healing process. Fibrogenesis is the active production of abnormal scars. It can be limited to a specific organ such as the lungs, liver, or kidneys or can affect multiples systems such as in systemic sclerosis. The reasons why fibrogenesis is often limited to a specific organ is poorly understood. Fibrotic scars contain mostly extracellular matrix (ECM) components and the fibroblast and myofibroblast cells which produce them. Fibrogenesis in most organ systems involves an epithelial layer which likely plays an active role in instigating fibroblasts to continue ECM production. The ECM of a fibrotic scar consists of predominantly fibrillar collagen of types 1 and 3 (1). Other major ECM constituents of fibrotic scars include fibronectin (2), elastin (3), glycosaminoglycans (4), and proteoglycans (4). Many different environmental insults and chemical poisons can instigate fibrotic changes. X-ray radiation (5), silica (6), asbestos (7), pesticide chemicals like diaquat and paraquat (8), and anti-neoplastic drugs like bleomycin (9) are all examples of irritants that can cause fibrotic changes especially in the lungs (9). All of the various types of organ fibrosis appear to have similar pathways of operation which rely on the abnormal activation of Transforming Growth Factor beta (TGFβ) cytokines (10-13). All of the above irritants and environmental stimuli are also known to directly or indirectly activate TGFβ to generate fibrotic changes. Frequently, damage caused by cancerous lesions can result in significant scarring and fibrosis which compromise organ function (14). Many other examples of later or end stage chronic disease exist in which fibrosis predominates and is critically involved in compromising organ function. Diabetes (15), asthma (16), hepatitis C viral infection (17), neurodegenerative diseases such as Alzheimer's disease (18) and many other chronic diseases are expected to benefit from an anti-fibrotic therapeutic drug.

Interstitial lung diseases (ILD) or pneumonias are a class of parenchymal lung diseases critically involving the alveoli (19). The alveoli of the lung, which are the sites of gas exchange, are grape-like shaped structures with ultra thin walls that divides epithelial cells from the endothelial cells that form the blood capillaries. This ultra thin wall or "interstitium" is produced by fibroblasts which reside in between alveoli. The

interstitium of the alveolus is the major site of injury in ILDs. Following a fibrotic instigating injury, fibroblasts proliferate and begin to accumulate ECM components in the interstitium. This process obliterates alveolar function which is dependent on thin wall layers for blood-gas diffusion. Alveolar epithelial cells, sensing the injury and fibrotic process, can undergo changes which cause them to dedifferentiate into mesenchymal fibroblasts. This epithelial to mesenchymal cell transition (EMT) is a hallmark of many fibrotic diseases. Bone marrow derived circulating fibroblast progenitor cells home to fibrotic wounds and can also contribute to overall fibroblast counts (20). As the disease worsens, fibroblasts can differentiate into myofibroblasts which contain large contractile structural components. These myofibroblast cells, which for example aide in pulling together normal skin wounds, represent a major effector cell of fibrogenesis for ECM production. Fibrotic changes are often found in diffuse patches throughout the lungs which appear to form a continuous reticulum towards the outer pleural layer (21, 22). It is thought that the mechanical stimulus of ventilation causes force related cell signals that often perpetuate fibrosis to the outer layers of the lung.

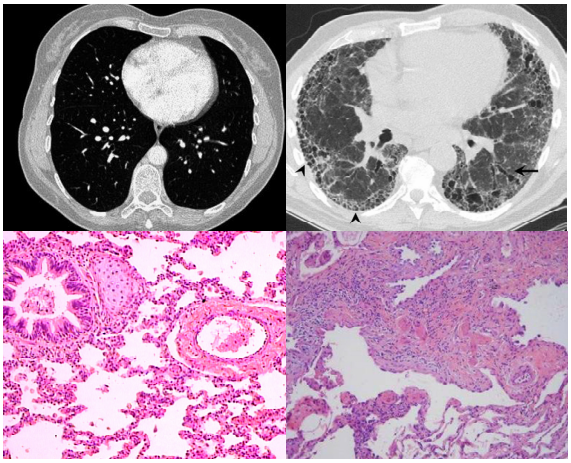

Figure 1.0. High resolution computed tomography scans and histology images of normal (left) and IPF (right) human lungs. IPF CT scans reveal peripheral and subpleural fibrosis which arrange themselves into linked reticular formations. Arrows point to pathologic honeycombing architecture which occur in advanced disease. IPF histology shows interstitial fibrosis beside areas of normal lung below. Arrow points to fibroblastic focus with activated epithelial layer surrounding it. Normal lung CT image taken from Science Photo Library website: http://www.sciencephoto.com /media/82467/enlarge. Normal lung histology taken from website: http://www.gwc.maricopa.edu /class/bio202/Respiratory/Normal.html IPF images adapted from Orphanet Journal of Rare Diseases 2008, 3:8.

Diffuse interstitial pneumonias are categorized by histological and radiological assessment. The most common histological presentation of interstitial pneumonia is the usual type. This usual interstitial pneumonia (UIP) is also call idiopathic pulmonary fibrosis (IPF). The term “idiopathic” simply indicates that this disease is of unknown origins. Other less common interstitial pneumonias include non-specific interstitial pneumonia, sarcoidosis, hypersensitivity pneumonitis, cryptogenic organizing pneumonia, desquamative interstitial pneumonia, and lymphoid interstitial pneumonia. These less common interstitial pneumonias

generally have a much more favorable prognosis with respect to IPF and are often treatable with immunosuppressive therapies (19).

Idiopathic pulmonary fibrosis is a deadly, progressive scarring disease with a worldwide prevalence estimated at 5 million individuals. It effects more men than women (20.2 vs. 13.2 per 100000), with a mean age of onset of 66 years, and an average survival of 2 to 5 years from the time of diagnosis. The initial symptoms of IPF include a non-productive cough and exercise induced dyspnea or breathlessness. Diagnosis of this disease is performed with a high resolution computed tomography chest scan which shows peripheral and subpleural reticular opacities. To confirm diagnosis, an open lung biopsy can be obtained for the histological presentation of UIP (23, 24). Figure 1.0 shows examples of normal and IPF lung CT scans with accompanying examples of normal lung histology. UIP is characterized by thick patches of scar tissue containing collagen, fibroblasts and myofibroblasts called fibroblastic foci. Epithelial cells surrounding these fibroblastic foci also grow to form abnormal thick layers. It is this interface between epithelial and fibroblastic mesenchymal layers where the underlying injury is thought to take place and be perpetuated (25). Environmental exposure to cigarette smoke, livestock, and various types of minerals such as asbestos and silica may predispose one to this disease but the term 'idiopathic' defines its general unknown origins. IPF is highly refractory to current medical intervention, with lung transplantation being the only treatment known to enhance life expectancy (23, 24). Lung transplantation has a survival rate of 49% after 5 years, amongst the poorest outcomes of major organ transplantation (26). Since compatible lung donation is relatively rare, patients with IPF are often left with no clinically proven alternative treatment options despite decades of focused research. Recent data identified in Han Chinese ethic populations have shown that genetic polymorphisms in the transforming growth factor beta 1 (TGFβ1) gene enhance susceptibility to IPF (27) and our lab has shown that TGFβ plays a central role in lung fibrosis pathogenesis in animal models (28-30).

1.1 Transforming Growth Factor Beta

TGFβ was discovered by Michael B. Sporn and Anita B. Roberts in 1981, and was later purified from bovine kidney extracts (31, 32). TGFβ is a cell signaling cytokine protein produced by all cells in the body in three separate isoforms (33). Each TGFβ isoform has its own unique promoter and distribution of tissue expression (34). Deletion of any

individual TGFβ isoform causes a lethal phenotype in mice. TGFβ1 null mice die of a wasting syndrome caused by massive autoimmune complications at around 20 days after birth, with no other obvious developmental deformities (35). TGFβ2 null mice

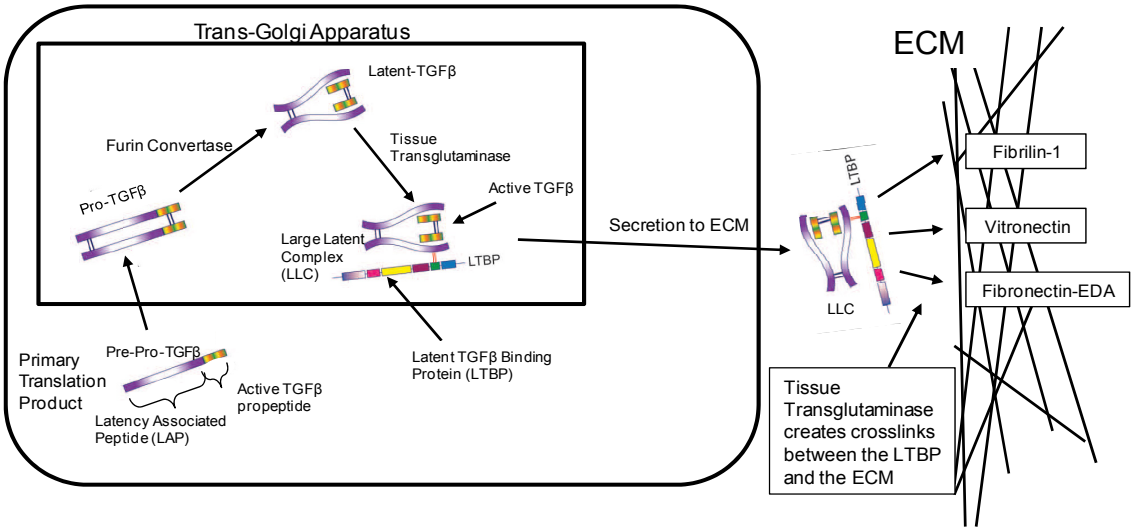

Figure 1.1. The synthesis and processing of TGFβ into its large latent complex. TGFβ pre-pro peptide forms homodimers before being shuttled to the trans-golgi apparatus. The Pro-TGFβ is cleaved to latent TGFβ by furin convertase. Tissue transglutaminase pastes the latent TGFβ to the latent TGFβ binding protein. Processing is followed by secretion into the extracellular matrix where tissue transglutaminase catalyzes covalent linkage formation with various protein components. Images adapted from Biernacka *et al.* Growth Factors (2011) 29:196-202.

have spinal column, craniofacial, inner ear, cardiac, eye, limb, lung and urogenital developmental defects and die at or before birth from complications due to lung deformation (36). TGFβ3 null mice are born with cleft palate and die from lung developmental deformities after about 20 hours (37). That each TGFβ isoform null mouse has a different lethal phenotype demonstrates the variety of developmental and immune regulatory functions performed by this cytokine. TGFβ is expressed as a large latent complex (LLC) of a latent TGFβ binding protein and latent TGFβ. Latent TGFβ1 and β3 are divided by the N-terminal latency associated peptide (LAP), which is cleaved by proprotein furin convertase from the C-terminal active TGFβ protein in the trans-golgi apparatus (38). Following cleavage, the LAP portion remains non-covalently wrapped around the active TGFβ (32). The latent TGFβ is then excreted by cells into the extracellular matrix (ECM) where it is covalently crosslinked to fibrillin-1, vitronectin, fibronectin-EDA, etc. by the activity of tissue transglutaminase (39, 40). Figure 1.1 shows the production, processing of latent TGFβ and its crosslinking to the ECM. Western blot analysis shows that TGFβ forms disulfide linked homodimers. The latent TGFβ complex and active TGFβ form 50kDa and 25kDa bands respectively (32). TGFβ is

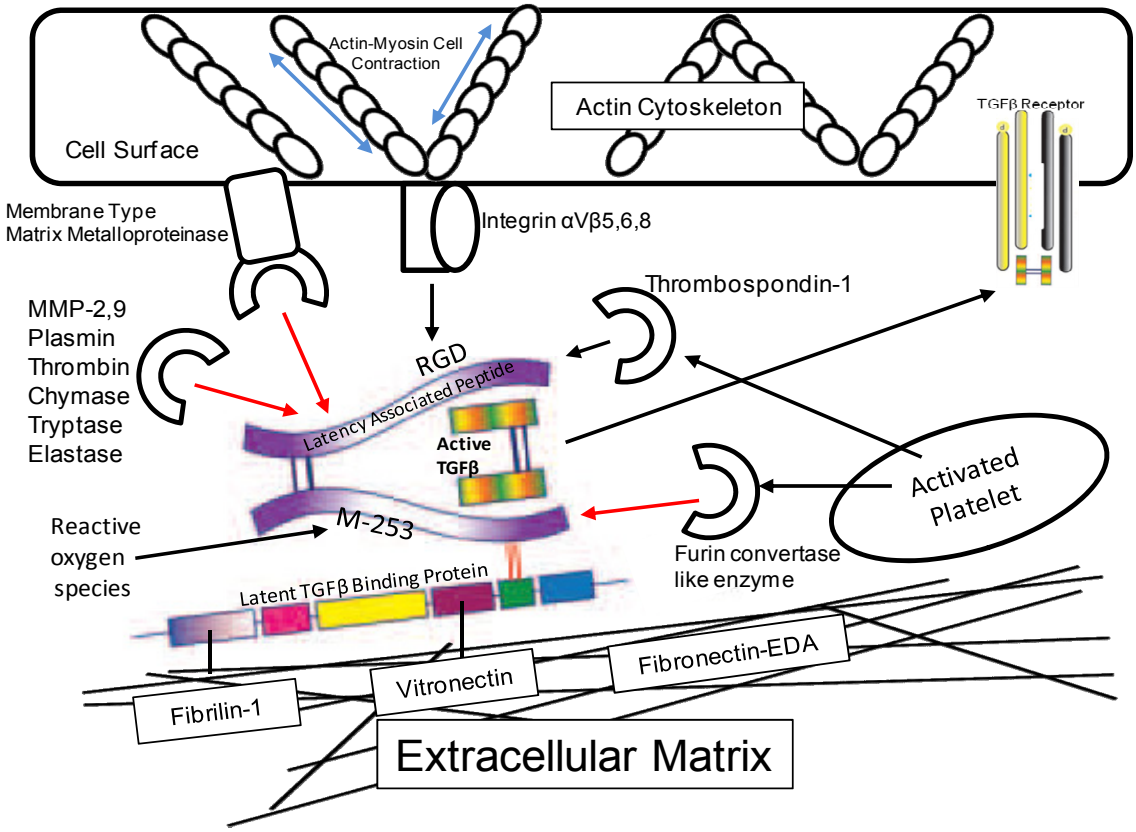

Figure 1.2. Activation of the TGFβ homodimer from its large latent complex in the ECM. TGFβ activation can proceed through mechanisms involving proteolytic cleavage of the LAP by MMP-2, -9, plasmin, thrombin, mast cell chymase and tryptase. TGFβ can be activated by conformational changes in the LAP by reactive oxygen species modification of methionine-253 and by binding of thrombospondin-1. Integrin αVβ5 and αVβ6 activate TGFβ by binding to the RGD domain in the LAP and causing a conformational change during cell contraction. Integrin αVβ8 works together with MT1-MMP to proteolytically cleavage the LAP peptide. The small active TGFβ is then freed to bind to its cell surface receptor. Activated platelets release thrombospondin-1 and an unidentified furin convertase-like enzyme which can also proteolytically cleave the LAP. Image adapted from Biernacka *et al.* Growth Factors (2011) 29:196-202.

also a highly hydrophobic protein, which has lead to numerous experimental difficulties. To keep TGFβ in solution it must adhere to an amphipathic protein such as blood serum albumin. The regulation of TGFβ activity is principally dependent on post-translational modification, removing the LAP portion from the small active TGFβ to allow for cell surface receptor binding. TGFβ activation can proceed through a number of situation dependent mechanisms. TGFβ can be activated by acidic pH (41), reactive oxygen species modification of methionine-253 in the LAP (42), proteolysis of the LAP by matrix metalloproteinases (MMP) -2, -9 (43), membrane type-MMPs (MT-MMP) (44), proteolysis by plasmin or thrombin (45), and non-proteolytic binding of

thrombospondin-1 to the LAP (46). Activated platelets can release thrombospondin-1 and a yet unidentified furin convertase like enzyme which also cleaves the TGFβ LAP (47). TGFβ can also be activated by a mechanism involving the binding of cell surface αV integrins to the LAP polypeptide. Integrins αVβ5 and 6 liberate TGFβ by a method dependent on cell contraction against latent TGFβ bound to a rigid ECM (48-50). Integrin αVβ8 activates TGFβ by proteolysis involving MT1-MMP (51). The mechanisms of TGFβ activation presented in Figure 1.2 are further discussed in detail in Chapter 2. Mechanical and contractile mediated TGFβ activation in the context of lung fibrosis form the focus of investigation for this thesis work.

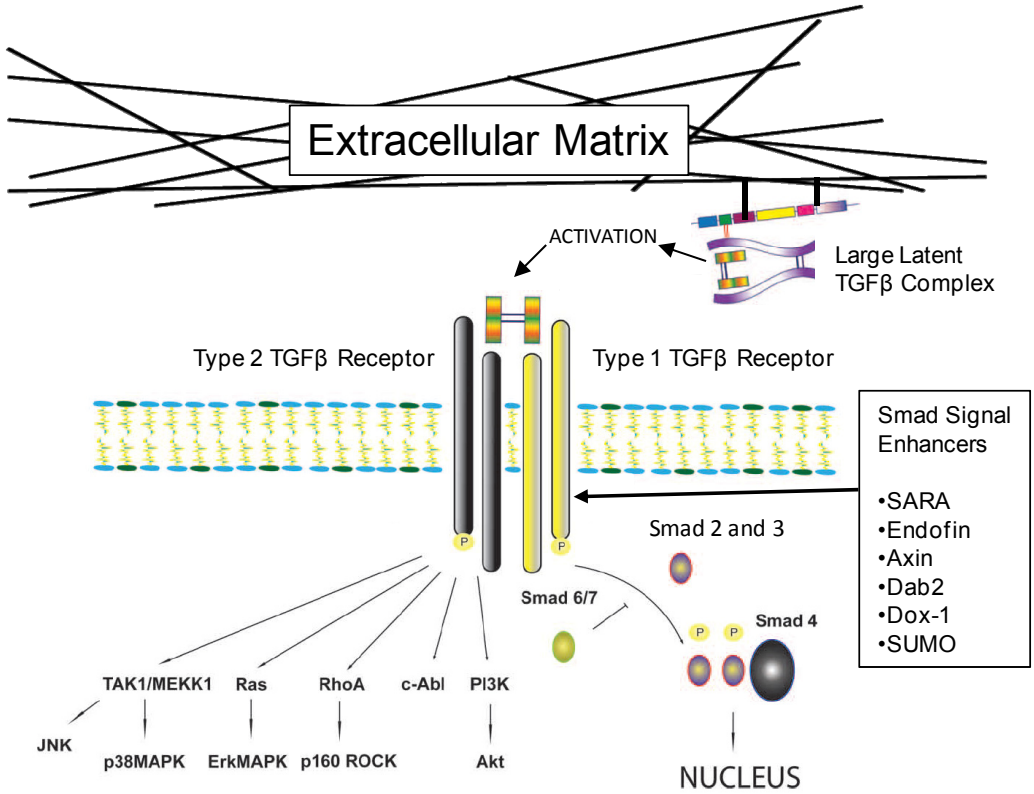

Figure 1.3. TGFβ cell signaling through the type 1 and 2 receptors. TGFβ initially binds to the type 2 receptor which auto-phosphorylates and recruits the type 1 receptor. The types 1 and 2 TGFβ then work together to phosphorylate Smads 2 and 3. Phospho-Smads 2 and 3 form hetero or homo-trimers with Smad4 which translocates to the nucleus to begin transcription. Smads 6 and 7 inhibit the phosphorylation of Smad 2 and 3. Other pathways activated by the TGFβ receptor include JNK, p38MAPK, ERK, Rho Kinase, c-Abl, and PI3K. SARA binds to the type 1 receptor and recruits Smads 2 and 3. Other enhancers of Smad2/3 phosphorylation include Endofin, Axin, Dab2, and Dox-1, and SUMO. Figure adapted from Biernacka *et al.* Growth Factors (2011) 29:196-202.

1.2 TGFβ Cell Signaling

There are three different types of TGFβ receptor. The type 2 receptor is involved in initial binding of the TGFβ active protein. The type 1 receptor is then recruited to the complex and is phosphorylated by the type 2 receptor (52). Type 3 receptor or betaglycan overexpression is involved in negative regulation of type 1 and 2 TGFβ receptor signaling in cardiac fibroblasts (53). Types 1 and 2 TGFβ receptor traffic into the cell via clathrin coated endosome and begin phosphorylating Smad2 (p-Smad2) and 3 (54-56). Figure 1.3 shows the activation of the TGFβ receptors and the downstream Smad and non-Smad signaling events. SARA, the Smad anchor for receptor activation binds to the type 1 TGFβ receptor and facilitates Smad2 and 3 activation (57). SARA is also important in recruiting endocytosis factors for TGFβ receptor internalization, an important step in signal transduction (58). Conjugation of the activated type 1 receptor with the SUMO protein enhances the recruitment of Smads 2 and 3 (59). Other facilitators of Smad signaling are Endofin, Axin, Dab2, and Dox-1(60). Cytoskeletal proteins like filamin, which crosslink actin microfilaments, act as a resting dock for unactivated Smad2 and 3. Cells deficient in filamin have limited TGFβ Smad2 signaling potential. Breakdown of these microtubules by nocodazole treatment enhances phosphorylation of Smad2 in the presence of TGFβ (61, 62). The cytoskeletal protein kinesin-1 ATPase binds to Smad2 and is required for microtubule associated movement of the activated Smad complex to the nucleus (63). In context of TGFβ activation, that Smad proteins are stored and released from an activated cytoskeleton will become important in later chapters. Phosphorylated Smad2 and 3 bind to the adaptor protein Smad4 to form a trimeric complex that travels to the nucleus (64, 65). Smads 2 and 3 form trimers with Smad4 with either two Smad2 or two Smad3 or mixture of all three components. In the nucleus, Smad2/3/4 acts as a transcription factor which participates in the upregulation or downregulation of Smad promoter element containing genes. The secondary binding of Smads with other transcriptional regulators results in the diversity, and often confusing, cell type and concentration dependent effects of TGFβ. Smad proteins are targeted by Smurf2 and NEDD4 HECT ubiquitin ligases for degradation which halts signal transduction. USP15 is the only deubiquitinylating enzyme known to restore activated Smad proteins before degradation (66). TGFβ receptor signaling is negatively regulated by many different methods. Smad7 binds to Smurf 1, Smurf 2, and E3 ubiquitin ligase which target the type 1 TGFβ receptor for

proteolytic degradation (67, 68). FKBP12 and Salt inducible kinase (SIK) associate with Smad7 and the type 1 TGFβ receptor and facilitates degradation (69, 70). SNX25 sorting nexin also binds to the type 1 TGFβ receptor targeting it for lysosomal degradation (71). Dapper2 also binds to the type 1 TGFβ receptor and initiates its degradation in lysosomes (72). TGFβ receptors can also be recycled back to the cell membrane by the activity of Rap2, a Ras GTPase which participates with Rab11 dependent endosomes shuttling (73).

The signaling of TGFβ can also affect other pathways aside from the main 'canonical' Smad pathway. TGFβ can induce MAP kinase signaling though p38, JNK and Erk (74, 75). The cell signaling protein ShcA can also be bound to and activated by the type 1 TGFβ receptor. Phosphorylated ShcA leads to downstream activation of Erk MAP kinases (76). TRAF6 also binds to the type 1 TGFβ receptor and is activated. TRAF6 association with TAK1 leads to downstream activation of both p38 and JNK MAP kinase pathways (77, 78). The phosphoinositol-3 kinase pathway is also activated under the TGFβ receptor which influences cell movement and apoptosis resistance (79). The contribution and importance of these non-Smad pathways to TGFβ driven fibrogenesis is currently unknown.

1.3 TGFβ Responsive Elements and Smad2/3/4 Promoter Control

Although TGFβ can signal through non-Smad pathways, the canonical Smad pathway confers many of this cytokine's primary effects. When the Smad2/3/4 trimeric complex reaches the nucleus it interacts directly with DNA in promoter regions called Smad binding elements (SBE). The Smad complex binds very weakly to an area of DNA encoding 5'-GTCT-3' (91). It was once thought that multiple SBE came together to form a stronger binding complex in general. However, SBE concatemers rarely contain more than four repeats, instead Smad proteins rely on binding cofactor partners to orchestrate transcription regulation via interaction with a common Smad interaction motif (90, 92). Transcription factors are constantly being discovered that bind to various components of the Smad complex. Pbx1, Prep1 (80), Ap1 family members (81, 82), FAST-1 (86-88), FAST-3 (89), Mixer/Milk, E2A/HEB/FOXH1 (83), FOXO family members (84), and p300/CBP (85) are all known transcription cofactors that bind to the Smad complex under various contexts presented in Table 1.0. SBE are found in many different genes playing positive or negative roles in transcription of TGFβ

responsive gene mRNA (92). For example, SBE are found along side Ap1 and Sp1 in the

Table 1.0 Smad Transcription Factor Binding Partners		
Transcription Factor(s)	Biological Context	Reference(s)
Pbx1 Prep1	Pbx1 and Prep1 bind to Smad2/3/4 to activate the follicle stimulating hormone gene promoter in immortalized mouse gonadotrope LβT2 cell lines.	(80)
Ap1 family members	Ap1 family members such as c-Fox and c-Jun bind to the Smad3/4 complex for gene regulation.	(81, 82)
E2A, HEB, FOXH1	E2A, HEB, and FOXH1 bind to Smad2/3/4 complex to regulate the lefty gene promoter in human embryo derived endoderm cells.	(83)
FOXO family members	FOXO family members such as FOXO-1, -3, and -4 bind to the Smad3/4 complex to regulate the p21Cip1 gene promoter in glioblastoma cell lines.	(84)
p300/CBP	p300 binds to Smad4 in a Smad2/3/4 complex to regulate genes in MDA-MB468 and COS-1 breast cancer cell lines.	(85)
FAST-1	FAST-1 binds to the Smad2/4 complex for promoter regulation of Mix.2 gene in early Xenopus laevis and mouse embryos. Disruption of this interaction prevents dorsoanterior axis formation in early embryos.	(86-88)
FAST-3	FAST-3 binds to the Smad2/4 complex to regulate the Mix.2 gene promoter during Xenopus laevis gastrulation.	(89)
Mixer Milk	Mixer and Milk bind to the Smad2/4 complex to regulate the goosecoid gene in early Xenopus laevis gastrula formation.	(90)

human TGFβ1 promoter, such that TGFβ signaling can upregulate its own mRNA message (93-97). Newly translated latent TGFβ protein does not immediately equate to more intracellular TGFβ signaling, since the primary level of regulation of TGFβ activity is at the post-translational level (98). It is suspected that cells maintain a latent TGFβ pool around them which is available for rapid activation under the proper conditions. This latent pool is constantly replaced in order to maintain of future rates of rapid protein activation.

1.4 TGFβ and Lung Fibrosis

Lung fibrosis is an abnormal wound healing process in which scar formations grow to overtake functional areas of blood gas exchange across the alveolar interstitial matrix. TGFβ both drives and augments lung fibrogenesis by the differentiation of epithelial cells into mesenchymal cells (EMT) (99-102), the differentiation of mesenchymal fibroblasts into myofibroblasts (103, 104), and the synthesis of interstitial collagen and other components of the extracellular matrix (105, 106), and the synthesis of numerous other secondary profibrotic mediators (107). It is this greatly enhanced synthesis of collagen in the alveolar interstitial layer which leads to the hallmark stiffness of the lungs which leads to organ failure. Injury to the alveolar interstitial layer continues throughout large reticular patches of lung until blood-gas diffusion is compromised (23). As the lungs stiffen, the physical force required for inspiratory breath increases, making breathing very laborious. At the same time, the force required to push blood through the lungs increases. This pulmonary hypertension causes the right heart to enlarge from the added pressure and often leads to heart failure. Patients often succumb to a combination of acute exacerbation, a poorly understood sudden worsening of symptoms, pulmonary hypertension, and blood gas exchange failure (23).

In 1996, it was discovered that the TGFβ$_1$ isoform but not TGFβ's 2 or 3 were overexpressed in histopathological examinations of IPF lung tissue (108). This and previous data from Anita Roberts' lab showing TGFβ$_1$ isoforms ability to stimulate collagen growth and fibrogenic signals, lead to a general focus on the TGFβ$_1$ for tissue fibrosis(105, 106). In their landmark publication, Jack Gauldie's lab showed that Adenovirus (Ad) driven transient overexpression of constitutively active TGFβ$_1$ resulted in persistent lung fibrosis upon intratracheal administration (30). This was the first time that a single cytokine had been found to induce all the fibrotic machinery required for

fibrogenesis in an animal model. Although other cytokines, when overexpressed, had been found capable of inducing some fibrogenic changes alone, these changes were all reversible if given enough time (107). Only a few cytokines when overexpressed by Ad produced pronounced fibrogenesis in the lungs. These cytokines were IL-1β, which greatly increases inflammation and produces sustained fibrosis, TNF-α, which produces inflammation and low level fibrosis, and GM-CSF, which produces inflammation and subsequent fibrosis (107). Upon closer observation, IL-1β effects were driven by subsequent activation of the TGFβ pathway (109). IL-13 was later shown to cause fibrosis by selectively stimulating the TGFβ pathway (110). IL-13 is known to induce expression of genes involved in parasite induced liver fibrogenesis in a manner that is independent of $TGF\beta_1$ cytokine or signaling through Smad3 (111). Manel Jordana showed in an allergic mouse model of house dust mite exposure that airway fibrosis could proceed independent of TGFβ signaling in Smad3 knockout mice as well as in the presence of TGFβ blocking antibodies (112). These results indicate that under certain conditions fibrosis can proceed with significant TGFβ involvement.

Although the signaling of a single cytokine is capable of activating lung fibrogenesis in a rodent model, this does not mean that this is the only mechanism of pathogenesis. With the invention of triple transgenic, inducible, surfactant apoprotein-C promoter constructs it became possible to achieve the expression of active $TGF\beta_1$ upon oral doxycycline administration. These mice produced in Jack Elias' lab were specially designed to ask the question of whether or not active $TGF\beta_1$ alone was sufficient to produce fibrogenesis in adult lungs without viral help. When adult conditional TGFβ expressing mice were given doxycycline induction, the initial response was a noted increase in epithelial apoptosis within 12 hours. After two days, inflammation in the form of macrophage appeared in the lungs and dissipated after ten days. An increase in collagen content was appreciated at day two and increased for as long as the mice received doxycycline. The fibrotic response was partially reversible following a month of doxycycline treatment. These data indicate that the context of $TGF\beta_1$ activity is as important as its activation itself (96). The Adenovirus control vector in Jack Gauldie's overexpression model is itself capable of tissue inflammation and cell death which predisposes the lungs to a fibrogenic stimulus from $TGF\beta_1$ (30). It is thought that the death of epithelial cells and their abnormal repair gives the crucial second hit that along

with plentiful active TGFβ$_1$ drives progressive tissue fibrosis. The reason of how and why TGFβ is continuously activated in lung fibrosis is a major question in the field.

The continuous activation of TGFβ is likely produced as a result of ongoing damage to the alveolar basement membrane, and is of central importance to the progression of IPF (113). TGFβ signaling through both Smad and non-Smad pathways leads to epithelial integrity loss, epithelial to mesenchymal transition, production of secondary fibrotic cytokines downstream of TGFβ, differentiation of fibroblasts to a myofibroblast phenotype, and extracellular matrix accumulation (109, 113). The Smad pathway of TGFβ signaling is indispensible to the main fibrotic stimulus. Smad3 null mice do not develop fibrosis upon intratracheal (IT) Ad driven constitutively active TGFβ$_1$ administration or to IT bleomycin (10, 29). These findings have lead to a focus on TGFβ activation mechanisms in hopes of finding a way to interfere with the fibrogenic stimulus.

1.5 Rationale and Hypothesis of Thesis

Mechanical TGFβ activation has been determined *in vitro* as a method by which fibroblasts and myofibroblasts sense and respond to the rigidity of the ECM around them (50, 114). As the scars stiffen during pathogenesis of lung fibrosis, it is thought that the rigid ECM presents a signal to the fibroblasts which is misinterpreted and leads to more collagen production. The active TGFβ cytokine hides within its LAP structure in the ECM (Figure 1.1), which makes this cytokine's activation dependant on conformational distortion or proteolysis of LAP. TGFβ activation is known to occur predominantly in vivo by cellular force dependent means acting through cell surface integrins bound to the LAP (Figure 1.2). Since the lungs are in constant motion, the stimulus of breathing, especially at higher inspiratory pressures which occur in IPF, could provide another diffuse tissue stimulus for TGFβ activation at the cellular level. These prior findings indicate that mechanical TGFβ activation may play an important role in IPF pathogenesis. Mechanical TGFβ activation in the context of lung fibrosis is further investigated in Chapters 2 and 3.

A great number of drugs have been described to be beneficial in the intervention of animal models of lung fibrosis initiated by IT bleomycin. Most of these drugs have been given as a prophylactic treatment and could thus act against the inflammatory response to bleomycin. Inhibiting the inflammatory response in the context of IT bleomycin halts the subsequent

fibrotic response. At diagnosis, patients with IPF lack a significant inflammatory response (23). Because of this, all anti-inflammatory drugs studied to date have never seen any therapeutic efficacy either in a model of fibrosis or in clinical trials (115). Warned by this and data from years of failed immunosuppressive corticosteroid therapy in IPF, our group has focused on the fibrogenic response itself to improve the study of therapeutic intervention. Our group has designed sophisticated methods towards a holistic approach to lung fibrosis modeling and drug intervention study. These methods are designed to look into more 'clinically relevant' outcomes in rodent model experimentation and focus on therapeutic intervention as opposed to prophylaxis (116). Non-invasive evaluations of lung fibrosis are further presented and discussed in Chapters 4 and 5.

The extracellular matrix has long been a focus of study in lung fibrosis. Collagen and other ECM components are highly expressed in lung fibrosis to the point where these molecules dominate the tissue structure (23). It is hypothesized that the underlying injury in lung fibrosis is one that distorts the ECM in a way that supports both epithelial cell death and TGFβ activation. Understanding the rate and nature of ECM turnover in lung fibrosis is a key goal in the discovery of underlying injury occurring in IPF. Collagen crosslinks are molecules that form during the maturation of collagen when arranged in the ECM. There are two different trifunctional collagen crosslinks called pyridinoline (Pyd) and deoxypyridinoline (Dyd). In this thesis is presented a novel method for assaying Pyd and Dyd by high pressure liquid chromatography (HPLC). It is thought that higher rates of mature collagen crosslink shedding indicate abnormal maturation of collagen and an enhanced fibrogenic process (117). Urological or serological assessments of collagen breakdown products are also beneficial since they do not involve invasive lung biopsy surgery and may indicate the severity of IPF progression. Collagen breakdown products are further presented and discussed in Chapters 6 and 7.

General Hypothesis

We hypothesize that the evaluation of collagen turnover markers and non-invasive analysis of lung function and density provide critical knowledge of the nature of the stiffened fibrotic microenvironment which demonstrates that cell contraction, mechanical stretch, and lung ventilation are stimuli which cause the persistent activation of TGFβ in animal models of lung fibrosis and these stimuli contribute to the persistent and progressive nature of IPF.

2.0 Introduction to TGFβ Activation

TGFβ activation has become one of the most central questions in the study of pathogenic mechanism driving pulmonary fibrosis. As noted earlier, TGFβ is created as a large latent complex (LLC) which is produced by a wide variety of cell types and is composed of the pro-peptide TGFβ latency associated peptide (LAP), the active TGFβ cytokine, and the latent TGFβ binding protein (Figure 1.1). During production of the LLC, the TGFβ latent protein is cut into two intertwined pieces which remain associated, sequestering the active peptide fragment within in a non-covalent manner. This latent complex is formed by furin convertase in the trans golgi apparatus (118). The LTBP is produced as separate protein which is bound to latent TGFβ via specific disulfide bonds during processing (119). Processing also involves the post-translational modification of LTBP by tissue transglutaminase. Tissue transglutaminase modifies glutamine residues in the LTBP and creates a covalent crosslink to ECM glutamic amino acid residues to provide an anchor for later activation. These transglutaminase crosslinking reactions can form in two ways. The first forms a glutamyl-lysine peptide bond. The second possible reaction forms a glutamyl-lysyl crosslinks containing a polyamine in between such as spermine (120). Both crosslinking reactions help to paste the TGFβ LLC into its ECM nest. There are many possible amino acid crosslinking residues in fibrilin-1, vitronectin, and fibronectin-EDA that bind to the TGFβ LLC (39, 40). Held within its ECM confined latent complex, the mature TGFβ homodimer remains hidden and cannot interact with its high affinity receptor (121).

2.1 Acid Activation of TGFβ

How and why TGFβ is activated is a constantly evolving story. The earliest methods of activation published involved the acid activation and proteolysis by the serine protease plasmin. Lyons *et. al.*, discovered that strong acid (pH= 1.5) or basic solutions (pH = 12.0) fully activated TGFβ from cell conditioned media. Mild acidic solutions (pH=4.5) and plasmin (0.1U/mL) activated 20% of the total TGFβ that were activated by strong acid means. This indicated to the researchers at the time that there were two pools of latent TGFβ, one that was readily activated and a larger pool that required harsh treatment (41, 122, 123). No further evidence of differing versions of latent TGFβ have been reported in the literature. Others have shown more recently that acidic bile

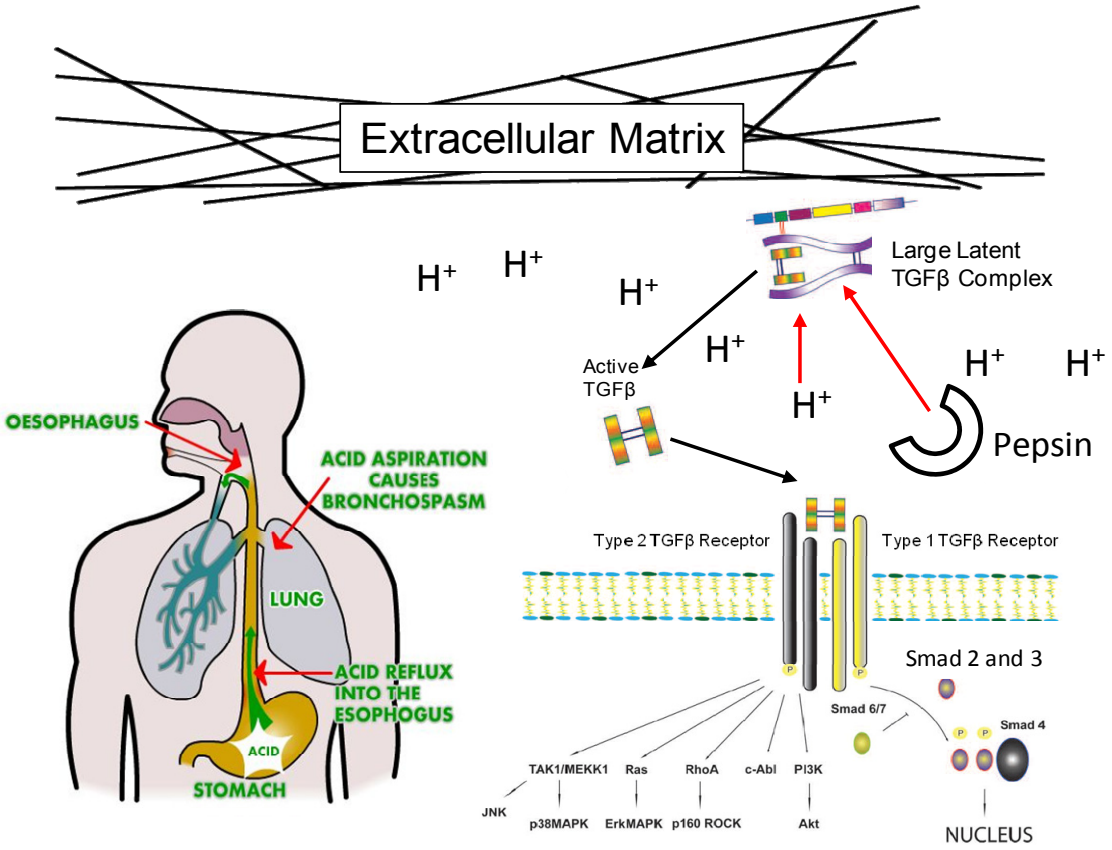

Figure 2.0. Gastroesophageal reflux aspirated into the lungs where it activates TGFβ. Hydrochloric acid and stomach enzyme pepsin liberate the active TGFβ homodimer by conformational change and proteolytic cleavage of the LAP respectively. Acid reflux diagram adapted from website: http://mylearningworld.com/admin/event/gerd.jpg. TGFβ figure adapted from Biernacka *et al.* Growth Factors (2011) 29:196-202. and

constituents present a plausible method of TGFβ activation following aspiration of stomach fluids into the respiratory tract (124). Gastro-esophageal acid reflux is known to be present in at least 90% of patients with IPF (125, 126). There is also a higher prevalence of hiatus hernia, a protrusion of the upper stomach into the diaphragm, amongst those with IPF (127). It has been hypothesized that stomach acid reflux could be a source of both constant lung epithelial injury and continuous TGFβ activation. Animal models have shown for the past 50 years that lung exposure to acid generates acute edema, hypoxemia, epithelial cell injury and in some cases interstitial fibrosis (128). Figure 2.0 describes how TGFβ is activated by gastric reflux. In a porcine bile exposure model, the causative agent was shown to be hydrochloric acid and the stomach enzyme pepsin (129). An interesting aspect of TGFβ biology is that the affinity of this cytokine for its receptor is very high and only small amounts of activated TGFβ

create a maximal cell response (98). Under this context, it is easier to envision how repeated acute gastric reflux could activate sufficient TGFβ over time. Other examples of low pH influencing TGFβ physiology are the resorption of bone by osteoclasts. Under the correct conditions, osteoclasts form adhesions to the bone surface through αVβ3 integrin binding (130). A pocket forms at the osteoclast-bone surface which is acidified by the delivery of acidic vesicles produced within the cell by osteoclast-specific vesicular proton pump Atp6i (131). The result is a bone surface pocket with a pH of 4.5 which is sufficient to activate TGFβ during bone demineralization (132-134). Contemporary to the acid activation discovery, it was found that heating latent TGFβ from chicken embryo fibroblast cultures to 100˚C for 3 minutes activated the protein (123). This is likely a result of heat dependent denaturing of the LAP surrounding the active TGFβ homodimer and likely has no direct physiologic relevance.

2.2 Reactive Oxygen Species and TGFβ Activation

Reactive oxygen species (ROS) are small oxygen containing molecules with a singlet high energy electron. This high energy electron confers strong reactivity to the molecule with functions including immune pathogen defense, redox homoeostasis, and cell signaling (135, 136). ROS can be created and used by the body to signal the presence of acute cellular injury(137) and attraction of innate immune cells (138), can be produced by immune cells to kill bacteria via myeloperoxidase (135), and influence cell function via activation of TGFβ (42, 139-141). Common ROS are superoxide anions O_2^-, hydrogen peroxide, and hydroxide radical $HO^{\cdot}$. Hydroxyl radicals can activate $TGF\beta_1$ directly by oxidation of methionine-253 within the LAP peptide. These redox reactions at methionine-253 cause a rapid conformational change in the LAP which releases the active homodimer. Other isoforms of TGFβ are refractory to direct activation by reactive oxygen species making the β_1 isoform unique as sensor of extracellular oxidative stress (142). In further support of this oxidative stress-TGFβ axis, Smad3 deficient mice are resistant to radiation exposure which produces ROS in the skin (143). It may be that O_2^- is more important in the context of pulmonary fibrosis. O_2^- enters cells through chloride ion receptors in lung fibroblasts and leads to the release of active TGFβ and collagen expression, whereas hydrogen peroxide did not activate fibroblasts (139). Excessive O_2^- is known to dismutate into more reactive hydrogen peroxide and hydroxyl radicals, the latter of which can activate TGFβ directly in the ECM. The animal

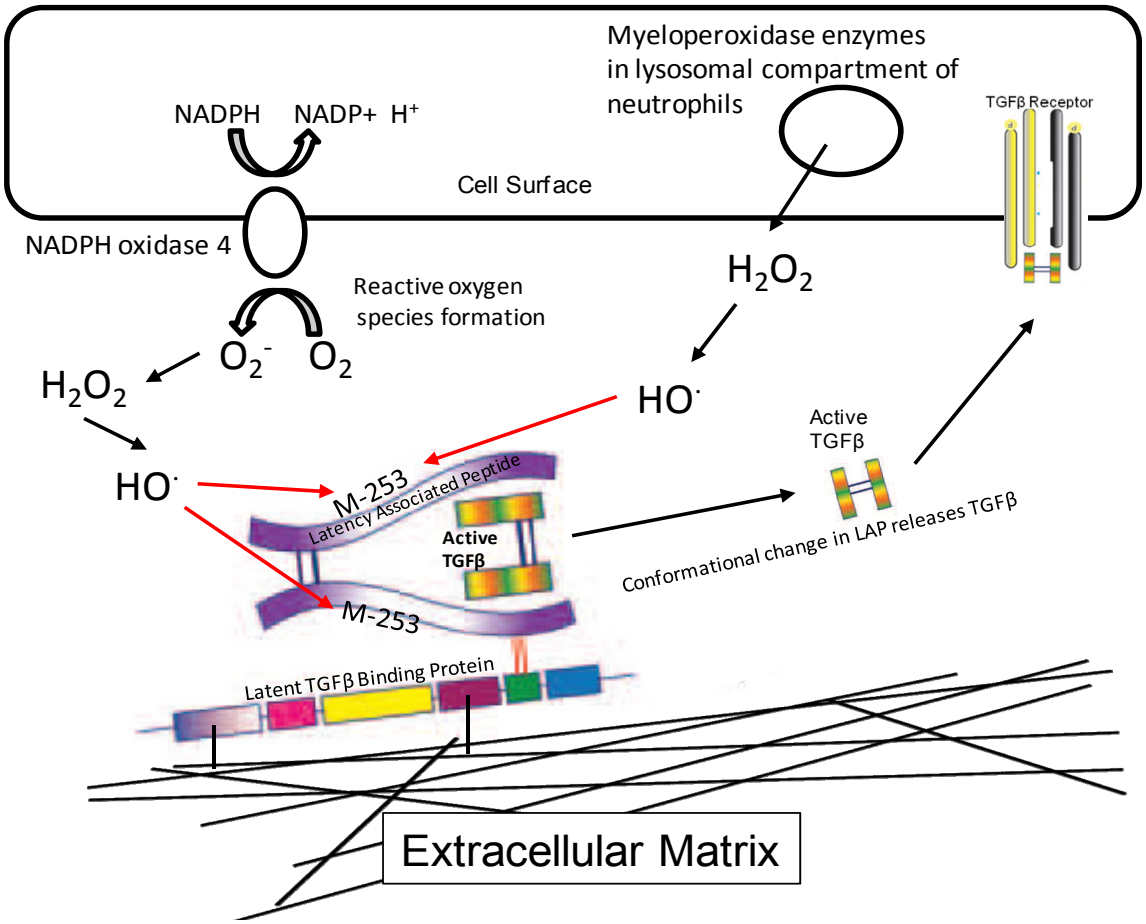

Figure 2.1. Superoxide radicals are created at the cell surface by NADPH oxidase. The superoxide radicals can then form hydrogen peroxide spontaneously which can then in turn form hydroxyl radicals. The active TGFβ homodimer is released from its large latent complex in the ECM by conformational changes caused by modification of methionine-253 in the LAP by hydroxyl radicals. Image adapted from Biernacka *et al.* Growth Factors (2011) 29:196-202.

models of exposure to bleomycin, paraquat, and thoracic irradiation are all known to generate fibrogenesis through ROS which are inhibited via strong anti-oxidants (144-146). Adenovirus driven active $TGF\beta_1$ overexpression in the lungs also increases the production of ROS which enhances fibrogenesis. Concomitant expression of adenovirus driven extra-cellular superoxide dismutase catalyzed the breakdown of TGFβ-dependant ROS in the lungs and also attenuated fibrogenesis (147).

ROS are thought to be important in the pathogenesis of IPF. O_2^- radicals are elevated in the blood of IPF patients over controls indicating an underlying deficiency in antioxidant glutathione regulation (148). Victor Thannickal's group have shown that the expression of NADPH oxidase-4 (NOX4) which produce O_2^- radicals, is elevated in IPF derived

fibroblasts and are critical for the development of myofibroblast phenotypes and collagen expression through Smad 2 and 3 activity (149, 150). Figure 2.1 demonstrates how TGFβ is activated by ROS. Hydrogen peroxide produced by IPF derived fibroblasts in response to TGFβ also signals to induce lung epithelial cell death which may be the important link to the second hit which is required for fibrogenesis (151). TGFβ enhanced production of ROS is thought to cause the further activation of more TGFβ residing in the tissue by directly activating methionine-253. It could be that this redox sensing system of $TGF\beta_1$ is causing a positive feedback loop which spirals out of control resulting in chronic fibrogenesis. To date, antioxidant therapies with high dose N-acetyl cysteine (NAC) in IPF have resulted in no significant improvements in lung function but do significantly delay progression of disease. Despite this improvement attributed to NAC, the disease remained terminal (152). These results indicate that although TGFβ activation may be partly attributed to the oxidative state of the ECM in the lung interstitium, other modes of TGFβ activation supplement or drive fibrogenesis.

2.3 Matrix Metalloproteinases, Serine Protease and TGFβ Activation

Matrix metalloproteinases (MMPs) are a large group of enzymes with partially overlapping functions capable of degrading specific constituents of the ECM to maintain tissue homeostasis. MMP biology is closely regulated by TGFβ signaling in the lungs. MMPs are produced as latent propeptides which are activated following their release into the extracellular matrix. Expression of pro-MMPs 2 and 9 is induced by TGFβ signaling in lung fibroblasts. Expression of MMPs 2 and 9 are also known to be elevated in fibroblastic foci from IPF lung biopsies (44). MMPs 2 and 9 are bound in their inactive propeptide form to cell surface marker CD44. Membrane type 1-MMP (MT1-MMP) activates pro-MMP2 and pro-MMP9 to their mature, high activity forms in concert with CD44 (153). MMPs 2 and 9 are capable of proteolytic cleavage of the TGFβ large latent complex to release the active homodimer (154). MT1-MMP has been shown to activate TGFβ in concert with αVβ8 integrins in lung epithelium (51). MT1,2,3,5-MMP were all upregulated in IPF lung biopsies. MT3-MMP was expressed in fibroblastic foci and was induced by TGFβ in IPF fibroblast cultures. Interestingly, the site of highest MT-MMP expression was MT1-MMP in IPF alveolar epithelium (44). These results highlight that both the fibroblast mesenchyme and the epithelium in the lungs are involved in TGFβ

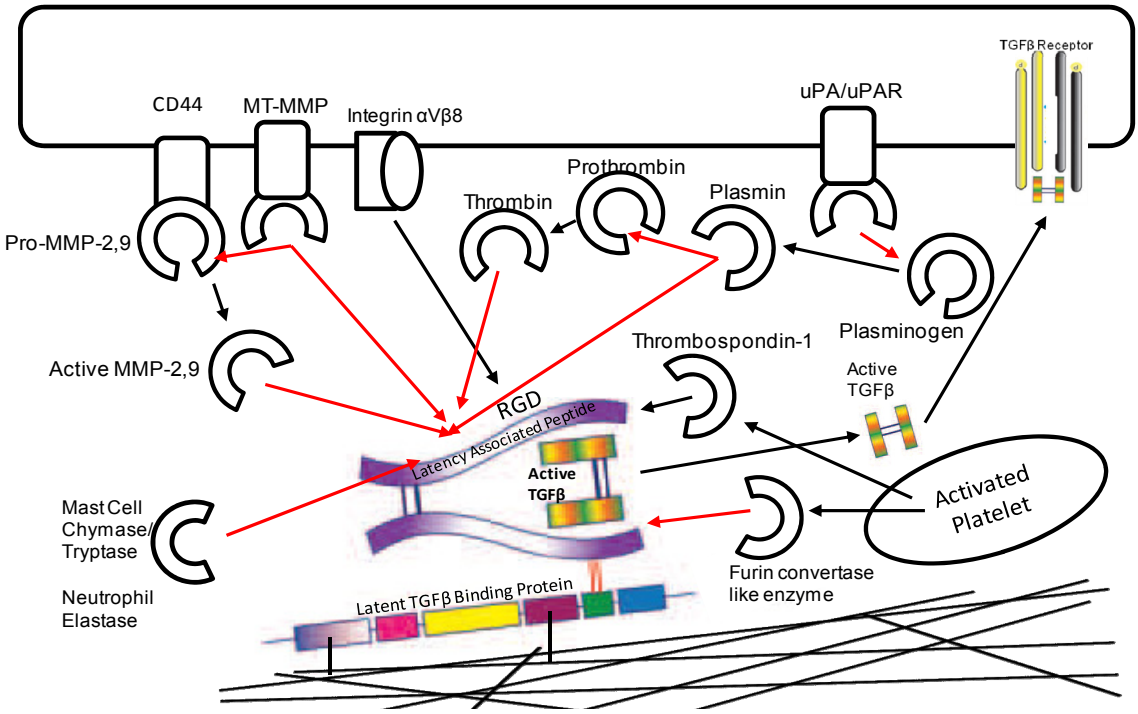

Figure 2.2. Protease and thrombospondin-1 mediated active TGFβ release from the ECM. proMMP-2 and -9 are bound to the cell membrane by CD44 receptor where they are activated by MT1-MMP. Active MMP2,9 and MT-MMP can cleave the latency associated peptide along with mast cell chymase, tryptase and neutrophil elastase. MT1-MMP works in concert with integrin αVβ8 which holds the RGD domain of the LAP in place. Plasminogen is activated by uPA/uPAR system and can cleave the LAP directly or indirectly by activating thrombin from prothrombin. Platelets release thrombospondin-1 which directly activates TGFβ by conformational changes in the LAP peptide. Platelets also release a yet unidentified furin-like convertase which also cleaves the LAP peptide. Image adapted from Biernacka *et al.* Growth Factors (2011) 29:196-202.

activation through MT-MMPs and perpetuate the fibrotic signal together. The co-localization of MT-MMPs expression with MMP2 expression in IPF biopsies also highlights MMP2 mediation of pathogenic TGFβ activation. As mentioned above, MMPs are heavily involved in the breakdown of ECM components. MMP2 breaks down collagen type 4 in the basement membrane underneath lung epithelium and causes the activation of TGFβ (43). Since TGFβ activates both the expression of more ECM products as well as MMP2 and 9 expression, it could that MMPs 2, 9 and TGFβ are involved in a positive feedback loop under fibrotic conditions.

The urokinase plasminogen activator (uPA) and its receptor (uPAR) are capable of activating plasminogen to plasmin which can in turn cleave the TGFβ LLC (45). Despite this, plasmin activation actually protects mice from bleomycin induced fibrosis. Mice that lack the plasminogen activator inhibitor-1 (PAI-1), a highly TGFβ responsive gene,

are protected from fibrogenesis induced by bleomycin. Plasmin activity results in the expression of prostaglandin E2 in normal and bleomycin treated mouse alveolar epithelium and lung fibroblasts cultures as well as in human fibroblasts. Plasmin activates hepatocyte growth factor (HGF) and downstream cyclooxygenase-2 (COX-2) which is involved in prostaglandin production. Fibroblasts cultured from IPF patients were unable to produce COX-2 in response to plasmin activity (155). These results indicate that although plasmin may activate TGFβ LLC directly, plasmin's general tissue effects are more restorative in function under normal conditions. Figure 2.2 describes known proteolytic methods by which the LAP is cleaved to release active TGFβ. The inability to produce prostaglandins in response to plasmin activity may allow plasmin to continue activating TGFβ without tight regulation.

2.4 Immune Cell Sources of TGFβ Activation

Immune cells store large quantities of latent TGFβ which can be released upon stimulation. Macrophage, neutrophils, and eosinophils especially have these latent stores within their cytosol. In response to tissue damage latent TGFβ is released into the site of injury. In the site of injury, the latent TGFβ can either be directly activated by acute phase enzymes plasmin and thrombin, activated by MMPs (2, 9, MT-MMP) at the cell surface or inserted into the matrix of the provisional wound. After macrophages secrete latent TGFβ, the protein is anchored to the cell membrane by thrombospondin-1 (TSP-1) bound to its cell receptor CD36 and the mannose-6-phosphate receptor (156). Latent TGFβ is then activated by plasmin in an uPA/uPAR dependant manner (157, 158). Macrophages are also capable of activating a B-cell produced IgG-TGFβ complex. This activation also occurs at the macrophage cell surface and requires Fc-γ receptors, which bind to IgG non-variable domains (159, 160). IgG-TGFβ complexes within some B-cells and plasma cells also exist in an activated state which may be due to IgG mediated dissociation of the LAP peptide from the latent TGFβ (161). TGFβ is critically important to immune cell suppression. Activation of tonsillar B cells with Staphylococcus Aureus Cowan increases the mRNA expression of $TGF\beta_1$ but causes a seven-fold increase in latent TGFβ protein secretion, of which only 10% is activated (162, 162). In contrast, the addition of lipopolysaccharide (LPS), a bacterial cell wall component, to spleen B-cells causes the release of TGFβ which is immediately activated (163).

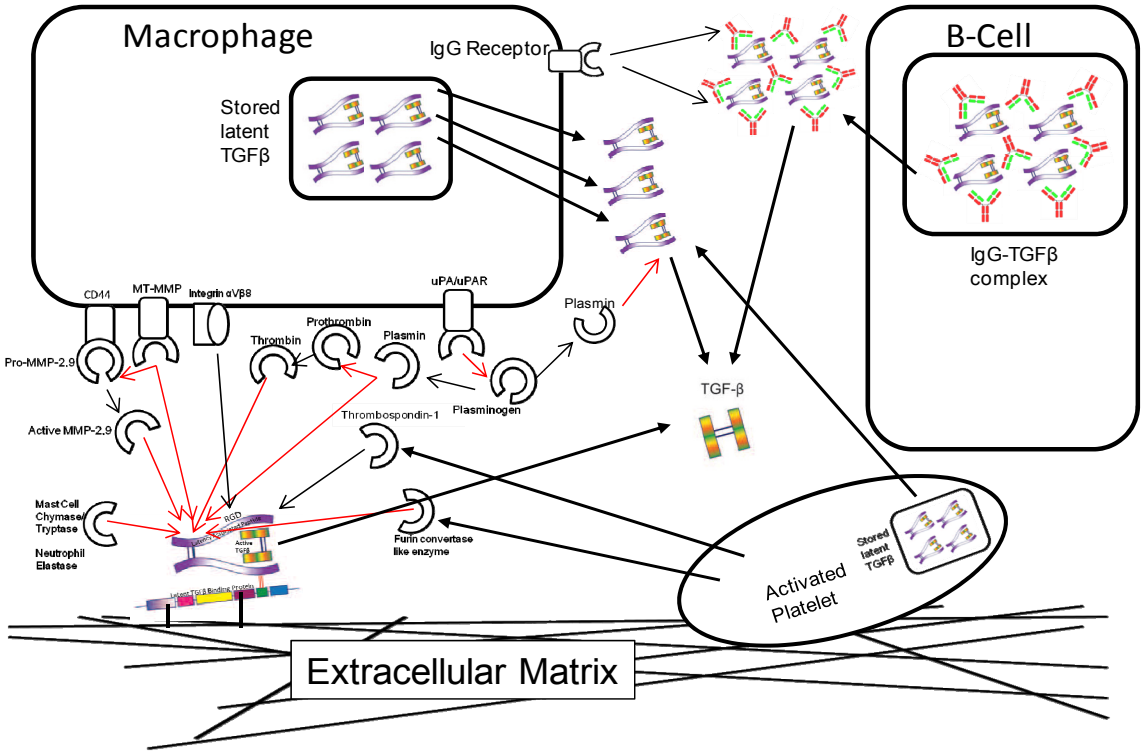

Figure 2.3. Immune cells use proteases to activate latent TGFβ. Latent TGFβ is stored in macrophage and platelets for rapid release. Plasmin and thrombin activate TGFβ released by macrophage platelets and B-cells. B-cells can carry IgG complexes of TGFβ which are activated by IgG receptors on macrophage. Antibody image taken from website: http://proteopedia.org/wiki/images/c/cb/Antibody_basic_structure.gif. Image adapted from Biernacka *et al.* Growth Factors (2011) 29:196-202.

Blood platelets are also a source of large quantities of latent TGFβ$_1$ (164). The acute coagulation enzyme thrombin stimulates both the activation of platelets to release latent TGFβ and the conversion of fibrinogen to fibrin in the assembly of the provision wound matrix (165, 166). This latent TGFβ is then subsequently activated later by a furin-like pro-protein convertase enzyme which is released by the platelet and is independent of TSP-1, plasmin, or thrombin (47). This furin-like enzyme has not yet been identified but represents an important link between the acute phase of wound healing and TGFβ activation (Private Communication from: Dr. Georg Brunner, Department of Cancer Research, Fachklinik Hornheide, University of Münster, Münster, Germany). Platelet derived latent TGFβ is found in α-granules alongside TSP-1 which can also activate TGFβ following platelet degranualation. Figure 2.3 illustrates the major routes by which TGFβ is activated by immune cell components. Glycoprotein-A repetitions predominant protein (GARP) also binds to latent TGFβ at the outer

membrane of platelets and regulatory T cells (167). GARP binds directly to LAP domain of TGFβ via non-covalent association and independently by covalent association through two disulfide bonds. The non-covalent binding of GARP was sufficient to outcompete LTBP for interaction with latent TGFβ and prevents latent TGFβ secretion (168). When membrane associated and disulfide linked to latent TGFβ, GARP permitted latent TGFβ activation via an integrin αVβ6 and αVβ8 dependent mechanism (169).

In the initial stages of fibroproliferative disorder, inflammatory sources are thought to play a stronger role in producing and activating TGFβ in the injury site. As the fibrotic process matures the tissue itself and the crosstalk between injured epithelium and mesenchyme take over from immune cell dependence. It is currently thought that inflammatory component diseases such as non-specific interstitial pneumonia could be precursors to full blown IPF (170). When IPF patients first enter the clinic with typical exercise induced dyspnea and non-productive cough, the hypothetical inflammatory phase of fibrogenesis has already passed. IPF biopsies mostly lack any significant immune cell infiltrates. The fibroproliferative stage of IPF, which is contemporary and successive to the hypothetical inflammatory phase, does not appear to be driven by immune cell interaction since IPF patients are refractory to immunosuppressive drug regimes (171).

2.5 Thromobospondin-1 and TGFβ Activation

Thrombospondin-1 is a matricellular protein that activates TGFβ directly and indirectly (46). TSP-1 unwinds the latent TGFβ from the LAP by a non-proteolytic binding mode which causes conformational changes which free the active homodimer (172). Of the knockout mice known to exhibit similar characteristics to the TGFβ null mice phenotypes, the first discovered was a knockout of TSP-1 (173). At the time that the TSP-1 null mouse was made, the leading candidate for TGFβ activation *in vivo* under normal physiologic conditions was plasmin. However, when the plasminogen null mouse was produced it quickly became apparent that this animal did not reproduce the phenotypes of the TGFβ null mice as was expected (174). The tetrapeptide (KRFK) from TSP-1 is capable of activating TGFβ *in vivo* on its own. Antibodies for the LAP inhibited binding of TSP-1 to TGFβ and its subsequent activation. The amino acid sequence LSKL peptide from the LAP region also competes with TSP-1 for latent TGFβ binding (173). Figure 2.2 illustrates TGFβ activation by TSP-1. However, mice that lack TSP-1 are not

protected from fibrosis instigated by IT bleomycin, which makes an antifibrotic drug based on TSP-1 inhibition less intriguing (175).

2.6 Integrin, Mechanical and Contractile Mediated TGFβ Activation

Integrins are a group of heterodimeric cell surface proteins many of which are involved in adhesion to the ECM (176). The two subgroups α and β contain 18 and 9 subunits respectively, forming at least 24 different combinations (177). Integrins form large complexes with the cytoskeletal structure which gives cells traction and adherence as they move through their environment. Many of the αV subunit containing integrins are known to bind to RGD amino acid domains which are abundant in ECM proteins (177). It was hypothesized that latent TGFβ could also be an integrin binding partner since it resides in the ECM and contains RGD in its pro-peptide domain. Further investigation from John Munger and Dean Sheppard's group showed that αVβ1 integrins were

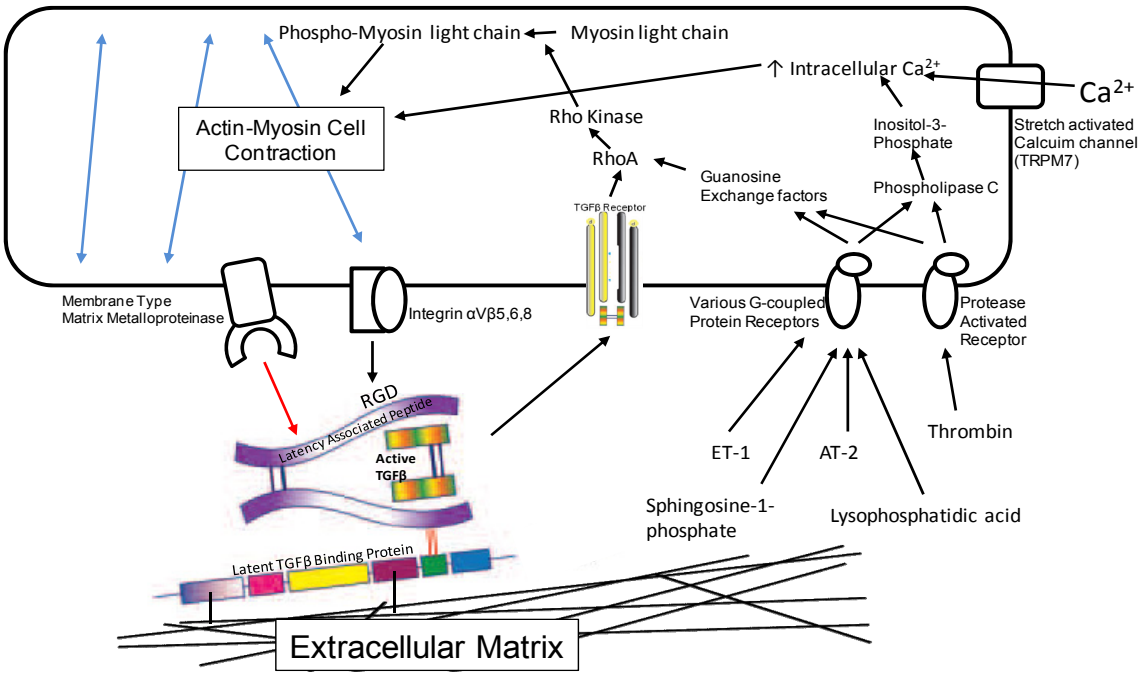

Figure 2.4. Integrin and contractile element activation of TGFβ. Integrins bind to the RGD domain of the LAP which is bound to the ECM through LTBP. Activation of TGFβ can proceed via any method which activates cellullar myosin-actin contractility which is potentiated though the cell surface integrins αVβ5,6. Integrin αVβ8 works with MT1-MMP to activate TGFβ by proteolytic cleavage. ET-1, AT-2, sphingosine-1-phosphate, lysophosphatidic acid, and thrombin are examples of agonists that function via G-coupled protein receptors to active contraction via the Rho and phospholipase C pathways. TRPM7 is activated by cell stretch and also increases contraction via intracelluar calcium influx. Image adapted from Biernacka *et al.* Growth Factors (2011) 29:196-202.

capable of binding to the RDG domain on the LAP of latent TGFβ_1 (178). Since TSP-1 also bound to TGFβ and activated it in a non-proteolytic manner, it was envisioned that perhaps αV integrins could activate TGFβ similarly. Null mice for integrin subunit β6, which only forms an integrin with its partner αV, showed some similar phenotypic characteristics to TGFβ_1 null mice with skin and lung inflammation (179). Work in integrin αVβ6 knockout mice showed that a link between the TGFβ_1 LAP and the integrin was required to drive subsequent bleomycin induced lung fibrosis (48). To confirm that integrin binding to the LAP RGD domain of TGFβ_1 was the dominant method of *in vivo* activation, an RGE mutant mouse was created. The LAP RGD modification to RGE abolished integrin binding in transgenic mice and reconstituted the same phenotype as the full length TGFβ_1 gene null mice (180). It was later found that TGFβ_3, but not TGFβ_2, could also be activated by αVβ6 integrins by binding to the LAPβ_3 RGD amino acid domain (181). Other αV containing integrins, αVβ5, αVβ8 were found to be able to bind to and activate TGFβ_1. Interestingly, αVβ8 integrin was able to bind to TGFβ LAP peptide but required MT1-MMP to cleave the LAP to release the active homodimer at the cell surface (51). Integrin αVβ5, expressed in human airway smooth muscle cells, was later found to activate TGFβ when stimulated with lysophosphatidic acid (LPA) or methacholine (49). Fred Grinnell's work with fibroblasts seeded in 3D collagen matrices shows that the rigidity of the environment a cell grows in has a great affects on its phenotype (182). Fibroblasts grown in loose collagen gels adopted a relaxed dendritic-like appearance, whereas fibroblasts grown in tight collagen gels differentiated into myofibroblasts with a dramatic tensile phenotype (183). TGFβ was shown to be responsible for the contraction of 3D collagen gels by causing the differentiation of fibroblasts to the myofibroblast phenotype (104). In 2003, Victor Thannickal's group showed that myofibroblast differentiation through TGFβ_1 was dependant on cell adhesion and integrin signaling via focal adhesion kinase (184). However, a positive link between TGFβ activation and cell perception of tissue rigidity via integrins was not made until 2007. Boris Hinz's group showed that myofibroblast activated latent TGFβ from the ECM via force of cell contraction in an integrin αV dependant manner. These experiments also showed that an intact cytoskeleton was required to produce enough force on the ECM to release the latent TGFβ bound to it. Figure 2.4 illustrates how TGFβ is activated by cell contraction. TGFβ activation was also dependant on the rigidity of the ECM, with less rigid matrices being less capable of releasing the active protein. This process also required that the latent TGFβ first be bound to the ECM via the LTBP (50).

This was the first indication that cells respond to tissue rigidity with TGFβ activation which results in mechanical signal transduction (mechanotransduction) *in vitro*.

That myofibroblasts activate TGFβ during contraction begs the question of how much force is required. Using single molecule force spectrometry and magnetic microbeads, the unfolding of the two LAPβ_1 domains surrounding the active TGFβ_1 was found to require ~40 picoNewtons (pN) of force. This force was only possible when TGFβ_1 was attached to LTBP and through it to the ECM. A single integrin is capable of generating force in the order of 40pN through cell contraction (114). Human airway epithelial cells are capable of producing sufficient contractile force to activate TGFβ in culture conditions without the differentiation to fibroblasts or myofibroblasts. Sphingosine-1-phosphate or LPA signaled through Rho kinase and non-muscle myosin to cause epithelial cells to contract and activate TGFβ in an αVβ6 integrin dependant manner (185, 186). Interestingly, TGFβ itself activates the Rho kinase pathway via non-Smad signal transduction and likely causes contraction on its own (73). In a study of TGFβ mediated collagen promoter response in cardiac fibroblasts, TGFβ was shown to activate a CCAAT binding factor CBF/NF-Y (187). TGFβ mediated contraction events could be yet another method by which cells continuously activate more TGFβ in a pathogenic positive feedback loop. Other agonists which stimulate cell contraction and are known to be upregulated in the context of IPF are thrombin, angiotensin-2 (AT-2) via angiotensin converting enzyme (ACE) upregulation, and endothelin-1 (ET-1) (188-190). Thrombin cleaves the protease activated receptor 1 (PAR1) receptor, a G-coupled protein cell membrane receptor, which induces intramolecular rearrangement in the cytoplasmic domain to begin signaling (191). PAR1 signals through Rho kinase pathway to induce cell contraction (50). Although PAR1 is more commonly researched with respect to thrombosis and platelet activation via thrombin, it is also expressed by lung fibroblasts. In the context of lung fibrosis, acute coagulation cascade mediator FXa activates thrombin to signal contraction of fibroblasts though αVβ5 and αVβ6 dependant manner (192-194). Endothelins are released from large precursors by endothelin converting enzyme. ET-1 is a powerful vasoconstrictive agonist produced mostly by the endothelium (195). ET-1 has a wide array of effects including contractility of smooth muscle and fibroblast cells (196, 197), mitogenic activity, and matrix metabolism which is critical for wound closure(103, 198). ET-1 induces myofibroblast phenotypes in lung fibroblast via activation of TGFβ. More recently, ET-1 was shown to

be capable of creating anoikis in fibroblasts independently of TGFβ, even though ET-1 expression is downstream of TGFβ signaling (199). AT-2 has some similarities to ET-1 as a potent vasoconstrictive agonist, cell mitogen and ECM maintenance (200, 201). ET-1 and AT-2 produce similar contraction in myofibroblasts to activate $TGF\beta_1$ (50).

A unique feature of the lungs is that they are under constant motion due to normal tidal ventilation. It could be that tidal ventilation itself is a stimulus for cell contraction via stretch dependent Ca^{2+} ion channels. Under normal circumstances Ca^{2+} channels such as transient receptor potential melastatin 7 (TRPM7) sense and transduce mechanical stresses and regulate lung epithelial cell volume (202). In the context of injury, TRPM7 mediated calcium 'flickers' at the leading edge of cells are used to induce movement in the desired direction. This helps epithelial cells to cover wound openings and for fibroblasts to enter into provisional ECM to aide in the functional ECM repair. In response to platelet derived growth factor (PDGF), a product downstream of TGFβ signaling (203), fibroblasts produced more asymmetric Ca^{2+} flickers and changed direction of travel (204). Subhendu Mukherjee *et al.* found that human lung fibroblasts respond to TGFβ with intracellular Ca^{2+} ion waves which cause contraction of the cells. Interfering with calcium handling at ryanodine channels or with endoplasmic reticulum based Ca^{2+} ion ATPase pumps caused a noted decrease in collagen and fibronectin expression in response to $TGF\beta_1$ (205). Since TGFβ activation requires ~40pN of force, which can be generated by a single integrin, it is likely that active TGFβ can cause contraction of cells which activates more TGFβ in the ECM. This represents yet another plausible positive TGFβ signal transduction feedback loop. If lung parenchymal cells contract in response to normal tidal pressure, it could be that elevated tidal pressure caused by lung fibrosis elevates cell contraction via TRPM7. It may be that TGFβ is activated during lung fibrogenesis due to the pressured tidal breathing effects at the whole organ level translated into cell contraction at the microscopic level.

In conclusion, there are many different mechanisms proposed over the past 15 years which could be responsible for the persistent activation of TGFβ required to generate a progressive fibrogenic program. Proposed mechanisms of positive TGFβ signal feedback include; gastric acid reflux, reactive oxygen species produced via NOX enzymes, and feedback from latent TGFβ cleavage by MMP2, 9, and MT-MMP. Under the hypothetical immune phase of fibrogenesis, lung macrophage and blood platelets can release latent TGFβ which is activated by plasmin at the cell surface in concert with TSP-

1 and CD36. The final proposed mechanism for generating a positive TGFβ signal feedback is via integrin αVβ(1, 5, 6, 8) mediated cell contraction against latent TGFβ bound to the ECM. This integrin dependent activation of TGFβ could be caused by contraction mediated by TGFβ itself though ryanodine and Ca^{2+} ATPase dependent mechanisms. All of the above mechanisms are likely to be involved in the pathogenesis of IPF but at varying stages of the disease. The final stage of disease which prompts the first clinical visit for IPF patients, involves mechanisms of TGFβ activation that must be identified if progress is to be made in designing anti-fibrogenic therapies. Currently a prominent mechanism of TGFβ activation, integrin dependent cell contraction activation represents a strong lead towards such a therapeutic drug. **We hypothesize that cell contraction, mechanical stretch, and lung ventilation in the context of abnormal scar tissue are stimuli which cause the persistent activation of TGFβ in animal models of lung fibrosis and these stimuli contribute to the persistent and progressive nature of IPF.**

3.0 Mechanical Force Dependant TGFβ Activation

3.1 Preamble

The activation of TGFβ is a prime focus for the discovery of pathways of intervention in the lung fibrotic disease process. Although many pathways have been found to contain plausible mechanisms by which TGFβ feeds forward to activate more TGFβ, mechanical activation has become prominent. In this chapter the mechanical activation of latent TGFβ is studied as it pertains to rodent models of lung fibrogenesis and in established IPF from biopsies. In order to study the effects of discrete amounts of force at the level of the TGFβ latent structure we designed and built a tissue bath equipped with a computer controlled servo-arm and force transducer. The design and specifications were adapted from the tissue bath used by Mara Ludwig's lab at McGill University, Montreal, QC. With these materials and models we asked the following questions of TGFβ activation in lung parenchymal tissue strips. Is the activation of TGFβ from fibrotic tissue related to duration or intensity of force of stimulation? Is mechanically liberated TGFβ dependent on the activity of serine proteases such as plasmin, thrombin, and MMPs? Is TGFβ activated from an artificially elevated latent TGFβ pool by mechanical means? Does mechanically activated TGFβ signal in the same tissue through the canonical Smad pathway under the TGFβ receptor? Does mechanically liberated TGFβ lead to downstream mRNA expression of early responder genes PAI1 and CTGF? Is TGFβ activation stimulated by force of contraction of cells by agonists such as ET-1 and AT-2? What are the effects on TGFβ activation when inhibiting ET-1 mediated contraction with the Rho kinase inhibitor Y-27632 (206)? Does the antioxidant NAC have an effect on the activation of mechanical TGFβ? Do αV integrins have an effect on mechanical TGFβ activation? Does force of ventilation activate TGFβ in fibrotic lungs by signaling through p-Smad2? And finally, is TGFβ activated mechanically in IPF tissue, signaling through the Smad pathway as in rodent models?

Investigation of the above questions represents the major bulk of this PhD thesis, the discussion and conclusions of which will be addressed in part in this text as well as in Chapter 8. Large portions of the results presented in this chapter are condensed in manuscript form for submission. Published or presented results include data pertaining to duration and intensity of TGFβ activation, p-Smad2 signaling, dependence on

protease activity, dependence on αV integrin activity, lung ventilation, and IPF tissue biopsies. All of the data presented in this chapter is the primary work of Aaron Froese. Technical help was provided by Jennifer Wattie (Department of Pathology and Molecular Medicine, McMaster University, ON) for all rodent ventilation experiments. The tissue bath was constructed by Bert Visheau (Health Research Services, McMaster University, Hamilton ON).

3.2 Methods Pertaining to Mechanical TGFβ Activation

Rat Lung Fibrosis Models

Female Sprague Dawley rats weighing 250g (Charles River, QC) were anaesthetized with isofluorane (Isoflo USP, Abbott Laboratories) with an Anesthetic Gas Vaporizer (Leica Microsystems Inc.) and given intratracheal instillations of recombinant A5 adenovirus expressing constitutively active porcine TGFβ1, latent porcine TGFβ1 or Delete control vector (30, 207) at $5x10^8$ pfu/rat in 200uL PBS (Lonza Group Ltd) and were sacrificed at Day 14 post instillation. All animal care was provided under the treatment guidelines of the Canadian Council of Animal Care. Rats given Ad latent porcine TGFβ1 were sacrificed at Day 7 for maximal tissue protein expression. Rats were sacrificed via CO_2 cull and lungs perfused with 10mL of sterile Krebs+ Bovine serum albumin (BSA) Buffer (NaCl (115.5 mM), KCl (4.6 mM), $NaHPO_4$ (1.2 mM), $MgSO_4$ (1.2 mM), $NaHCO_3$ (22 mM), D-glucose (11 mM), $CaCl_2$ (3.3 mM), BSA (0.125g/L), pH=7.4) into the pulmonary artery (Sigma Aldrich). Lungs were removed on block and cut transversely in 10x2x2 mm sections. Lungs strips were then placed in ice cold Krebs+BSA buffer prior to use in the 1D tissue bath.

1D Mechanical Stretch and Tissue Bath Model

A 1D horizontal tissue bath was constructed with dimensions 3x1x1cm. A force transducer and a servo-control arm were used in tandem with a digital controller interface (Models 400A, 322C, 604C, Aurora Scientific Inc.). Trimmed tissue strips were pasted to metal clips via ethyl 2-cyanoacrylate based adhesive (Electron Microscopy Sciences, Inc.) and attached to a hook on the force transducer and servo-arm in the tissue bath with the help of a dissecting microscope (Figure 3.1). Tissue strips were equilibrated in the bath for 26 minutes after which the tissue wash solution was taken following 4 minutes of resting incubation in the bath prior to mechanical stimulation. Mechanical stimuli were 0.1x resting length of the tissue in amplitude for 4-15 minutes and a bath sample was taken immediately afterward. Resting tension was set using a manual actuator controlling the stage upon which the servo controlled arm was mounted. Following stimulation, tissues were taken out of the bath and incubated in

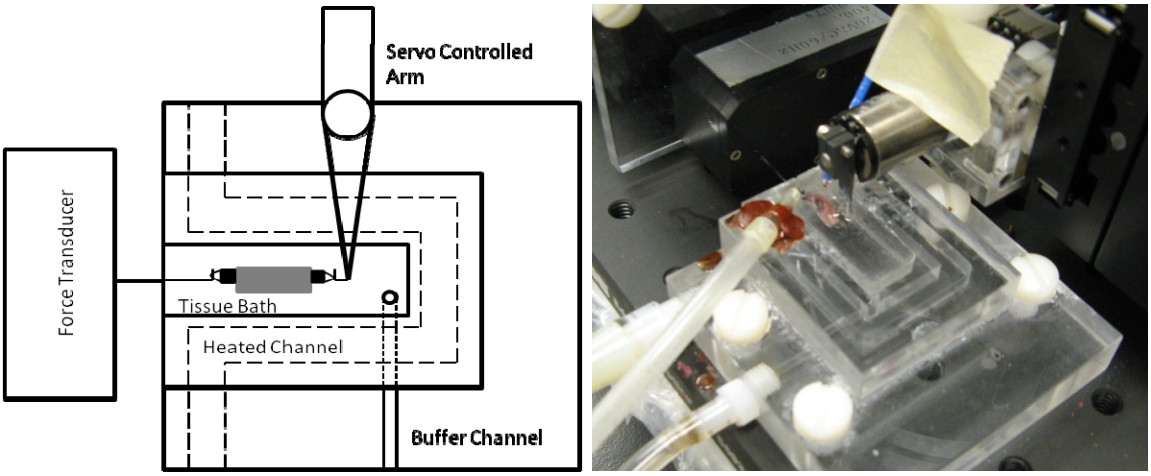

Figure 3.1. Top-down schematic (left) and graphic (right) representation of the *ex vivo* lung tissue bath model.

Krebs+BSA solution for 6 hours with the following: Complete EDTA-free Protease inhibitor cocktail (1X, Roche Diagnostics GmbH), TAME (1mM, Sigma-Aldrich Co.), GM6001 (60uM, EMD Millipore Inc.) Tissues strips were then frozen in liquid nitrogen and stored at -80˚C. To study the impact of antioxidants, N-acetyl cysteine (Cat# A7250, Sigma Aldrich, Inc.) was added to the tissue during the 30 minute wash phase prior to mechanical stimulation. Experiments with tissue contraction involving Endothelin-1 and Angiotensin-2 (Cat# H6995.0005 and Cat# H-1705.0025, Bachem California, Inc.) proceeded with 10uM ET-1 or 100uM AT-2 for 15 minutes. Y27632 Rho Kinase inhibitor

(Cat# 53-B85, Reagents Direct, Inc.) was added with the wash solution for the 30 minutes prior to ET-1 stimulation. In all cases tissue bath solution samples were taken directly after tissue stimulation for analysis via the PAI1/Luciferase cell reporter assay. All bath equipment was washed with distilled water to remove Krebs buffer following experimentation. No significant bacterial contaminations were ever discovered in tissue bath samples taken for the TGFβ reporter cell assay. Static tissue elastance was measured by reading the force one second before and one second after a length increase of 0.01 times the resting tissue length and analyzed as in Equation 1.0. The initial tissue tension for the static elastance test was set to 5mN.

Static Tissue Elastance (mN/cm) = $\frac{Force(2) - Force(1)}{Length(2) - Length\ (1)}$; (Equation 1.0)

TGFβ Reporter Cell Assay

The Mink lung epithelial cell assay with the PAI1/Luciferase construct (208) was used to determine biologically active TGFβ levels. Reporter cells were grown in Dulbeccos' Modified Eagle Medium (Lonza, Inc.) supplemented with 10% Fetal Bovine Serum, 2mM L-glutamine, 100 units/mL Penicillin, 100 ug/mL Streptomycin, and 250 ug/mL the antibiotic Geneticin (also called G-418) (Invitrogen, Inc.) and placed in an humidified tissue culture incubator at 37˚C with 5% CO_2 (HeraCell 240, Mandel Scientific Company Inc.). Media was renewed every 2 days or when splitting cells upon confluence into new flasks. Cells must be maintained in fresh Geneticin which is critical to maintain optimum TGFβ responsiveness. Media could not be used if it was more than 1 week old as Geneticin degrades gradually with time. Cells were split by first aspirating media and from the tissue culture plates followed by washing with sterile phosphate buffered saline (Lonza, Inc.). Phosphate buffered saline was removed and replaced by a small volume of 0.25% Trypsin and 0.05% Ethylene-diamine-tetra-acetic acid (Invitrogen, Inc.) in phosphate buffered saline (3mL for a 150 cm^2 plate). The cells were then placed in the incubator for 2 minutes to allow for the Trypsin and ethylene-diamine-tetra-acetic acid to remove all the cells from the plate. The 3mL of solution was washed across the plate with an automatic pipetter to loosen all of the cells into suspension. The 3mL cell suspension was then added to 7mL of normal media and placed in a 50mL centrifuge tube (Falcon, Fisher Scientific Inc.) then centrifuged (Allegra X-12R, Beckman Coulter Inc.) at 300 x g for 5 minutes to gently settle all the cells to the bottom. The cell pellet

was then resuspended in fresh media and plated in dilutions as needed. A 1 in 30 cell dilution attained confluence in 2-3 days and a 1 in 3 dilution reached confluence in the next day.

Bioassay for TGFβ activity was performed by harvesting cells to a concentration of $1.6x10^5$ cell/mL and plating them into a 96 well plate at 100uL per well. The outside wells of the 96 well plate were not used since these wells experience more evaporation overnight than the well further inside. Cells are washed after initial plating with Assay Medium containing a Dulbeccos' Modified Eagle Medium plus L-glutamine and 0.2% sterile Bovine Serum Albumin (A2934, Sigma Aldrich Inc.). Following pipetting into 96 well plates, reporter cells were left to attach for 3 hours in the incubator. Samples to be assayed were diluted 4X or (15X, 30X, 75X) in assay medium. A duplicate set of samples was made and heated activated to 80˚C for 5 minutes in order to detect Total TGFβ, which includes all soluble latent TGFβ in a sample. Recombinant human $TGF\beta_1$ (R+D systems, Inc.) was also mixed with Assay Medium and used as a reference standard. At 3 hours, the media was aspirated and washed with sterile phosphate buffered saline (Lonza, Inc.). The phosphate buffered saline was then aspirated and the diluted samples and references were added at 100uL per well. The assay was allowed to grow overnight in the incubator for 16 hours at which point the plates are removed. Luciferase assay lysis buffer (BD Monolight Luciferase 3X Cell Lysis Buffer, Becton Dickinson Company) was prepared by diluting 3X in sterile water. The assay medium was aspirated from the plates and 100uL of 1X lysis buffer was added per well. The assay plates were then spun in an orbital shaker (DS500 Orbital Shaker ,VWR Inc.) at 150 rpm for 30 minutes at room temperature. Luciferase luminescence substrate buffer was made by mixing the contents of Table 3.0. Samples and standards (45uL) were plated into an opaque luminescence plates for final analysis in a luminometer (Lumistar, BMG LabTech Inc.). The amount of substrate buffer added to each well was 110uL. The luminometer was set to read the emanating light at maximum sensitivity for 10 seconds, 2 seconds after substrate buffer addition. Raw luminescence data was converted to TGFβ in pg/mL through analysis of the standard curve. Biologically active TGFβ values were expressed as a percentage of active over total TGFβ or simply as active TGFβ in pg/mL.

When not in use, TGFβ reporter cells were frozen by first lifting the cells from their plates via Trypsin treatment and placing them in cold normal media supplemented with 10% dimethylsulphoxide. Vials of cold cells were placed in the -20˚C freezer for 1 hour and then placed in the -80˚C overnight. The cells were then placed in long term liquid nitrogen storage until needed. When needed again, cells were thawed rapidly by taking them from the liquid nitrogen storage and resuspending them in normal 37˚C media followed by centrifugation at 300 x g. Cell pellets were washed in fresh media to remove the dimethylsulphoxide and placed in new sterile flasks. Approximately 1 million cells were plated into a 75cm^2 plate and placed into the incubator at 37˚C. The following two mornings afterwards, the new cultures were washed with fresh media to remove dead cells.

Table 3.0 Luciferase Luminescence Substrate Buffer		
Reagent Name	Final Concentration	Reagent Source
Tricine	20 mM, pH=7.8	Cat# T9784, Sigma Aldrich Inc.
$Mg(CO)_3Mg(OH)_2 \bullet 5H_2O$	10 mM	Cat# 227668, Sigma Aldrich Inc.
Dithiothreitol (DTT)	33.3 mM	Cat# DTT001, Bioshop Inc.
D-Luciferin	800 uM	Cat# L9504, Sigma Aldrich Inc.
Adenosine Triphosphate	750 uM	Cat# A3377, Sigma Aldrich Inc.
10mL of Substrate Buffer was sufficient to run one 96 well plate in the luminometer. All reagent were stored as concentrated stocks in a freezer at -20˚C.		

Homogenization

Frozen lung strips were homogenized with a TH homogenizer (OMNI International, Kennesaw GA) in a volume (10X the mass of the sample, eg. 25mg tissue → 250uL) of plasma membrane lysis buffer (HEPES (10mM), KCl (10mM), pH 7.9). IGEPAL detergent was added to the samples to a final concentration of 1% (v/v) and vortexed for 10 seconds. Samples were then spun down at 18000 x g for 15 minutes at 4˚C. The supernatants were then removed and the pellets resuspended in RIPA buffer (IGEPAL (1% v/v), Sodium Deoxycholate (1% w/v), SDS (0.1% w/v), NaCl (150mM), Na_3PO_4 (10mM), pH 7.2). Resuspended pellets containing nuclei were then vortexed for 15 seconds and again after 10 minutes. Samples were kept on ice at all times following homogenization and promptly frozen at -70˚C in several aliquots. Both plasma membrane lysis and RIPA buffers contained protease and phosphatase inhibitors (PMSF

(1mM) (Sigma Aldrich Inc.), Roche Complete Protease Inhibitor Cocktail (1X) (Roche, Inc.), NaF (1mM), Na_3VO_4 (1mM)) (Sigma Aldrich, Inc.).

Western Blotting

Western blotting for phospho-Smad2, α-tubulin, and phospho-Smad3 was performed using a 10% polyacrylamide gel electrophoresis. Table 3.1 shows the ingredients and protocol for assemble of the polyacrylamide gel. The resolving gels were produced first in a 50mL centrifuge tube (Becton Dickinson, Inc.). The stacking gels were mixed at the same time in a separate 15 mL tube (Becton Dickinson, Inc.). Tetramethylethylenediamine crosslinking agents were added after the Western gel apparatus (Mini Protean Tetra Cell, BioRad Inc.) was prepared for loading. After the resolving gels were added, a thin layer of isopropanol (Caledon Laboratories Ltd.) was added to keep the gel surface from forming a curved meniscus. After 15 minutes the gel is hardened and the isopropanol were removed so that the gel surface can be dried with paper towels. The stacking gel is then added on top of the resolving gel with a 15 well comb provided in the Mini Protean Kit (BioRad Inc.). After 15 minutes the hardened gel can be placed into the Mini Protean Gel Apparatus for tissue homogenate loading.

Table 3.1 Polyacrylamide Gel Synthesis List		
Resolving Gel (30 mL)		
Distilled Water	11.8 mL	Produced from an Elix Water Purification System, Millipore Inc.
30% Acrylamide:Bisacrylamide (29:1)	10 mL	Cat# ACR002.5, BIS001, Bioshop Inc.
1.5 M Tris, pH 8.8	7.6 mL	Cat# TRS001.5, Bioshop Inc.
10% Sodium Dodecyl Sulfate	300 uL	Cat# 161-0416, BioRad Labs Inc.
10% Ammonium Persulfate	300 uL	Cat# AMP001, Bioshop Inc.
Tetramethylethylenediamine (added to mixture to begin crosslinking)	30 uL	Cat# 161-0801, BioRad Labs Inc.

Stacking Gel (9 mL)		
Distilled Water	4.8 mL	Produced from an Elix Water Purification System, Millipore Inc.

30% Acrylamide:Bisacrylamide (29:1)	1 mL	Cat# ACR002.5, Cat# BIS001, Bioshop Inc.
0.5 M Tris, pH 6.8	2 mL	Cat# TRS001.5, Bioshop Inc.
10% Sodium Dodecyl Sulfate	100 uL	Cat# 161-0416, BioRad Labs Inc.
10% Ammonium Persulfate	100 uL	Cat# AMP001, Bioshop Inc.
Tetramethylethylenediamine (added to mixture to begin crosslinking)	12 uL	Cat# 161-0801, BioRad Labs Inc.

Tissue homogenate samples (20 uL) were placed in 200uL PCR tubes (Diamed Inc.) with 5uL of 5x Reducing buffer concentrate (0.313 M Tris = pH 6.8, 10% sodium dodecyl sulfate, 0.05% bromophenol blue, 50% glycerol, 2.5% β-mercaptoethanol). The tissue homogenate samples were then heated to 90˚C for 5 minutes to remove intramolecular protein disulfide bonds via the β-mercaptoethanol reducing reaction. The tubes were then cooled and briefly spun down to collect condensates before loading into the polyacrylamide gels. The Mini Protean Gel apparatus was submerged in Tris/Glycine/SDS Running buffer (Cat# 161-073, BioRad Inc.) and connected to the Electrophoresis power pack (Power Pac Basic, BioRad Inc.) and set to run at 90 Volts for 2 hours. This voltage and duration allows for adequate separation of protein components for p-Smad2 and α-tubulin. After 2 hours the gel proteins were transferred onto polyvinylidene fluoride membrane (Biotrace PVDF transfer membrane, Pall Corporation) for 2 hours using the same Mini Protean Kit submerged in Tris/Glycine buffer (Cat# 161-0734, BioRad Inc.) supplemented with 20% methanol (Caledon Laboratories Ltd). The amperage of the protein transfer apparatus was held constant at 270 mA and the voltage was allowed to vary.

After 2 hours the polyvinylidene fluoride membranes were trimmed and placed into Western washing buffer (part of Q-Dot 625 Western Blotting Kit, Invitrogen Inc.). Rinsing membranes involves washing in western washing buffer for 5 minutes with 3 changes of buffer solution. The blocking buffer was added to the membrane with shaking on a rocking shaker (Rocking Platform, VWR Inc.) at room temperature for 1 hour. The first antibody used was Rabbit anti-Phospho-Smad2 (Cat. #3101, Cell Signaling Technology, Inc.) which was placed in wash buffer at a concentration of 1:2000. Incubation of western membranes in primary antibody was done on an orbital shaker (DS500 Orbital Shaker, VWR Inc.) over night at 4˚C. The membrane was then

rinsed and the secondary biotinylated anti-Rabbit IgG antibody was added at a concentration of 1:2000 in washing buffer. Secondary antibody was incubated with the membrane for 1 hour with rocking at room temperature. The secondary antibody solution was then removed and the membrane rinsed again. Finally, the streptavidin labeled QDot 625 reagent was added to the membrane at a concentration of 1:2000 in the supplied blocking buffer. The QDot 625 reagent was allowed to bind to the secondary antibody for 30 minutes at room temperature with rocking. The reagents were then washed off and the membrane was read in a ChemiDoc XRS Imaging System (Bio-Rad Laboratories, Inc.). Densitometry measurements were performed with ChemiDoc XRS Imaging System Software and were normalized to a control sample when studies required more than one blot.

After the initial protein was assayed in the imaging system, the membranes were placed in 5mL of Restore Western Blot Striping buffer solution (Cat# 21062, Thermo Scientific Inc.) for 25 minutes at room temperature with rocking. This removes the antibodies from the membrane for further analysis of other proteins.

Rabbit anti-Phospho-Smad3 and Rabbit anti-α-tubulin (Cat. #9520, Cat. #2144, Cell Signaling Technology, Inc.) were used to assay rat p-Smad3 and human and rat α-tubulin respectively. P-Smad3 and α-tubulin antibodies were detected using an anti-rabbit IgG linked to horseradish peroxidase (Cat. #7074, Cell Signaling Technology, Inc.) secondary reagents instead of more costly QDot reagents. Both p-Smad2 and α-tubulin antibodies were also used for human sample western blotting. The protocol was the same as above except that blocking and antibody solutions contained 5% milk powder (Carnation fat-free skim milk powder, Smucker Foods of Canada Corp.) in washing buffer. The anti-p-Smad3 and anti-α-tubulin antibodies were both used at 1:2000 concentration for primary incubation. Following anti-Rabbit HRP incubation for 30 minutes at room temperature, the membranes were washed. The chemiluminescence reagent (ECL, GE Healthcare Ltd.) was added and allowed to incubate with on the membrane for 1 minute before being read in a ChemiDoc XRS Imaging System (Bio-Rad Laboratories, Inc.). Again, densitometry measurements were performed with ChemiDoc XRS Imaging System Software and were normalized to a control sample when studies required more than one blot.

RNA isolation

RNA isolation was performed with an UltraClean Tissue and Cells RNA Isolation Kit (Mo Bio Laboratories). The tissue was first homogenized in the provided kit buffer using the TH homogenizer. The homogenate was then treated with a second kit buffer solution and then placed into the RNA isolation microcentrifuge filter. As the filter was spun down, the RNA remains bound to the filter column. On column RNA was then washed twice with 70% ethanol followed centrifugation to remove ethanol. The dried columns are then eluted with ribonuclease free water.

cDNA Production

cDNA was then prepared from isolated RNA solution using the First Strand RT Kit (Invitrogen, Inc.). Briefly, RNA was quantified using a NanoDrop ND-1000 spectrophotometer (Thermo Fisher Scientific Inc.). This method quantifies RNA by its UV absorption spectra reading and the Beer Lambert Law. The extinction coefficient for ssRNA at 260nm was 0.025 $(ug/ml)^{-1}$ cm^{-1} which yields ug quantities of pure RNA upon reading at 260nm. 1 ug of RNA per sample was taken and place in solution with 1uL of 10X DNAse I buffer, 1 unit of DNAse I enzyme (Invitrogen, Inc.) and water to a final volume of 10uL. This removes all trace DNA contaminants from the RNA sample prior to cDNA creation. DNase I reaction mixture was incubated at room temperature for 15 minutes followed by enzyme inactivation with 1uL of 25mM EDTA and heating to 65˚C. Next 50ng of synthetic random hexamer DNA primers are added to the mixture as well as 1uL of a 10mM dNTP mixture (containing all nucleotides in equal concentration). This reaction was heated to 65˚C for 5 minutes to anneal the DNA primers to the RNA. After this the First Strand buffer is added 4uL of 5X solution, 2uL of 25mM Mg_2Cl_2 as an enzyme and dNTP cofactor, 2uL of 0.1M DTT as an anti-oxidant, 2uL of 40 units/uL RNAse Out reagent which inhibits ribonucleases, 2uL of 200U/uL Superscript reverse transcriptase enzyme (Invitrogen, Inc.). Water was added to a total volume of 20uL. The following reaction cycle was performed 10 minutes at 25˚C, followed by 50 minutes at 50˚C, followed by 5 minutes at 85˚C using a Mastercycler gradient polymerase chain reaction (PCR) machine (Eppendorf, AG, Hamburg, Germany). Finally, 1 uL of 200U/uL RNAse H which degrades left over RNA was added to the reaction and incubated at 37˚C for 20 minutes. The cDNA from this reaction was stored at -20˚C until Real Time Polymerase Chain Reaction procedure.

RT-PCR Analysis

Real Time PCR was performed with the 7500 Fast Real-Time (RT) PCR system (Applied Biosystems, Inc.). Taqman 2X RT-PCR master mix at 10uL was used with 1uL of the following 20X Taqman cDNA Gene Probes: 18S Euk rRNA Part# 4352930E, β-2-Microglobulin (β2M) Part# Rn00560865_m1, PAI1 Cat# Rn00695641_m1, CTGF Rn00573960_g1 (Applied Biosystems, Inc.). cDNA preparations were diluted 1/6 in water and 5uL per sample was added to each Taqman reaction well. Each sample was assayed in duplicate. The PCR reaction cycle was performed according to the manufacturer's automated protocols for comparative ddCT analysis. Cycle threshold (CT) value refers to the cycle when the baseline probe signal threshold was exceeded and depends directly on the amount of initial cDNA template. The algorithm for the calculation of the CT value was a proprietary secret. Data in CT mean values for each gene (PAI1, CTGF) was analyzed with respect to housekeeping genes (β2M, 18S). Equation 1.0 shows how absolute gene expression values were calculated.

$$Abs.expression = 2^{-(Gene\ CTvalue - Housekeeping\ Gene\ CTvalue)}$$; (Equation 2.0)

Each data point was expressed as fold increase over the average absolution expression of the control group or first time point group samples.

Rodent Lung Ventilator Model

Rats were treated with Adenovirus as above. On Day 14, a half hour prior to sacrifice, the rats were given 1000U/kg Sodium Heparin as an intraperitoneal injection and then sacrificed via CO_2 cull 30 minutes later. The lungs were intubated and extracted carefully to avoid puncture and the pulmonary artery catheterized. The lungs were then floated in a tissue bath of phosphate buffered saline held at 37˚C and connected to a FlexiVent rodent ventilator (SciReq Inc., QC). The pulmonary artery catheter was connected to a Krebs+ BSA buffer solution held 30 cm above the lung tissue (Figure 3.2). Lungs were ventilated with a tidal pressure of 5 cmH_2O for 20 minutes as a control treatment. After removing the left lobes, the right lobes were given a ventilation challenge of a total lung capacity measurement every 20 seconds for 20 minutes. Elastance measurements during ventilation were made with the FlexiVent SnapShot-90 physiologic properties test. Lungs were then cut into 2 mm wide transverse sections

and incubated in Krebs+ BSA buffer including protease inhibitors for 6 hours. Lungs strips were then frozen in liquid nitrogen and stored at -80˚C.

Human Lung Tissue Experiments

All tissue was collected with patient and family consent in compliance with the Research Ethics Board of McMaster University. Control lung tissue was collected from patients undergoing biopsy for cancer diagnosis. Lung fibrosis tissue was collected from patients undergoing biopsy for the diagnosis of usual interstitial pneumonia or non-specific interstitial pneumonia. Following biopsy, all tissue was stored in RPMI cell culture media for 1.5 hours. In preparation for analysis in the 1D tissue bath apparatus, the tissue was washed in cold Krebs+ BSA and sectioned into 10x2x2 mm strips.

Figure 3.2. Image of rodent ventilator model. The lungs were suspended in PBS held at 37˚C. The pulmonary artery was perfused with Krebs + BSA buffer held 30 cm above the tissue.

Statistical Analysis

All data were expressed as a mean +/- standard deviation unless otherwise noted in the text. Statistical analysis between two groups was performed using a non-parametric Student's t test. Statistical analysis between multiple groups with one control group was performed by a one way ANOVA test, with Dunnett's multiple comparison test (post hoc). Analysis was performed with GraphPad Prism 5.0 (GraphPad Software Inc.), in all cases a p-value less than 0.05 was considered significant.

3.3 Results of Mechanical TGFβ Activation Experiments

Mechanical activation of TGFβ in fibrotic rat lung tissue

In order to study the effects of mechanical stimuli on lung parenchymal tissue we developed a tissue bath model which would allow for precise measurement and production of tensile force. To that end we placed a sensitive force transducer and a servo controlled arm oriented horizontally in a tissue bath (Figure 3.1). We modeled the tension of breathing in the tissue bath by setting the resting tissue tension to 15mN and cyclically stretching the lung strip with a length change of 10% of the resting tissue length. We asked the question of whether TGFβ is activated by cyclic stretch in this tissue bath model during active fibrogenesis in the rat at day 14 post-Ad active TGFβ. Note that Ad-driven transgenic active TGFβ expression ends around day 9, making this model an analysis of endogenous rat TGFβ activation at day 14. We compared the tissue bath wash solution 4 minutes before stimulation and 4 minutes afterward.

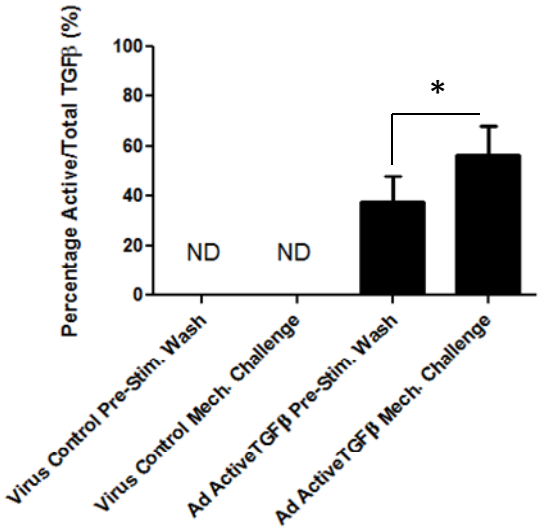

Figure 3.3. Activation of TGFβ in rat fibrotic lung strips following mechanical stimulation in a tissue bath. PAI/Luciferase reporter assay data expressed as a percentage of active over total TGFβ. Data is averaged from lung strips given between 5 and 15 mN of tensile force for 4 minutes. N= 48 with 6 separate experiments with a mean difference of 19.2% ± 4% (SEM), * p<0.05.

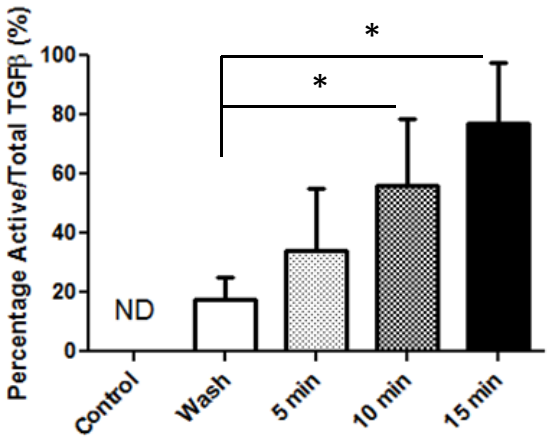

Figure 3.4. Activation of TGFβ in rat fibrotic lung strips with respect to duration of mechanical stimulation in a tissue bath. Individual lung strips were given three different timed treatments at 5mN initial tension in serial succession. Data is a representative of at least 3 separate experiments. Means +/- SD. N=5 strips, ANOVA tested significant difference p<0.05, with Dunnet's post hoc significant difference * p<0.05 between wash and both 10 and 15 minute groups.

These solutions were tested using the TGFβ cell reporter assay. Figure 3.3 shows a significant increase in the percentage of active to total TGFβ. Percentage TGFβ activity

normalization was required due to the "patchy" nature of lung fibrosis models and the high degree of variability between sample slices. Each tissue slice has a unique amount of ongoing fibrogenesis and its own variable ability to respond to tensile force. Virus control tissue did not respond to mechanical stimuli by releasing detectable TGFβ levels. The bath solution analysis, taken directly following mechanical stimulation, does not allow enough time for tissue expression of the TGFβ gene. These data indicate that TGFβ is activated in a post-translation modification event from resting ECM stores in a manner that is tensile force dependant and also independent of circulating blood cell factors which have been washed away during pulmonary artery perfusion. Virus control experiment data strongly highlight the role of mechanical TGFβ activation during a fibrogenic pathobiological state.

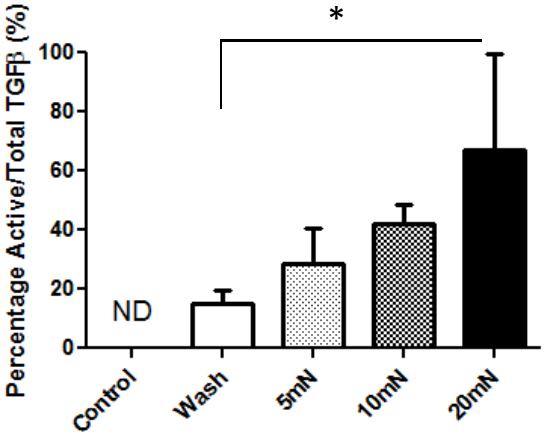

Figure 3.5. Activation of TGFβ in rat fibrotic lung strips with respect to tensile force in a tissue bath. Individual lung strips were given three different tensile treatments from 5mN to 20mN in serial succession. Data is a representative of at least 3 separate experiments. Means +/- SD. N=5 strips, one way ANOVA tested significant difference $p<0.05$, with Dunnet's post hoc significant difference * $p<0.05$ between wash and 20 mN groups.

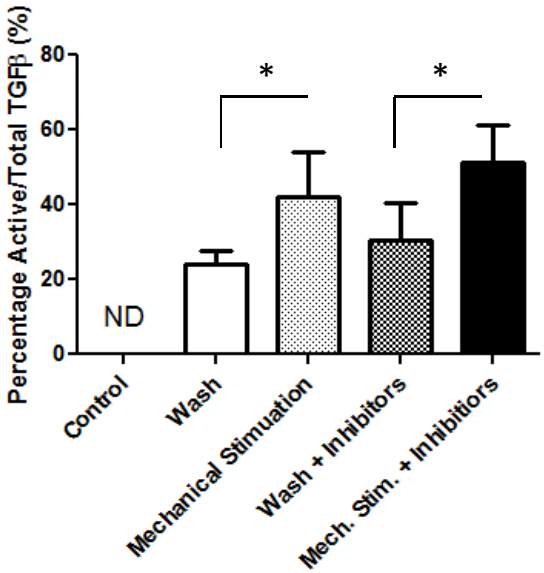

Figure 3.6. Activation of TGFβ from rat fibrotic lung strips with contrast to protease inhibitors cocktail treatment. Individual lung strips were challenged twice, once without pan-protease inhibitor cocktail + 1mM TAME + 60uM GM6001. Data is a representative of at least 3 separate experiments. Means +/- SD. N=5 strips, t-test significance difference of * $p<0.05$ between the following groups: wash to mech. stim., wash + inhibitors to mech. stim. + inhibitors.

Next we asked whether the duration of stretch impacted the activation of TGFβ from fibrotic tissue. Figure 3.4 shows that as the duration of stretch increases, the

percentage of active/total TGFβ released from the sample increase as well. Afterwards, we asked whether increasing the initial tensile force, while holding the stimulus time constant, activates increasing amounts of TGFβ. Figure 3.5 shows that as the initial applied tension increases, the percentage of TGFβ released significantly increases in response. These data indicate that mechanotransduction of TGFβ activation is a real time response to varying tissue tension both in respect to duration and amplitude of stimulus.

Next we asked whether serine protease and MMPs were a major component to the mechanical activation of TGFβ during fibrogenesis. In order to study the effects of proteases in context of this 1D tissue bath stretch model, we employed pan-protease inhibitors and pan-MMP blockers. Figure 3.6 shows that an equivalent amount of TGFβ is released from tissue with or without the presence these inhibitors following two serial challenges with differing tissue bath conditions. These results indicate that the lung scars are activating TGFβ in a method that could not be explained by serine protease or MMP activity.

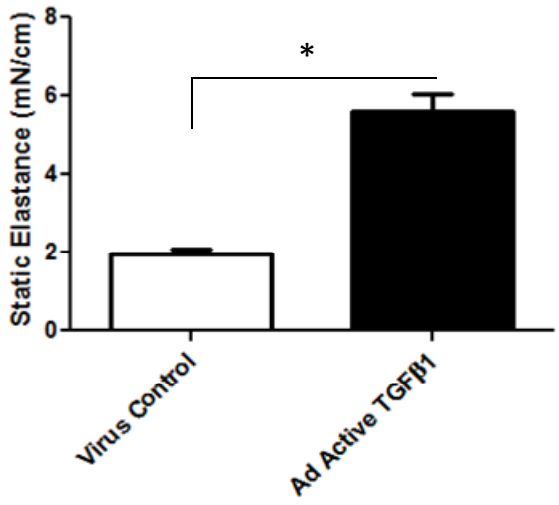

Figure 3.7. One dimensional static elastance of rat lungs strips used in the tissue bath model. Data is averaged together from least 4 separate experiments of at least 6 strips each. Means +/- SEM with * $p < 0.05$.

In has been noted in the past that the rigidity of the matrix on which cells grow affects their ability to activate TGFβ in response to contractile agonists or mechanical force (50). Although the stiffness of fibrotic lung slices did significantly increase over control slices (Figure 3.7), we found that there was no correlation between the static elastance of individual strips and their ability to activate TGFβ (data not shown). This suggests that the general stiffness of the lungs is not as critical to mechanical TGFβ activation as was previously suspected from in vitro studies.

TGFβ signaling events following mechanical stimulation

Past studies have indicated that TGFβ signals through the Smad2/3 pathway, and that this pathway is critical to the main fibrogenic process (29). We asked whether the rat fibrotic lung strips respond to mechanically activated TGFβ with downstream phosphorylated Smad2 activity. We performed standard western blotting techniques with homogenized nuclear fractions of stimulated and non-stimulated tissue. At 6 hours

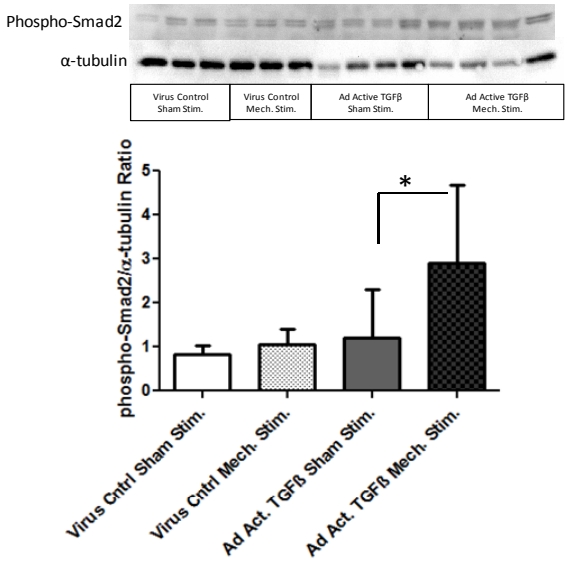

Figure 3.8. Phosphorylated Smad2 activity of rat fibrotic lungs 6 hours following mechanical stimulation at 15 mN for 4 minutes. Tissue was homogenized and nuclear fractions were used. This data is expressed with respect to α-tubulin loading control. This densiometric data is representative of at least 3 separate experiments. N=7 per group with TGFβ sham and challenge groups reaching significant difference, * p<0.05.

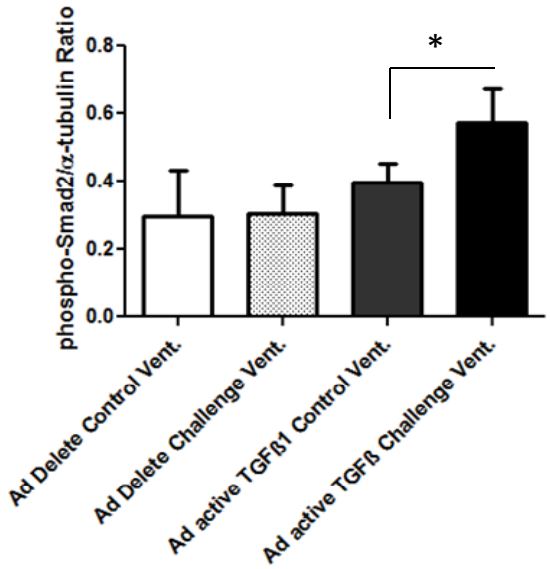

Figure 3.9. Phosphorylated Smad2 activity of rat fibrotic lungs 6 hours following mechanical ventilation. Tissue was homogenized and nuclear fractions were used. This data is expressed with respect to α-tubulin loading control. This densiometric data is cumulative with at least 3 separate experiments per virus group. Means +/- SEM with TGFβ control and challenge ventilation groups reaching significant difference, * p<0.05.

following mechanical stimuli the levels of p-Smad2 are significantly elevated in challenged tissue over controls (Figure 3.8). These data strongly suggest that the active TGFβ released during mechanical stretch are affecting the tissue itself.

Smad2 signaling in mechanically ventilated fibrotic rat lungs

The tissue bath model we developed is elegant in its ability to ask mechanistic questions concerning the mechanotransduction of TGFβ during fibrogenesis. However, this model lacks clear correlation to the clinical setting. To address this concern, we asked the question; do lungs undergoing fibrogenesis respond to mechanical ventilation by activating phosphorylated Smad2. To answer this question we gave rats Ad active TGFβ1 or control virus and removed the lungs at day 14 and placed them on a rodent ventilator (Figure 3.2). The lungs were suspended in a solution of PBS, held at 37˚C, and were perfused through the pulmonary artery with Krebs Buffer at 30 cmH_2O pressure. The lungs were then ventilated at a resting/control pressure of 5 cmH_2O for 20 minutes. After the control ventilation the left lung lobes were tied off by suture thread and removed. The remaining lobes then received base line ventilation with the added challenge of a measurement of total lung capacity every 20 seconds for 20

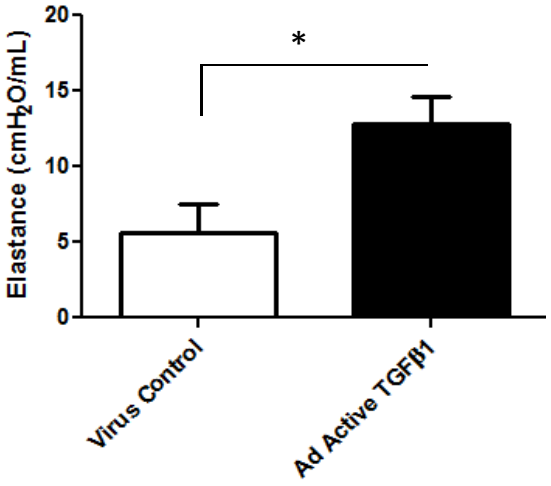

Figure 3.10. Ventilation model elastance of fibrotic and control rat lungs taken out of the chest cavity. Data is averaged from 3 separate experiments. Means +/- SEM with * $p < 0.05$.

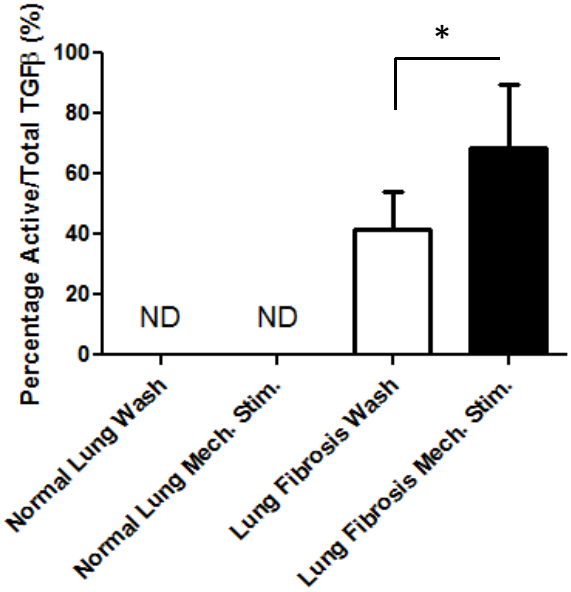

Figure 3.11. Activation of TGFβ in human fibrotic lung strips following mechanical stimulation in a tissue bath. PAI/Luciferase reporter assay data expressed as a percentage of active over total TGFβ. Number of separate experiments (UIP = 2, NSIP = 1, Control = 2). Data from NSIP and UIP were grouped together. Mean +/- SD with lung fibrosis wash and mechanical stimulation groups reaching significant difference, * $p<0.05$.

minutes. Each total lung capacity measurement lasted 6 seconds and reached a final pressure between 25 and 30 cmH_2O. The challenged and control lungs were, following removal, cut into slices and incubated in Krebs buffer at 37˚C in the presence of protease inhibitors for 6 hours. After 6 hours the lungs were frozen and stored for analysis of phosphorylated Smad2 activity. Figure 3.9 shows that there is a significant increase in phosphorylated Smad 2 activity in fibrotic lungs in comparison to control lung ventilation. We also noted a significant increase in the whole organ elastance of fibrotic lungs in comparison to virus control specimens (Figure 3.10). These data highlight the clinical relevance of TGFβ mechanotransduction findings for UIP or ARDS patients undergoing lengthy higher pressured ventilation. More ventilation pressure will activate TGFβ and should worsen the fibrogenic pathogenesis through the effects of phosphorylated Smad2.

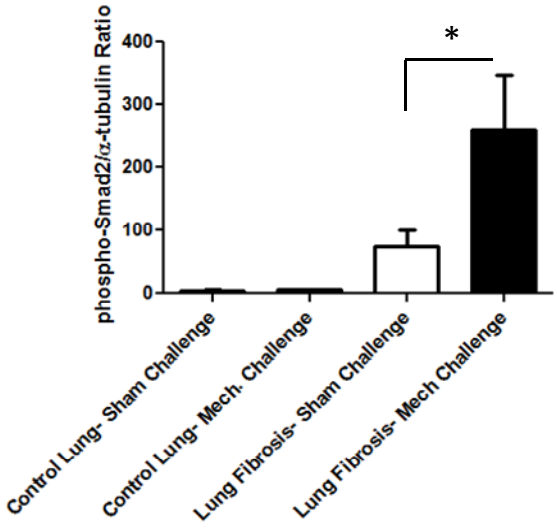

Figure 3.12. Phosphorylated Smad2 activity of human fibrotic lung biopsy tissue 6 hours following mechanical stimuli in a tissue bath. Tissue was homogenized and nuclear fractions were used. This data is expressed with respect to α-tubulin loading control. Number of separate experiments (UIP = 2, NSIP = 1, Control = 2). Data from NSIP and UIP were grouped together. Mean +/- SD with lung fibrosis wash and mechanical stimulation groups reaching significant difference, * $p<0.05$.

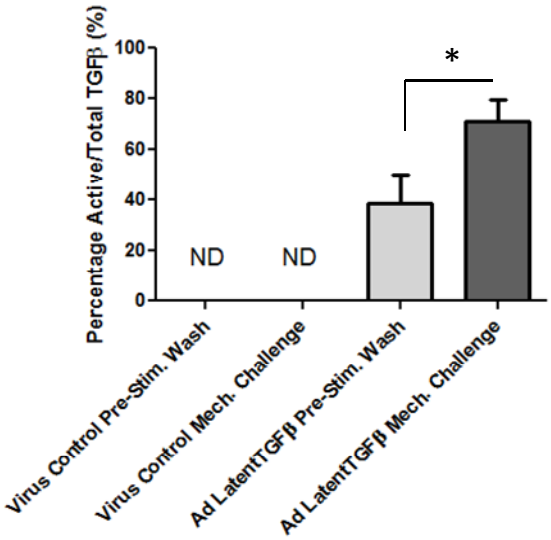

Figure 3.13. Activation of TGFβ in latent TGFβ overexpressing rat lung strips following mechanical stimulation in a tissue bath. PAI/Luciferase reporter assay data expressed as a percentage of active over total TGFβ. Data is averaged from lung strips given 15 mN of tensile force for 4 minutes. N= 7 with 3 separate experiments with a mean difference of 32.3%, * $p<0.05$.

TGFβ mechanotransduction in human pulmonary fibrosis biopsies

Human lung fibrogenesis, as noted in IPF, is a process that occurs sub-clinically over many years. It may be that rat fibrogenesis, initiated by Ad active TGFβ1, misrepresents the true human disease process with respect to TGFβ mechanotransduction. To address these concerns we collected human pulmonary fibrosis biopsy specimens and control lungs and studied them in the tissue bath model. Figure 3.11 shows that human lung fibrosis parenchymal strips release active TGFβ in a similar manner to the rat model data. Also of significance, the human control lungs did not release detectable quantities of TGFβ following stimulation. Next we asked if the TGFβ activated during mechanical stretch signals through Smad2 in human pulmonary fibrosis tissue. Figure 3.12 shows that 6 hours following mechanical stimulation, phosphorylated Smad2 is found in tissue homogenate nuclear fractions. We noted that phosphorylated Smad2 levels in established lung fibrosis were at least an order of magnitude higher than the rat lung fibrosis model. Also, control lung tissue did not respond to mechanical stimuli with a significant increase in phosphorylated Smad2. These data indicate that TGFβ is released following mechanical stimulation in human lung fibrosis tissue in a manner that is similar to the rat model and underscores that the mechanical activation of TGFβ is specific to a pathobiological wound healing state through the phosphorylation of Smad2.

Mechanical TGFβ activation in a latent TGFβ overexpression model

When first assayed, Adenovirus mediated overexpression of latent TGFβ_1 did not lead to any significant fibrotic changes to rat lung tissue on histological examination. Even though large quantities of total TGFβ could be detected in the lung homogenates of these animals, the TGFβ needed to be activated to have its tissue effects (30). We asked the question if latent TGFβ produced in abundance in the lung parenchyma could yield the same mechanotransduction as seen in the Ad active TGFβ_1 model but in the absence of tissue damage and fibrosis. Rats were sacrificed on Day 7 and subject to the same mechanical stretch as in the fibrotic models. Latent TGFβ overexpressing rats produced significantly more percentage active/total TGFβ upon tissue stretch than in the wash solution (Figure 3.13). Static elastance was found to be increased on average by 1.1mN/cm for latent TGFβ overexpressing lungs (Figure 3.14). This indicates that these lungs still underwent a slight but statistically significant change in architecture even

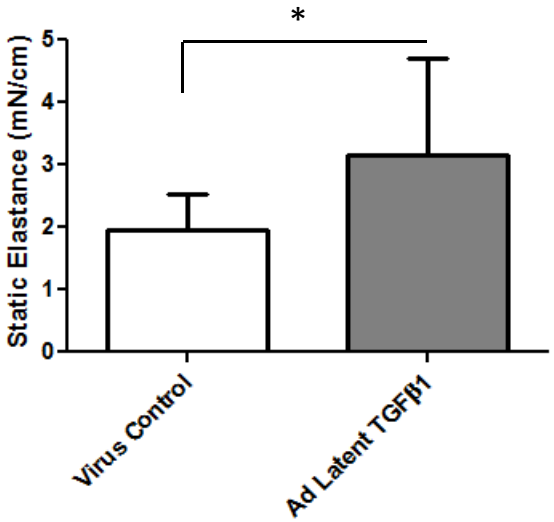

Figure 3.14. Static elastance for latent TGFβ overexpressing rats at Day 7. Data collected from at least 3 separate experiments with a mean difference of 1.1mN/cm, * $p < 0.05$.

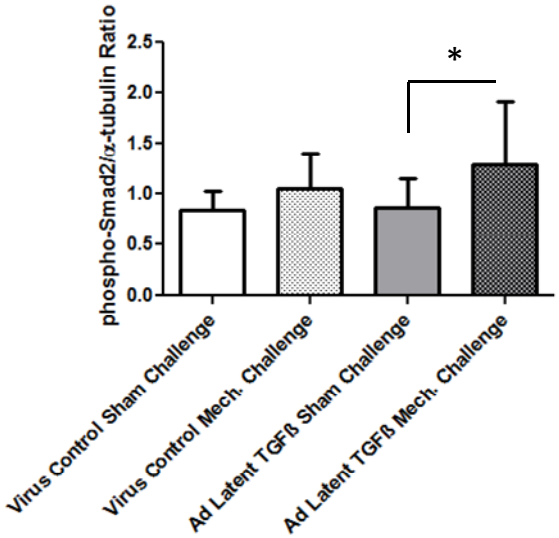

Figure 3.15. Phosphorylated Smad2 activity of latent TGFβ overexpressing lungs 6 hours following mechanical stimulation. Tissue was homogenized and nuclear fractions were used. This data is expressed with respect to α-tubulin loading control. This densiometric data is representative of at least 3 separate experiments. N=7 per group with TGFβ sham and challenge groups reaching significant difference, * $p < 0.05$.

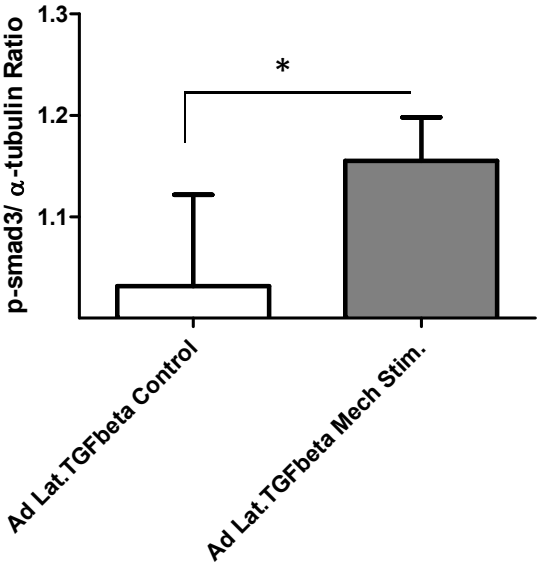

Figure 3.16. Western densitometry of p-Smad3 over α-tubulin of latent TGFβ overexpressing lungs. Lungs were stimulated with between 5 and 15 mN of force for 4 minutes followed by 6 hours of incubation at 37˚C. Representative blot is shown of 3 separate experiments. Means with standard deviation, N=4 per group with statistically significant difference of * $p < 0.05$. Virus control groups were not analyzed within these experiments.

though no differences could be detected by standard histological analysis or

hydroxyproline collagen quantification (30). Smad2 phosphorylation was also increased in the same tissue after 6 hours of incubation at 37˚C (Figure 3.15). p-Smad3 was also found to be elevated with respect to untreated controls (Figure 3.16). These data together indicate that when present in high abundance, latent TGFβ will undergo some mechanotransduction to the nucleus with p-Smad2 signaling. Signaling of the

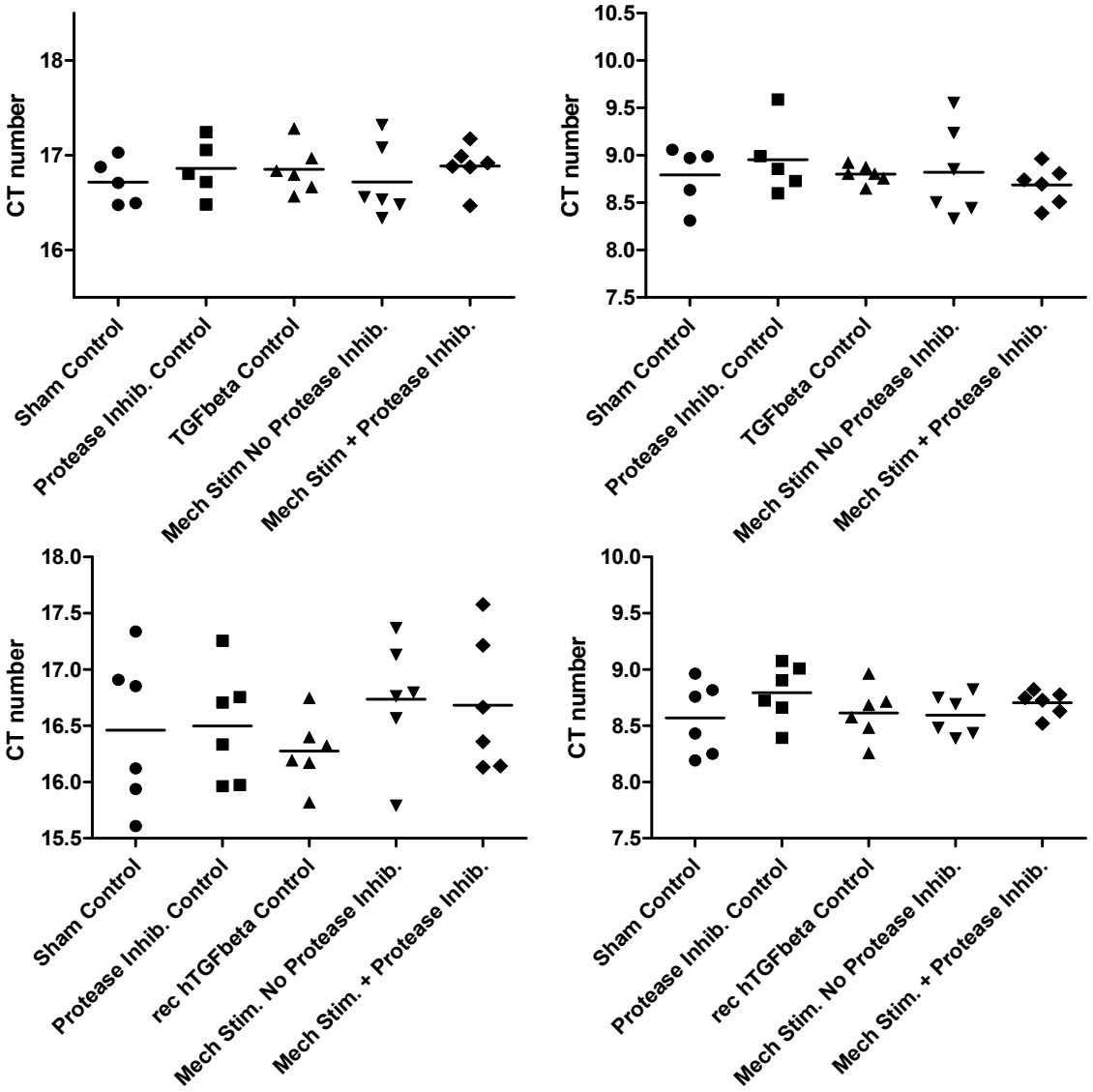

Figure 3.17. RT-PCR analyzed mRNA expression of house keeping genes β-2-microglobulin (left) and 18S (right). In two separate experiments (top and bottom) which both received Ad latent $TGF\beta_1$ and were sacrificed at Day 7.

Smad2/3/4 complex into the nucleus would activate early responder genes plasminogen

activator inhibitor (PAI1) and connective tissue growth factor (CTGF) with respect to housekeeping genes 18S and β-2-microglobulin. In order to test whether mechanical TGFβ signaling activated mRNA expression of these early responder genes, real time PCR analysis was performed on rat tissue overexpressing latent $TGF\beta_1$ at Day 7. Figure 3.17

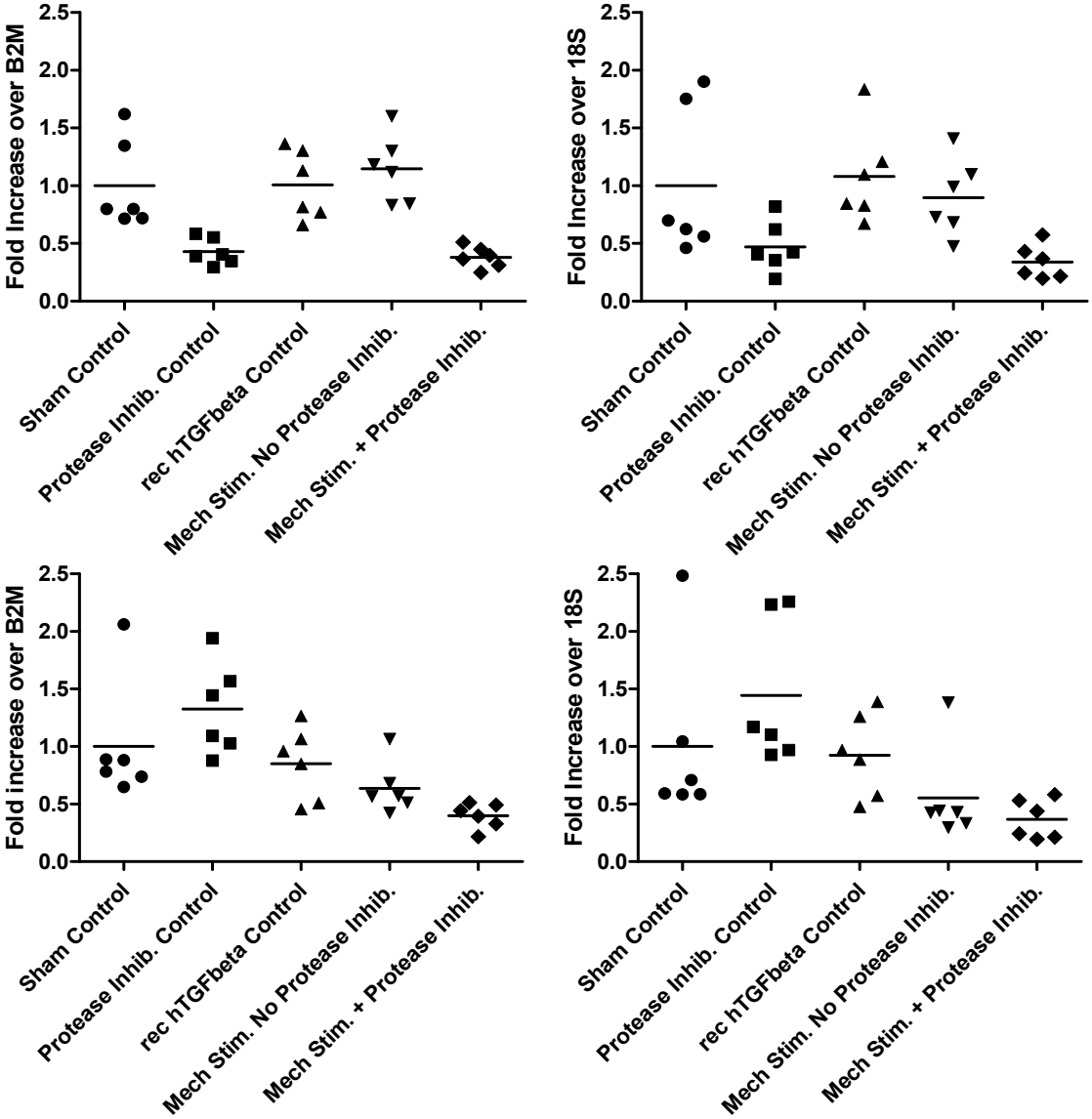

Figure 3.18. RT-PCR analyzed mRNA expression PAI1 and CTGF levels in latent TGFβ overexpessing lung strips 6 hours post mechanical stimulation. Lungs were stimulated for 4 minutes with 15 mN cyclic mechanical stretch force. Recombinant TGFβ was used as a positive control to see if a significant maximal response could found. None of the above groups reached statistically significant difference by one way-ANOVA analysis.

shows that the 18S gene varied less between treatment groups then did β-2-microglobulin. Figure 3.18 shows data for two separate experiments indicating that

early responder genes are not upregulated at 6 hours post-mechanical stimulation. The latent TGFβ model was chosen over the fibrotic model because the fibrotic model is known to elevate PAI1 and CTGF as a result of ongoing injury response to active TGFβ overexpression. It was hypothesized that latent TGFβ overexpression would allow for a lower baseline in PAI1 or CTGF expression at the start of the mechanical stretch experiment, which would allow for a significant difference reading 6 hours post stimulation. Recombinant TGFβ was used to treat the lung slices as a positive control for TGFβ activation. Protease inhibitors were also used in order to see if further lowering the baseline activation of TGFβ in controls would separate them from mechanically stimulated groups. Other time points were tested post stimulation to see if prolonging exposure to 12ng/mL recombinant TGFβ would allow for more PAI1 and CTGF expression. Figure 3.19 shows that at no time point following recombinant TGFβ addition did the lung strip yield more PAI1 or CTGF mRNA that was significantly different from non-treated time matched controls.

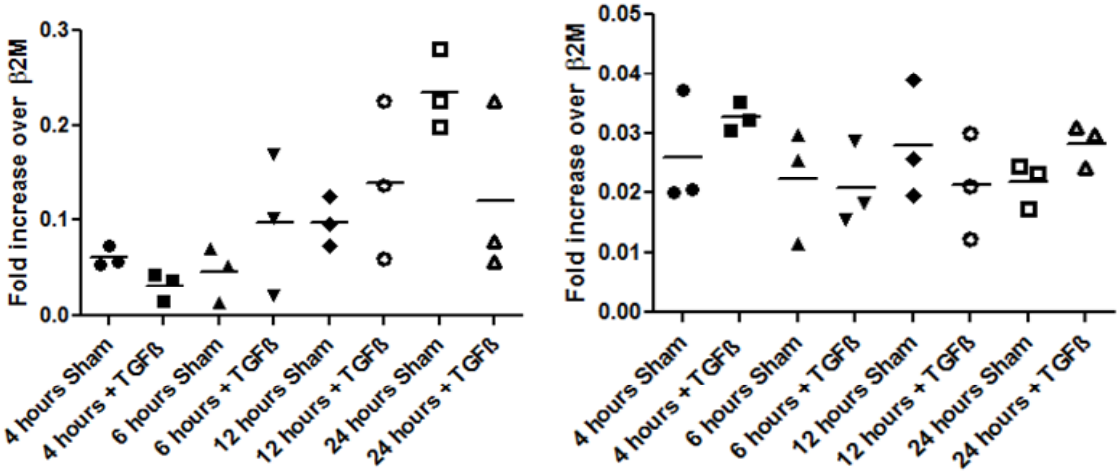

Figure 3.19. RT-PCR analyzed mRNA expression PAI1 and CTGF levels of naïve rat lung slice treated with 12ng/mL recombinant human $TGF\beta_1$. None of the above paired time groups reached statistically significant difference by non-parametric Student's T-test.

Intervention with N-acetylcysteine in fibrotic rat lung strips

As noted in Chapter 2, reactive oxygen species have strong effects on the activation of TGFβ *in vitro* and *in vivo*. N-acetylcysteine (NAC) is a strong anti-oxidant used recently in an IPF drug trial (209). The findings of the trial were that NAC prevented the deterioration of vital capacity and DL_{CO} lung functional parameters but did not prevent reduce mortality. These encouraging results indicate that modulation of ROS in IPF via antioxidant NAC could be an important part of an effective future multipronged approach. We set out to ascertain whether NAC could impact the activation of TGFβ from fibrotic rat lung tissue. We first assayed whether or not a single lung parenchymal strip could produce the same intensity of TGFβ release after two separate but equal stimuli. After multiple experiments and under various experimental procedures we concluded that the insult to the tissue from the first stimulus makes the second stimulus much more difficult to predict. Figure 3.20 shows an experiment on the effects of 100uM NAC on TGFβ release from tissue strips. The reduction in active TGFβ in the second stimulation in rat parenchymal lung strips was a common occurrence. One explanation of this is that fibrotic parenchymal lungs strips contain a specific pool of TGFβ in the ECM that would take more than 30 minutes to replace in order to release the same amount of TGFβ during the second mechanical stimulus event. The *ex vivo* nature of this experiment and the fact that the tissue is in a constant process of decay following sacrifice indicate that no two stimulus events will be equivalent for this model.

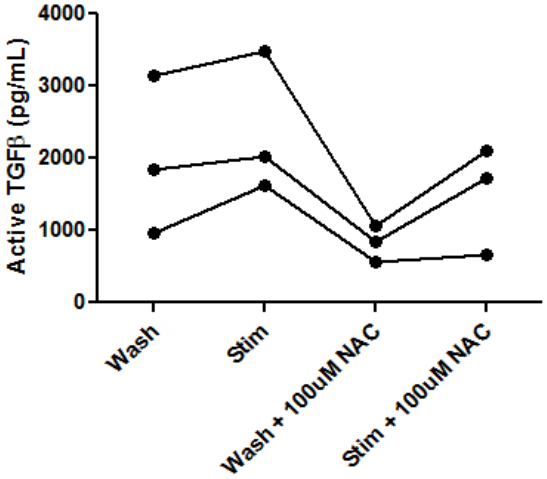

Figure 3.20. Experiment showing the effects of anti-oxidant N-acetyl cysteine on TGFβ activity in fibrotic lung strips. Wash phase was for 30 minutes followed by a 1D mechanical stimulation for 6 minutes at 6 mN. Data shown is not controlled for total TGFβ due to erratic data values. There was no significant change in TGFβ activity when NAC was used.

Contraction of fibrotic ex vivo lung strips

The mechanism proposed by Boris Hinz (50) indicates that any contractile agonist should be able to activate TGFβ via integrin αVβ5,6 binding directly to the RGD domain in the

ECM (Figure 2.4). It is known that endothelin-1 and angiotensin-2 are upregulated in IPF tissue and BAL fluids (188-190). These data lead us to ask whether or not ET-1 and AT-2 cause contraction of fibrotic lung strips to release active TGFβ. Figure 3.21 shows a characteristic ET-1 mediated contraction of fibrotic parenchymal lung strips. An early indication that this model would not be useful for inhibitor intervention studies was that the tissue tension relaxed slowed but did not reset to baseline following extensive bath

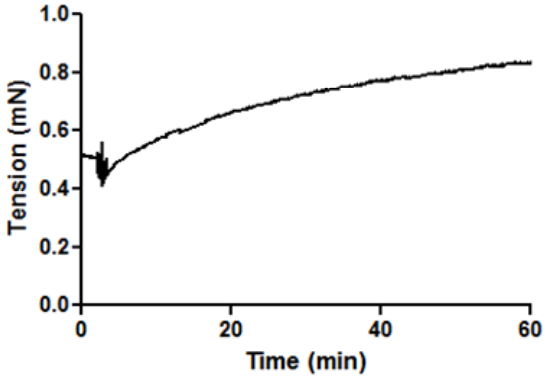

Figure 3.21. Representative fibrotic lung parenchymal strip contraction following addition of 10uM ET-1 to the bath solution. Tissue typically produces 0.4 to 0.5 mN of force per contraction. Parenchymal lung strip tension did not return to baseline following wash even with 2 hours of active rinsing.

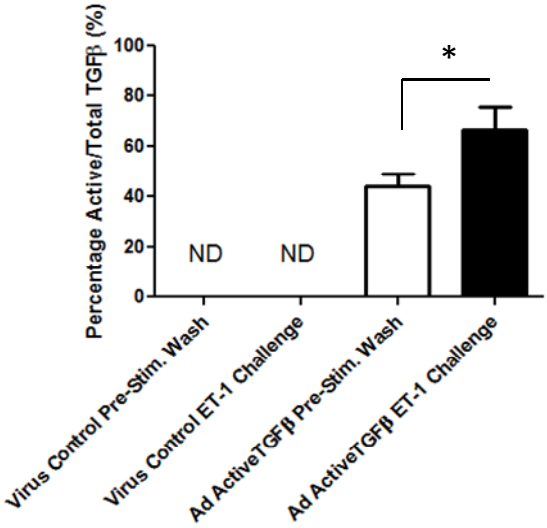

Figure 3.22. TGFβ following 15 minutes of contractile stimulation with 10uM ET-1 in fibrotic rat lung strips. N=5 per group representative of 3 separate experiments. Significant difference exists between final two groups, * $p<0.05$.

solution rinsing over 2 hours. When fibrotic rat lung tissue was assayed after 15 minutes of 10uM endothelin exposure there was a significant increase in active/total TGFβ release (Figure 3.22). Although many experiments were repeated we could not find a consistent subsequent activation of p-Smad2 after 6 hours (Figure 3.23). In order to show changes in TGFβ release due to inhibition of ET-1 mediated contraction we first set out to demonstrate if ET-1 could cause two consecutive contraction events which produce equivalent amounts of active TGFβ. Figure 3.24 shows an experiment indicating that fibrotic rat lung strips produce unpredictable amounts of TGFβ following a second ET-1 mediated contraction. Second contraction events were noted to be much lower than the initial contraction. These data indicated that this model would very likely be unsuitable for asking questions of interference of contraction on TGFβ release. It may be that once myofibroblasts or other resident contractile cells in fibrotic lung parenchyma respond to non-physiologic ET-1 levels, their internal signaling pathways

are set for a sustained contraction that takes hours to reset following removal of ET-1. With this in mind, we investigated if ET-1 mediated contraction could be inhibited by

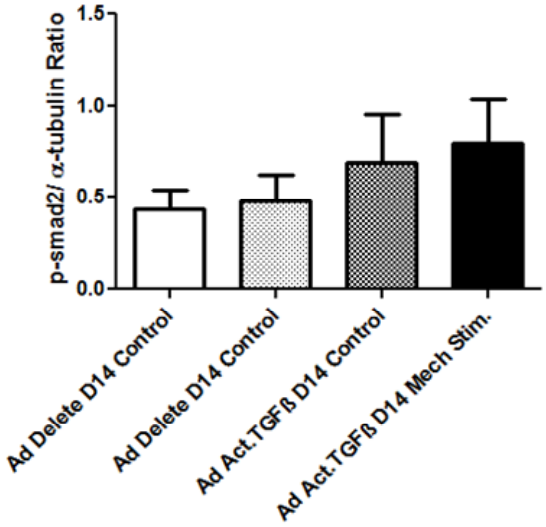

Figure 3.23. Western densitometry for p-Smad2 with respect to α-tubulin for virus control and fibrotic rat lung strips treated with 10uM ET-1 for 15 minutes and then incubated for 6 hours at 37˚C. At least 5 per group, representative of 5 separate experiments. No significant difference was noted between the final two groups.

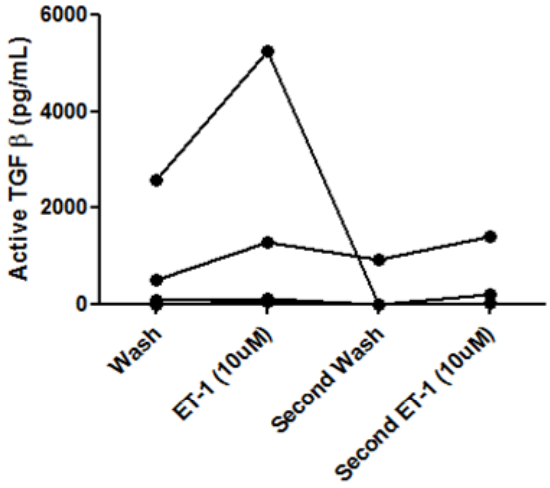

Figure 3.24. TGFβ released by ET-1 (10uM) mediated contraction of fibrotic rat lung strips. One experiment showing inconsistency of second contractions events for fibrotic strips.

addition of a contractile inhibitor during a second ET-1 stimulus event. Inhibition of ET-1 mediated contraction by Rho kinase inhibitor Y-27632 contraction resulted in a >50% reduction in contractility of fibrotic parenchymal lung strips. However since the control experiments with two consecutive ET-1 treatments also had a ~50% reduction in tension on the second treatment, we could not be certain that Y27632 had any effect. Since experimentation in this model with contractile inhibitors did not produce interpretable results we cannot discount a contraction-independent mechanism for direct activation of latent TGFβ by the ET-1 peptide. That p-Smad2 activity was not elevated significantly after 6 hours indicates that there is likely no physiological relevance for ET-1 mediated release of TGFβ in fibrotic rat lung strips in this model.

Angiotensin-2 also causes the contraction of fibrotic rat lung strips at 100uM concentration similar to ET-1 (Figure 3.25). AT-2, however produces very little contraction in parenchymal lung strips (~0.1 mN) in comparison to ET-1 (~0.4 mN). Although many experiments were repeated, AT-2 mediated activation of TGFβ in fibrotic lung strips was inconsistent. Figure 3.26 (left) shows data from one experiment

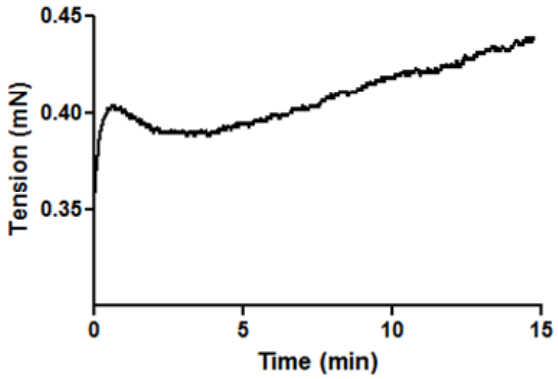

Figure 3.25. Fibrotic lung parenchymal strip contraction following addition of 100 uM of Angiotensin-2 to the bath solution. Tissue produces ~0.1 mN of force per contraction. The AT-2 model was not robust, many tissues did not contract. There was no correlation between non-contracting tissue and TGFβ release.

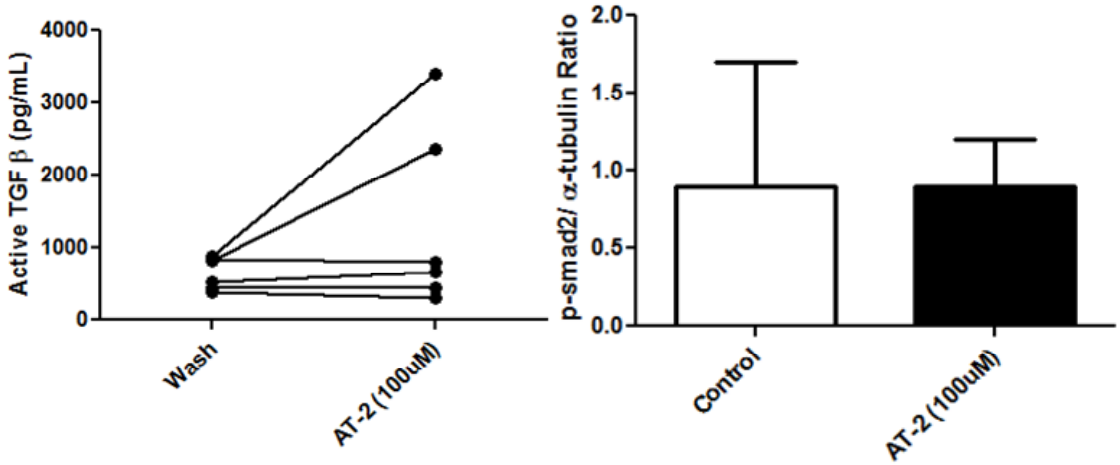

Figure 3.26. Active TGFβ release (left) by angiotensin-2 mediated contraction of fibrotic rat lung strips. Roughly half of the strips did not respond to AT-2 in this experiment. No significant difference between the wash and the stimulated tissue was found even after removing non-responding strips from analysis. Western densitometry (right) for p-Smad2/α-tubulin of fibrotic rat lung strips treated with sham control or 100uM of AT-2 for 15 minutes and then assayed after 6 hours of incubation at 37˚C. Data displayed as means plus standard deviations. No significant differences were found in 3 separate experiments.

were half of the lungs strips responded with TGFβ activation following addition of AT-2 to the bath solution. There was no correlation between non-responding tissue and TGFβ release into the bath solution. Figure 3.26 (right) shows that there are no significant changes in downstream p-Smad2 activation 6 hours following AT-2 stimulation. These data demonstrate that this tissue bath model is not a good model for

the experimental investigation of the effects of AT-2 on active TGFβ release from fibrotic lung strips.

3.4 Discussion of Mechanical TGFβ Activation in Fibrotic Lungs

TGFβ is a pleiotropic cytokine involved in organ development, cell differentiation and maintenance of extracellular matrix homeostasis(35-37), immune regulation(210), epithelial to mesenchymal transition(99), and fibroblast to myofibroblast transformation(211). TGFβ is known to be post-translationally activated *in vitro* by serine proteases thrombin and plasmin (212), neutrophil elastase (213), mast cell tryptase (214) and chymase (215), MMP's 2, 9 (154), membrane type 1- MMP (Figure 2.2) (216), and *in vivo* by conformation changes induced by thrombospondin-1 (173). Integrins subtypes containing αV also physically link the LLC with the cell cytoskeleton and have been demonstrated to be directly involved in TGFβ activation *in vivo* (Figure 2.4) (180, 217). Under the conditions of contraction in rigid ECM, myofibroblasts were able to physically pull apart the LLC to release the TGFβ active homodimer (50). How TGFβ is activated during lung fibrogenesis remains a subject of strong debate.

We identified mechanical ventilation as a physiologically relevant stimulus of the TGFβ signal transduction during lung fibrogenesis. We developed a model capable of placing discrete amounts of force on ex vivo lung parenchymal strips while analyzing tissue elastance properties. This model was ideal for mapping out the release of active TGFβ from lung strips and later following intracellular signal events.

We found that TGFβ is activated by mechanical tension in fibrotic tissue and is positively dependant on time and force of stimuli. These results imply that higher pressure and longer ventilation will worsen existing fibrotic scarring through a TGFβ dependant manner. Results from control tissue indicate that lungs must undergo a strong abnormal wound healing process and engage the cellular machinery involved in lung fibrogenesis before TGFβ mechanotransduction can become a process for persistence and progression. Protease inhibitors had no effect on the activation of TGFβ from fibrotic lung parenchymal strips. This indicates that TGFβ is not being activated during mechanical stimuli in a plasmin, thrombin, etc. dependant manner. It may be that some other protease that is important to mechanical TGFβ activation was still active in the context of the pan-protease inhibitor cocktail. However, there is no way to test all

possible TGFβ activators with the reagents available. At least serine/threonine proteases (eg. plasmin, thrombin) and MMPs (1,2,3,8,9) were inhibited by the cocktail representing a great many enzymes which could directly cleave the TGFβ latent complex or be involved in cell contraction to indirectly activate TGFβ. Although thrombin is known to activate TGFβ via a PAR1- αVβ6 integrin dependant method (192), inhibition of thrombin did not in of itself block TGFβ release or signaling. Other known major sources of TGFβ activation are dependent on integrin cytoskeleton interactions with the LLC in the ECM. Integrins may turn out to be the major source of TGFβ activation during mechanotransduction. We found that there was no correlation between amount of TGFβ activated and tissue elastance (data not shown). This data indicates that unlike in myofibroblast cultures (50), fibrotic lung tissue can undergo TGFβ mechanotransduction without a clear dependence on underlying ECM elastance, or that elastance measured in this manner does not reflect the microenvironment of the cells.

TGFβ released during mechanical stimuli activates p-Smad2 in the nuclei of stretched lungs 6 hours following. This data demonstrates that TGFβ activated by mechanical stimuli has a physiologic role in the tissue as opposed to having an impact on reporter cells afterward. Virus control lung strips did not activate Smad2 following stimuli indicating that this mechanical TGFβ activation was limited the fibrogenic diseased state. We also looked at early TGFβ responder genes PAI1 and CTGF. We found a visible trend favoring more PAI1 in fibrotic tissue strips that did not reach statistical significance at 6 hours post-stimulation. This may be a limitation of the *ex vivo* lung strip bath model due to tissue degradation as we found that approximately two thirds of the original p-Smad2 signal was lost at 6 hours post stimulation in comparison to freshly harvested and snap frozen tissue.

The ventilator model showed that there was also a significant p-Smad2 signal following ventilation challenge at 6 hours similar to the 1D tissue bath model. Art Slutsky's group have shown with their ARDS model of acid instillation and mechanical ventilation challenge that rodent lungs produce enhanced TGFβ and β-Catenin expression 3 days following (218, 219). Cabrera *et al.* also showed that ventilator induced lung injury was causing EMT in lung, another pathway which is known to be controlled by TGFβ (99-102). Mechanical ventilation did not change p-Smad2 signaling in virus control lungs, again indicating that this TGFβ mechanotransduction was limited to the fibrogenic diseased state. These data agree with Cabrera *et al.* which showed that mechanical

ventilation alone in normal mice was insufficient to enhance TGFβ or β-catenin mRNA expression 3 days later. Tissue elastance from ventilator experiments showed an increase in elastance in fibrotic lungs from control lungs, which confirms the 1D tissue bath model data.

Data from Sakamoto *et al.* 2011, and Watanabe *et al.* 2011, found that acute exacerbations were more likely to occur in patients with IPF following mechanical ventilation and oxygen supplementation (220, 221). We found that human lung fibrosis tissue activated TGFβ in a similar manner to rat lung fibrogenesis models. Although TGFβ is known to signal branch into the many downstream pathways, the canonical Smad pathway is known to be critically important to the maintenance of the fibrogenic stimulus (109). It is now clear that mechanical stimuli acting on human fibrotic tissue force the activation of the TGFβ signalling pathway via Smad2. It is likely that long term TGFβ mechanotransduction activates a positive feedback loop in IPF tissue that results in further fibrotic changes. Human control lungs did not release detectable TGFβ following stretch or respond with phosphorylated Smad2 activity. These data indicate that a TGFβ mechanotransduction feedback loop may only be possible under the pre-existing conditions of tissue fibrosis.

We proposed that enhanced latent TGFβ production in the lungs would create a situation that allowed for mechanical TGFβ activation. Other groups have reported that latent TGFβ overexpressed in the lungs could be activated by exogenous means. Arnold Brody's group showed that adenovirus driven latent TGFβ overexpression in the lungs of mice could be activated by reactive oxygen species produced by asbestos exposure (222). Our data shows that overexpressed latent TGFβ was activated by mechanical stretch force and that these forces lead to downstream activation of p-Smad2 in the same tissue. Although these lungs had a significant increase in tissue elastance, these measurements do not correlate with the incidence of tissue fibrosis or collagen production and was still roughly half as rigid as fibrotic model lung tissue (30). These data suggest that the proposed dependence on tissue rigidity for mechanical TGFβ activation may not be as important during fibrogenesis as latent TGFβ availability itself (50). The lack of fibrosis in these tissues suggests that latent TGFβ overexpression and subsequent mechanical activation could be important to the initial stages of IPF pathogenesis.

We studied the effect of strong antioxidant N-acetyl cysteine on the mechanical activation of TGFβ. We found instead that the fibrotic tissue strip model produces difficult to interpret results with the second stimulus. Nonetheless, we could find no impact of NAC on TGFβ release into the bath solution when fibrotic rat lung strips were mechanically stimulated.

Cell contraction is currently the most prominent mechanism studied in the context of mechanical TGFβ activation. Contractile agonist ET-1 was able to cause TGFβ activation following the tightening of fibrotic rat lung strips. These results are similar to those found by Wpiff *et al.* in myofibroblast cultures. Downstream signaling of TGFβ released by ET-1 mediated contraction events did not upregulate p-Smad2 to the nucleus 6 hours later, although a trend was very visible. Unfortunately, multiple contraction events produced unpredictable results in fibrotic lungs strips, which created difficulties during attempts on contractile antagonist intervention studies. Although AT-2 did produce some contraction this was almost negligible in comparison to ET-2. AT-2 did cause significant TGFβ activation in some tissue strips but in an inconsistently manner that could not be predicted by tissue rigidity. Since inhibition of ET-1 mediated TGFβ activation did not produce interpretable results, we cannot disprove that a contraction-independent mechanism exists in which ET-1 liberates the active cytokine by directly binding to latent TGFβ.

In summary, under the conditions of lung fibrogenesis in the rat and in established human lung fibrosis, TGFβ is activated following mechanical stretch or via ventilation challenge which leads to a downstream activation of phospho-Smad2 which transits to the nucleus. These studies shed mechanistic light on the observation that ventilation of acute IPF and ARDS patients leads to fibrogenesis and worsening of prognosis. This phenomenon is not evident in human or rat control lungs, supporting that TGFβ mechanotransduction is limited to the pathobiological state in tissue fibrosis. These observations provide strong supporting evidence that mechanical stimuli contribute to pathological TGFβ activation and add to the persistent and progressive nature of IPF.

4.0 Introduction to Non-Invasive Evaluations of Lung Fibrosis

The development of novel technologies has had a profound impact on the study of lung fibrosis. However, keeping pace with technological improvements is a constant challenge. This chapter sheds light on these advancements and what is possible to accomplish in a pre-clinical drug treatment trial in the context of pulmonary fibrosis. Special consideration will be given to non-invasive methods which allow the researcher to follow drug treatments longitudinally. This can reduce the cost of experimentation as well as enhance the accuracy of evaluation of efficacy of drugs. Efficacy evaluations are enhanced since the study can exclude subset groups to be euthanized before and during fibrogenesis, instead focusing on the primary endpoint following the fibrogenic period. Fewer animals required to power a drug efficacy trial also decreases the cost of expensive experimental drugs and reduces the amount of time needed to evaluate the results. Lung fibrogenesis can be evaluated non-invasively by a variety of means. Advanced imaging with high resolution computed tomography (HRCT), positron emission tomography (PET), nuclear magnetic resonance imaging (MRI) analysis, lung function experimentation, blood serum and cell analysis are diagnostic methods functioning without major organ tissue removal.

4.1 Fibrocytes as Non-Invasive Markers of Fibrosis

The persistence and progression of IPF is highly complicated. It is currently not possible to tell if a patient will survive longer or progress quickly with this disease. This has motivated researchers to find other prognostic markers and tools to help identify patients in the course of pathogenesis. These efforts have focused on blood serum and cell based markers, urological analysis, and next generation imaging technologies. Of these evolving technologies, the analysis of fibrocytes has found some grounds a prognostic tool. Fibrocytes are bone marrow derived mesenchymal progenitor cells which are known to home to sites of tissue injury. Fibrocytes participate in tissue repair by differentiating in to fibroblasts, myofibroblasts, and producing ECM components in response to TGFβ or endothelin-1 (ET-1) (223-226). Fibrocytes are characterized by the expression of collagen types 1 and 3 and hematopoietic surface markers CD34, CD43, CD45, and LSP-1 (227-230). Fibrocytes do not have lymphocyte markers CD3, CD4, CD8, CD19, or CD25 (227). Fibrocytes also express chemokine receptors CCR2, CCR7, and CXCR4(228) which are used in homing to sites of tissue inflammation (228).

Chemokines are small protein ligands which are released by one cell type to draw in another cell type through a tissue or from the blood stream (231). Work by Bob Strieter has shown in animal models that interfering with the trafficking of fibrocytes to the lungs by blocking CXCL12 chemokines during bleomycin fibrogenesis significantly attenuates disease severity (223, 225). Interestingly, fibrocytes have been recently found to correlate with the stage and severity of bronchiolitis obliterans, a fibrosing disease of the trachea and bronchi following lung transplantation (232). Work in our laboratories discovered that, during acute exacerbations of IPF, levels of fibrocytes appear to temporarily increase. Elevated levels of fibrocytes also indicated poor prognosis for patients with IPF apart from other lung diseases (233). Fujiwara *et. al.* have provided further recent evidence that fibrocytes correlate with disease progression, percent vital capacity lung function test, and sialylated carbohydrate antigen (KL-6), another marker of disease severity (234). Moises Selman's group has positively identified fibrocytes in 8 out of 9 tissue samples from IPF patients with immunofluorescence and confocal microscopy. CXCL12, a chemokine implicated in the recruitment of fibrocytes to the lung was highly expressed in IPF alveolar epithelium and was significantly elevated in blood serum and bronchioalveolar lavage (BAL) fluid (235). Whether fibrocytes contribute to or resist the IPF disease process is unclear, however their use as a marker of disease severity makes a strong case for their use as a diagnostic tool in IPF clinical management.

4.2 Blood Born Markers of Lung Fibrosis

The search for blood born markers of fibrogenesis was in its prime during the latter half of the 1990's. No markers in BAL have proven useful in the diagnosis of UIP over non-specific interstitial pneumonia, a similar but less severe disease (236). A mucin-like glycoprotein named KL-6 is also elevated in the BAL and serum of various forms of interstitial lung disease (237). Elevated KL-6 is not specific to ILDs as it has also been found in breast cancer (238), colorectal cancer (239), lung tuberculosis(240), and non-small cell lung cancers (241). Manufactured by type II pneumocyte, KL-6 was found to be a predictor of survival and decreased gradually after treatment of a small 14 member group of rapidly progressing IPF patients with a high dose corticosteroid treatment (242). KL-6 has been evaluated in other studies correlating its elevation to lung

inflammation, however these studies have to date been in small populations with ILD which may be unrepresentative of the larger IPF population.

Surfactant protein A and D (SP-A and D) are protein constituents secreted by type II pneumocytes into the fluid in the lungs which maintains a low alveolar surface tension (243). SP-A and D are elevated in IPF and other inflammatory lung diseases (244). It could be that the hyperplasia of type II pneumocytes in the vicinity of the fibrotic lung parenchyma causes this increase in serum SP-A and D, especially if the alveolar epithelial and endothelial vessel barriers have been compromised (244). Takahashi *et al.* showed in a 3 year study of 52 IPF patients that the levels of SP-A and SP-D were normal in stable patients. Of the patients that succumbed to disease the levels of SP-A and SP-D were normal in only 25% of individuals. Greene *et al.* followed a population of 142 IPF patients to predict survival. They showed that SP-D, but not SP-A, was elevated 56% over controls when adjusting for a variety of factors including smoking status, forced vital capacity (FVC), Partial pressure of arterial oxygen (PAO_2), total lung capacity (TLC), and forced expiratory volume for one second (FEV_1) (244). More recently a study of 82 IPF patients by Kinder *et al*. showed that those with a 49ng/mL elevation in serum SP-A over controls had a 3.3 fold increased risk of death one year following initial diagnosis. The Kinder *et al.* study saw no link between SP-D and risk of death (245). These discrepancies in various studies and the large standard deviations found when measuring SP-A and SP-D demonstrate that these biomarkers are still unsuitable for routine clinical indication of survival (246).

The chemokine CCL-18 has been shown to be upregulated in IPF serum. This protein is known to cause the chemotaxis, or trafficking of B cells, T cells, dendritic cells, hematopoietic progenitors, fibroblasts, and monocytes (247). Rodents lack a gene that corresponds to CCL-18, making study of protein limited to human biopsy and cell culture work. The corresponding receptor for this ligand has not yet been found (248). This molecule is constitutively expressed in normal lungs and also plays a role in the alternative activation of macrophage. Alveolar macrophage cultured from IPF patients indicate that CCL18 regulates collagen production in lung fibroblasts (249). Prasse *et al.* published a study involving 72 IPF patients indicating that CCL18 serum concentration predicts changes in FVC and TLC after a 6 month period and a significant risk of mortality was associated with CCL18 concentrations above 150 ng/mL (247).

4.3 Lung Functional Parameters as Evaluations of Fibrosis

Interstitial lung diseases have a high incidence of decreasing lung function in spirometry test which can help indicate course of disease. In early stages of IPF, the diffusion capacity for carbon monoxide (DL_{CO}) and TLC can be close to normal controls. The prevalence of emphysema and fibrosis in smoking IPF patients may also confound TLC and FEV_1 values to make them appear closer to average. This is likely due to the expanding lung volume of emphysematous tissue compensating as the solid fibrotic scars grow. DL_{CO} and vital capacity are the generally accepted parameters to monitor disease progression (250).

Clinical trials for a number of possible drugs to treat IPF have had the benefit of yielding additional data of lung disease physiology. A study of the affects of antioxidant NAC on 155 IPF patients showed that a TLC of >62% of predicted and a DL_{CO} of >43% together predicted survival rates one year later. Independently, DL_{CO} and TLC were not predictors of survival one year later (209). Data mining from a trial of IPF treatment with interferon gamma showed that for those on placebo control treatment, patients that survived until 72 weeks had no change on average in FVC (251, 252). Further evaluation of the trial noted that one year mortality risk was 2 times higher with patients that had a decrease of 5 to 10% in FVC and that a fall in FVC between 2 and 6% was still clinically meaningful (253). This trial also noted that a decrease of greater than 50 meters in a six minute walk distance test resulted in a 4.27 fold increase in risk of death after one year and that a decrease by 24-45m was considered to be clinically meaningful (254). In a separate study of 80 IPF patients, a fall of FVC by 10% was associated with a significant increased mortality risk after 6 months (255). Although these drug trials have proven unsuccessful, the data used has resulted in an improved understanding of the relationship between lung function and disease progression and time based mortality risk.

4.4 Fibrogenesis Reporter Mice

Collagen promoter beta-galactosidase (LacZ) reporter mice have been produced by Fragiadaki *et al.* to look into the molecular pathways activating collagen expression in kidney fibrosis. This group have combined the collagen promoter with the expression of CCN2 or connective tissue growth factor (CTGF) which gave rise to interstitial fibrosis

upon aristolochic acid exposure (256). The group was able to map out the growth of collagen expressing cells during disease progression. None have tried this approach to study lung fibrosis which would also greatly benefit from the enhanced interpretation of fibrogenesis data.

4.5 Advanced Imaging Technology

High resolution computed tomography is the first diagnostic tool used in the diagnosis of IPF. Evaluative studies have shown that the specificity the 'confident' HRCT pattern can be correctly interpreted in 90% of cases. Since, the 'confident' HRCT pattern can be found in only 80% of biopsy proven IPF patients, surgical lung biopsy is still required for positive diagnosis (257-259). Surgical biopsy is generally considered to be safe for IPF patients but age and lung function related challenges can be strong contraindications. The mortality rate 90 days after biopsy surgery was found to be only 1.5% for patients with IPF (260). Lung biopsy is also a painful surgical procedure which likely decreases patient moral, especially if IPF is positively identified.

The use of nuclear magnetic resonance imaging (MRI) can also be used to analyze lungs non-invasively. Proton MRI signal-to-noise ratios are poor since the lungs are filled with air spaces that have much less water than solid tissues (261). This difficulty has lead researchers toward the use of hyperpolarized gases such as ^{3}He. ^{3}He is sparingly soluble and therefore does not enter into the blood stream or surrounding tissues (262). Because hyperpolarized noble gases have a much higher signal to noise ratio, they can be imaged directly after being inhaled by patients during MR imaging. The lungs can also be assessed for regional ventilation deficiencies and alveolar surface parameters (261). Hyperpolarized ^{3}He is expensive to produce however and requires specialized equipment to transport which greatly reduces widespread utility. Only one article has been published showing the use of hyperpolarized ^{3}He for IPF patients undergoing lung transplantation. Their data shows the characteristic and numerous defects in ventilation due to fibrotic scaring and collapse of pulmonary architecture. Image resolution was also an issue in this article which used relatively large voxel (volume pixel) sizes of 4x2.5x10 mm (263).

The use of PET imaging requires that the contrast molecule be a positron emitting isotope. Common examples of these isotopes in use today are 18-Fluorine and 125-

Iodine. These isotopes are can be used in the construction of molecules with significant metabolic activity cancerous or fibrotic tissue. For example radiolabelled 18-F-deoxyglucose (FDG) is used to highlight heavy use of glucose in contrast to surrounding less glycolytic cells. This allows tumor and immune cells to be highlighted during routine cancer imaging. Use of FDG in the monitoring of IPF is currently undergoing validation but was noted to have favorable short term reproducibility (264). One study of 36 IPF patients showed that FDG uptake in the lungs correlated with FVC and overall health score. Lung FDG uptake was elevated in all 36 patients and was especially elevated in regions that appeared in HRCT scans as reticular or honeycomb formations (265). Lung fibrosis is a disease that involves the construction and turnover of large quantities of collagen, the main protein constituent of scar tissue. Collagen contains relatively large amounts of the amino acid proline. To image the development and turnover of collagen in vivo, Renee Labiris' group has used radiolabelled 18-F-proline as a PET contrast agent (266, 267). Figure 4.0 illustrates how active fibrogenesis is labeled by 18-F-proline in the context of Ad TGFβ_1 modeled lung fibrosis. Rodent lung fibrosis models show that sites of lung fibrosis have greatly enhanced uptake of 18-F-proline (268, 269). Preclinical concepts such as mapping of collagen turnover in real time with 18-F-proline represent a superior method of evaluating fibrogenesis and will greatly enhance the determination of anti-fibrotic drug efficacy.

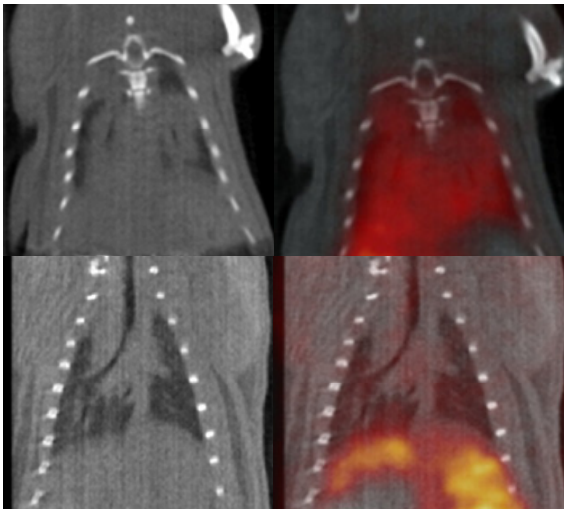

Figure 4.0. Positron emission tomography images of ^{18}F-proline uptake in the lungs of Ad TGFβ_1 exposed rat (top) and control rat (bottom). The CT image shows the accumulation of high density fibrosis at Day 7 post viral administration (top left) in comparison to the control rat (bottom left). The right column shows PET images fused with CT images showing accumulation of radiolabelled proline signal in Ad TGFβ_1 (top right) but not control lungs (bottom right). The uptake of proline denotes active collagen synthesis. The control rat accumulated proline in the liver as anticipated. Images taken from Labiris *et al*. 2006.

4.6 Antigen Specific Imaging Technology

Antigen specific imaging technology relies on an affinity enhancing agent to target an imaging contrast molecule. The most impressive techniques in validation today use one of two methods for detection; MRI and positron emission tomography (PET). The detection of a specific antigen in an organ or tissue can be achieved using a variety of ligands. The most common ligand used is the antibody protein, or a derivation of the antibody structure. Smaller, single chain variations of antibodies have been noted to perform with better pharmacokinetics following IV injection (270). Once in the body, the antibody binds to a specific antigen with varying levels of affinity. This makes finding an efficiently binding antibody vital in order to improve the contrast of antigen specific imaging techniques. Antibodies carry various side chains and surface groups which are chemically ligated to the desired contrast agent. Some contrast agents for MRI analysis include superparamagnetic iron oxide nanoparticles (271), gold nanoparticles (272), and gadolinium^{3+} ions (273). In the case of Gd^{3+} ions, the contrast agent must be placed in a protective carrier or chelating complex which keeps the ions from exerting highly toxic effects. In fact, Gd^{3+} freed by improper chelation during contrast agent production has been directly implicated in the formation of a fibrocyte dependant systemic fibrotic disease called nephrogenic systemic fibrosis (274). The latest initiatives are to employ nanotechnology to the production of contrast agents to increase efficiency. Recently superparamagnetic iron nanoparticle and quantum dot copolymers were labeled with surface antibodies to identify tumor cells *in vitro* and *in vivo* MRI (271). Analyses like these present promising avenues of diagnostic imaging in which the pathogenic tissue can be visualized over time. To my knowledge no antibody directed imaging techniques have been used to visualize lung fibrosis. However, the use of fibroblast specific surface antigens specific antibodies labeled contrast agents could be a possible avenue to visualize fibrotic changes over time.

In conclusion, a non-invasive approach including imaging technologies, lung function and exercise testing can be applied to any rodent model of lung fibrosis. This allows drug trials to proceed without interruption to their end without euthanasia, reducing animal numbers needed to power trials and the time required for analysis. The following chapter presents published and unpublished data collected by Kjetil Ask and myself in which high resolution computed tomography (CT) imaging, lung function

measurements, exercise testing where used to characterize fibrogenesis non-invasively. The purpose of this study was to determine if non-invasive methods could provide the same or better information as classical approaches. Kjetil Ask was the primary author of the paper that was published and performed most of the work involved. Aaron Froese was involved in animal care and assisted in the exercise experiments to determine VO_{2max} (the maximal rate of oxygen consumption during exercise), animal CT scanning, and analysis of CT data. Aaron Froese was not involved in the Ashcroft scoring of histological sections or rodent ventilation experiments (116).

5.0 Non-Invasive Evaluations of Lung Fibrosis

5.1 Preamble

For the investigation of lung fibrosis, animal models have played a central role in the discovery of pathologic activity. However, no drug treatments with clinical efficacy have been reported for lung fibrosis or indeed for any known fibrotic disease with the exception of pirfenidone (275, 276). Pirfenidone slows down progressive decline in lung function for IPF patients but does not prevent death (277). We rationalized that the divergence in the approaches to investigation of lung fibrosis in animal models skews the interpretation of experimental results. This difference between human and animal model interpretation is largely based on the evaluation of lung fibrogenesis over a fixed time period. A great many drug compounds have been found to have efficacy in experimental models of lung fibrosis. Of this large group, only a small fraction of anti-fibrotic drugs have been investigated as therapeutics and even fewer have been involved in clinical trials (115). Examination of anti-fibrotic drugs has been largely designed as prophylactic intervention against the inflammatory phase of the bleomycin induced lung fibrosis rodent model. This inflammatory phase, which may not exist in advanced IPF (171), is likely an inappropriate treatment target. Experimental lung fibrosis assessment uses histology and hydroxyproline analysis to quantify collagen accumulation and yield data of a single moment in the chronic disease process. In contrast, clinical trials of IPF detect lung function and survival improvements over many months, relying on exercise tests and radiology (23, 253, 254). In the published manuscript entitled “Comparison between conventional and "clinical" assessment of experimental lung fibrosis” we endeavored to ask whether or not non-invasive experimentation could give similar results to classical assessments of lung fibrosis (116). We made a detailed investigation of the later stage of a non-inflammatory rodent model of lung fibrosis (30). These assessments included changes in lung micro CT densities, lung functional parameters, and exercise testing which have the advantage of repetitive analyses that do not require euthanasia. We propose that the use of non-invasive measurements will yield a higher quality interpretation of anti-fibrotic therapeutic outcomes.

Some of the data presented in this chapter is included in the publication in the Journal of Translational Medicine in 2008 and is displayed here with permission. Data shown from the article is indicated in the corresponding figures below. Kjetil Ask was the primary author of the paper and performed a major portion of the work involved. Aaron Froese was involved in animal care and assisted in the exercise experiments to determine VO_2max (the maximal rate of oxygen consumption during exercise), animal CT scanning, and analysis of CT data (116).

5.2 Methods Pertaining to Non-Invasive Evaluations of Lung Fibrosis

Rat Lung Fibrosis Model

Female Sprague Dawley rats weighing between 200 to 250 grams (Charles River Laboratories, Inc.) were anesthetized with isofluorane (MTC Pharma, Inc.) with an Anesthetic Gas Vaporizer (Leica Microsystems Inc.) and given intratracheal instillations of recombinant A5 adenovirus expressing constitutively active porcine TGFβ_1, or delete control vector (30, 207) at $1x10^8$ pfu/rat in 300uL phosphate buffered saline (Lonza Group Ltd) and were sacrificed at 14, 21, 35, and 56 days post instillation by abdominal aorta bleeding under isofluorane induced anesthesia. Animal care was provided under the treatment guidelines of the Canadian Council of Animal Care.

Histology

Rat lungs were moved following sacrifice and inflated in 10% buffered formalin (Fisher Scientific, Inc.) for 24 hours to a final pressure of 20 cmH_20. After fixation in formalin was complete, the lungs were cut into 1 cm wide slices and processed for paraffin embedded sectioning with a Peloris II Tissue Processor (Leica Microsystems GmbH, Wetzlar, Germany). Paraffin embedded lung sections were section at 3 micrometers with a histological microtome (Model: RM2235, Leica Microsystems GmbH, Wetzlar, Germany). Masson's Trichrome and Picrosirius Red staining protocols were performed for standard histological investigation of lung fibrosis.

Masson's Trichrome Staining. Lung sections were first deparaffinized by placing the slides in xylene (Fisher Scientific, Inc.) for 5 minutes at room temperature in a fume hood. Next the slides were rehydrated by placing them in 100% ethanol for 5 minutes,

95% ethanol for 5 minutes, 70% ethanol for 5 minutes followed by a wash in single distilled water for 5 minutes. Slides were then fixed again in Bouin's solution (Bouin's Solution: 75% saturated picric acid, 10% formaldehyde, 5% glacial acetic acid (Fisher Scientific, Inc.) for 1 hour at 55˚C. The slides were then washed in tap water for 5 minutes. The slides were then stained for 10 minutes at room temperature in Weigert's iron hematoxylin working solution which is a 1:1 solution of two stocks. Weigert's stock solution A contains 1 g of Hematoxylin in 100mL of 95% ethanol. Weigert's stock solution B contains 4 mL of 29% $FeCl_3$, 1 mL of concentrated HCl in 95 mL of distilled water. The slides were then rinsed in warm tap water for 10 minutes then rinsed briefly in distilled water. The slides were then stained for 10 minutes at room temperature in Biebrich Scarlet Acid Fuchsin solution (0.09% Biebrich scarlet (Sigma Aldrich, Inc.), 0.01% Acid Fuchsin (Sigma Aldrich, Inc.), 1% acetic acid). The slides were then washed in distilled water for 5 minutes. The slides were then placed for 10 minutes in phosphomolybdic-phosphotungstic acid solution (2.5% phosphomolybdic acid (Sigma Aldrich, Inc., 2.5% phosphotungstic acid (Sigma Aldrich, Inc.)) which ensures that the collagen fibrils become greenish-blue. Without rinsing, the slides were placed in Aniline Blue solution (2.5% Aniline Blue (Sigma Aldrich, Inc.), 2% Acetic Acid (Fisher Scientific, Inc.) for 5 minutes. The slides were washed briefly in distilled water and then placed into 1% acetic acid solution for 5 minutes to further differentiate colors. The slides were then rinsed quickly in distilled water. The slides were then dehydrated rapidly in 95% ethanol and then 100% ethanol followed by xylene. This dehydration step must be done quickly to avoid removal of staining dyes. Finally, the slides were mounted with coverslips in xylene compatible mounting medium (Fisher Scientific, Inc.)

Picrosirius Red Staining Protocol. Paraffin embedded sections were first deparaffinized in xylene for 5 minutes followed by 5 minutes in 100% ethanol, 5 minutes in 95% ethanol, 5 minutes in 70% ethanol followed by washing in distilled water. The slides were then placed in Wiegert's Iron Hematoxylin working solution (contents detailed above) for 10 minutes. The slides were then washed in tap water for 10 minutes. The slides were then placed in Picrosirius Red staining solution (0.1% Sirius "Direct Red 80" in saturated picric acid (Sigma Aldrich, Inc.)) for 1 hour at room temperature. Slides were then washed in tap water containing 0.005% acetic acid. The slides were then dried to remove most of the excess water. The slides were then placed in 100% ethanol twice for 5 minutes each to remove all water from the slides and then placed in xylene

for 5 minutes followed by mounting with a xylene compatible mounting medium (Fisher Scientific, Inc). The slides were then observed under a cross-polarizing light filter to observe brightly colored collagen which appeared yellow to orange.

Ashcroft scoring of severity was performed on Picrosirius red stained slides focusing on 20 fields per slide at a magnification power of 200X. Three investigators were blinded and asked to assign fibrotic severity to each histological field with a numerical score between 1 and 8 (278).

Quantitative Colorimetric Hydroxyproline Assay

Rat lungs were frozen in liquid nitrogen and then stored at -80˚C until homogenization. Rat lungs were homogenized using an Ultra Turrax T25 tissue homogenizer (Staufen, Germany) in 5 mL of phosphate buffered saline. Tissue homogenate is diluted by taking 1 mL of the resuspended solution and mixing it in 9 mL of double distilled H_2O (Elix Water Purification System, Millipore Corp.). A 2 mL aliquot of each sample was then freeze dried overnight in pre-weighed bottles using a FreeZone Freeze Drier (Labconco, Inc.). The freeze dried samples were then placed in 10 mL Teflon® lined screw cap test tubes with 2 mL of 6 M HCl (Fisher Scientific, Inc.). The samples were then hydrolyzed in acid overnight at 110˚C. The samples were then neutralized with concentrated sodium hydroxide (Bioshop, Inc.) keeping note of the volume of sodium hydroxide used for final quantification calculation. Separately, a set of pure hydroxyproline (Sigma Aldrich, Inc.) standards in 2 mL double distilled H_2O were created ranging in concentration from 0 to 5 mg/mL. To the samples and standards was added 500 uL of chloramine-T solution (50mM chloramine-T, 30% ethylene glycol monomethyl ether, 50% solution of (260mM citric acid, 1.46M sodium acetate, 850mM sodium hydroxide, 1.2% glacial acetic acid) in water.) Samples were incubated at room temperature for 20 minutes after which 500 uL of 3.15 M perchloric acid was added. The samples were mixed and incubated for a further 5 minutes. Then 500 uL of a solution of p-dimethylamino-benzaldehyde (1.34 M p-dimethylamino-benzaldehyde dissolved in ethylene glycol monomethyl ether) was added to each sample. The samples were incubated at 60˚C for 20 minutes at which time the color change occurs. The samples were aliquoted at 100uL per well into a 96 well Elisa plate for absorbance reading in an Elisa spectrophotometric plate reader (SpectraMax, Molecular Devices, Inc.) set to 560 nanometers absorbance detection. Results were calculated using Beer's Law using linear regression on the hydroxyproline

standard absolute absorbance values (279). Hydroxyproline values were expressed as a fold increase over virus control lung sample values.

Animal Lung Imaging

Computed tomography of rodent lungs was performed under vaporized isofluorane anesthesia (MTC Pharma, Inc.) using the Micro-CT portion of the X-SPECT scanner (Gamma Medica, Inc.). Figure 5.0 shows a picture of the scanner used for computed tomography of rats during fibrogenesis. Rats were placed into cylindrical Plexiglass® containers equipped with Hepa-filters and scanned with normal breathing through 512 angles. The reconstructed CT images were 155 micrometers cubed in volume pixel (voxel) size. All imaging data was reconstructed and analyzed using Amira® Software (Mercury Computer Systems, Inc.). The densities of each the voxels in the image stacks were converted to Hounsfield Units (HU) using a Matlab program (MathWorks, Inc.) by calibration with a tube of water taped to the rat's chest set to 0 HU and with normal air set to -1000 HU. The image data was filtered for noise reduction through a Gaussian 3D voxel filter with a sigma value of 2. Reconstructed and density corrected 3D images were analyzed for fibrotic and normal lung areas by selecting the contents of the rib cage using a region-growing tool. The surfaces of whole lungs were generated for pictorial display with respect to the density of each voxel. 3D lung surface image surfaces help to locate high density fibrosis within the organ by limiting the densities included in the image. Whole lung images were also used to create of 3D density histograms. These density histograms help to note which densities are lost and gained during the fibrogenic process.

Figure 5.0. X-SPECT small animal scanner (Gamma-Medica, Inc.). This scanner performed all micro-CT assessments of rat lung density during lung fibrogenesis. Image taken from www.gammamedica.com.

Rodent Lung Physiology

Animals were placed under anesthesia with 100 mg/kg of Ketamine (Parke-Davis, Inc.) and 10mg/kg of Xylazine (Bayer Healthcare, Inc.) and intubated through the oropharynx and ventilated with 10 mL/kg/breath with a Flexivent rodent ventilator (Model 5.1, Scireq, Inc.). Figure 5.1 shows an image of a Flexivent rodent ventilator. Pressure volume loops were measured after letting the rat expire in a passive way for 1 second with 2 cmH_2O of positive end expiratory pressure. The pressure was measure during a 7 step increase and 7 step decrease in air volume at 40mL/kg per step. The Salazar-Knowles equation k value was used to describe the curvature of the higher half of the pressure-volume loop (280). Stiffness of the lungs was determined from the inspiratory lower half of the volume loop as the volume of air required to attain 20 cmH_20 of pressure.

Figure 5.1. Flexivent rodent ventilator. This apparatus was used to create pressure volume loops for the investigation of lung physiology in the context of pulmonary fibrosis models. Image taken from the www.SciReq.com

Exercise Physiology

The assessment of gas exchange capacity under exercise was performed with a flow-through respirometry system (Sable Systems, Inc.) which measures oxygen and carbon dioxide levels in a connected air tight container equipped with a speed controlled treadmill (Columbus Instruments, Inc). The movement of carbon dioxide and water free air was tuned with an electric mass flow controller (Sierra Instruments, Inc.) Figure 5.2 shows the experimental and schematic setup of the rodent exercise physiology lab. The maximal oxygen consumption rate (VO_2max) was determined as the treadmill increased the rats' exercise output. VO_2max was measured with three criteria. 1) Rats could not keep their position on the treadmill. 2) No change was noted in oxygen usage rate VO_2 after the treadmill speed was increased, c) the ratio of carbon dioxide use to oxygen use was greater than 1. Pulse oximetry (MediTech Inc.) was used as another measurement

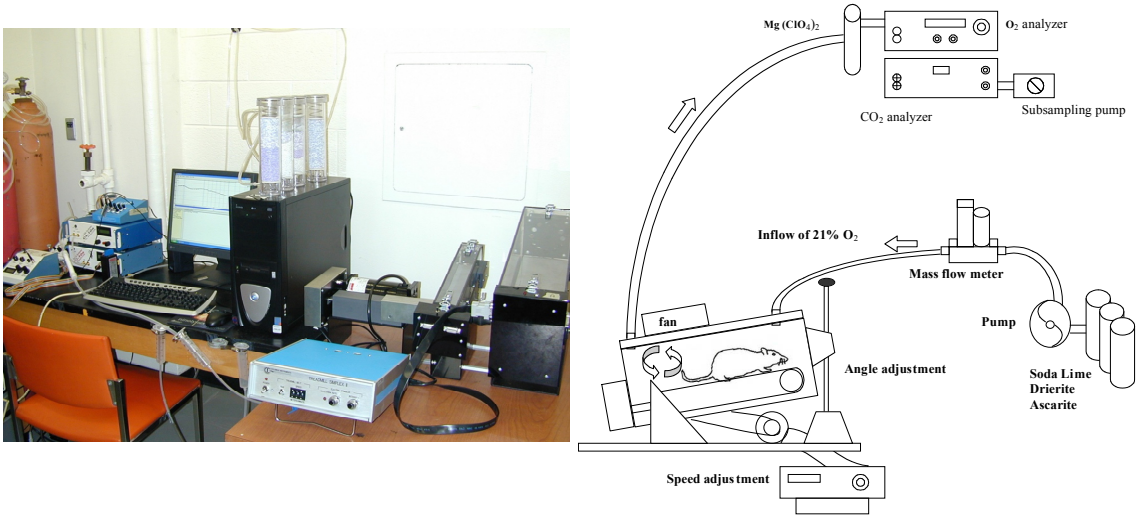

Figure 5.2. Rodent treadmill and exercise physiology equipment. The rat is placed into the air tight treadmill chamber were the air flow is monitored closely for changes in oxygen and carbon dioxide. As the rat runs it attains its maximum mass-specific oxygen consumption. Rats with modeled lung fibrosis are have impaired oxygen exchange capability and would not be capable of running as far. This experiment was designed to be similar to the 6 minute walk test use for IPF physiological measurements.

of lung function by analyzing blood oxygen saturation of the hind foot pad following treadmill exercise.

5.3 Results of Non-Invasive Evaluations of Lung Fibrosis

Standard Evaluation of Pulmonary Fibrosis

The lung fibrosis models benefit from the assessment of significant biochemical mechanisms collected following euthanasia. This allows the investigator to look into pathobiological processes during fibrogenesis as well as in a therapeutic context. The standard evaluations of lung fibrosis are the collagen quantifying hydroxyproline assay or Woesnner's colorimetric assay and a histological assessment with Ashcroft objective scoring (278, 279). The Ad activeTGFβ_1 model of lung fibrosis was re-evaluated in order to contrast standard assessments to non-invasive investigations (30). Figure 5.3 shows images taken from normal and fibrotic rat lungs with Picrosirius Red and Masson's Trichrome stained histology. The interpretation of severity score was performed along with standard hydroxyproline quantification. Figure 5.4 shows that the Ashcroft index increased significantly and was sustained following administration of Ad TGFβ_1. We observed partial bronchiocentric fibrosis with associated loss of lung architecture which persisted out to 7 months post vector instillation. Figure 5.4 also shows how the

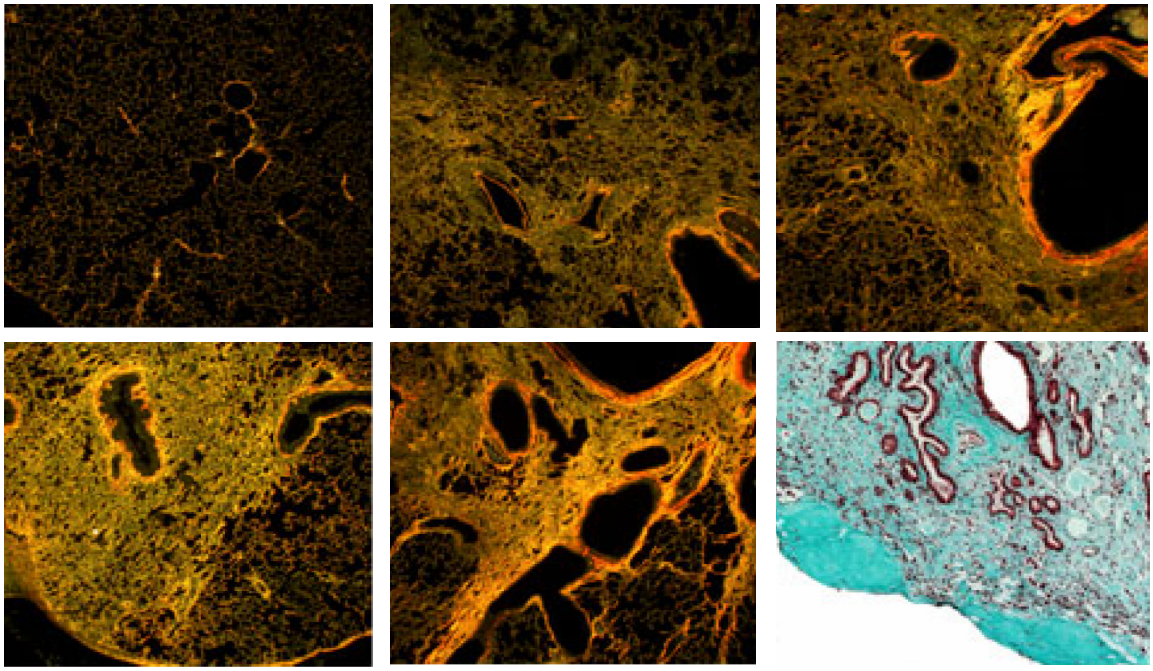

Figure 5.3. Rat lungs histological images taken from representative fields during Ashcroft scoring. Picrosirius red staining was used for all Ashcroft staining. The final image is stained with Masson's Trichrome which colors collagen fibrils blue. Image identification: Naïve lungs (top left), Day 14 Ad TGFβ_1 (top center), Day 21 (top right), Day 35 (bottom left), Day 56 (bottom center), Day 225 (bottom right). These images indicate the persistent nature of this rodent lung fibrosis model. Images taken from Ask *et al.* 2008.

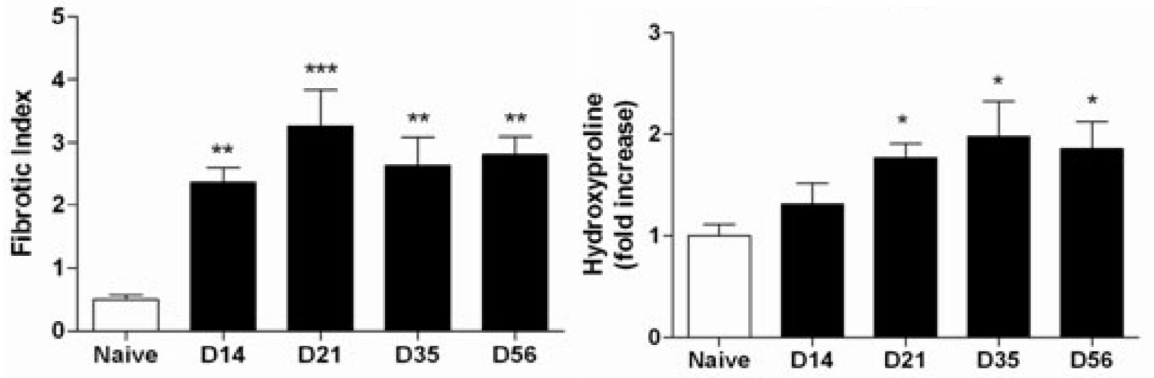

Figure 5.4. Ashcroft indexing of fibrotic severity in lung histology (left). Three independent, blinded investigators scored 20 fields per histological slide. One way ANOVA with Dunnett's multiple comparison analysis shows that the fibrotic score was significantly different amongst groups.
The quantification of hydroxyproline in comparison to control rat lungs using the Woesnner's colorimetric method (right). N= 4 to 6 per group with * $p < 0.05$, ** $p < 0.01$, *** $p < 0.001$ vs. naïve group. Graphs and data taken from Ask *et al.* 2008.

hydroxyproline content in rat lungs increases during fibrogenesis in response to Ad TGFβ_1, peaking at around day 35 post instillation.

Non-Invasive Imaging Evaluation of Lung Fibrosis

The analysis of computed tomography images of the fibrotic rat lungs allows for observation of higher density regions with progression of the disease model. With voxel sizes of 155 um^3 and reconstruction of image data to standardized densities, CT images provided a window into disease progression that normally requires euthanasia. We first validated the micro-CT scanner to determine the variation in total lung volume over 10 separate scans of one rat. Figure 5.5 shows the variation in CT scan images and densities over 10 scans. The total lung volume coefficient of variation was 2.6%. Figure 5.6 shows how experimental data from CT scans can indicate changes in lung density

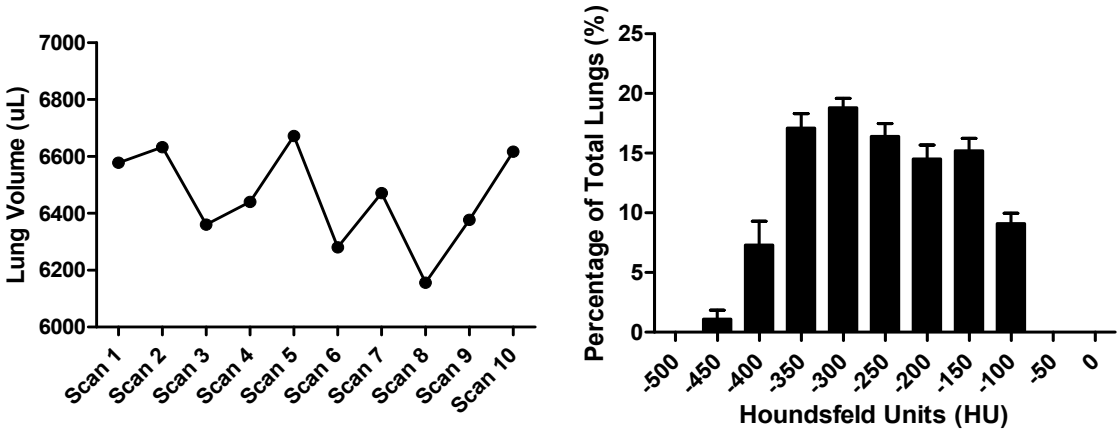

Figure 5.5. Validation of micro CT for one rat scanned ten times. Volume of lungs calculated over ten different successive scans, the coefficient of variation was 2.6% (left). Percentage of total lung volumes at various calculated CT densities (right). The data is expressed as means and standard deviations.

over time. With the onset of lung fibrosis, a shift to the right in Hounsfield density histograms was seen indicating increasing density in lung regions between -200 and 100 HU. We followed a group of rats up to 7 months after vector instillation and observed that the same higher density fibrotic regions persisted. Analysis of the percentage of lung densities between -600 and 200 HU revealed an increase in lower density regions indicating a compensating mechanism to tissue thickening. We observed that the percentage of normal lung densities found between -400 and -200 HU decreased significantly in fibrotic animals. Investigation of these higher density regions of CT images with histology revealed close correlation with the presence of tissue fibrosis and dense collagen deposition. Figure 5.7 shows an example of close correlation between higher CT densities and lung fibrosis in histological images. These data underscore the use of CT images in routine investigation of lung fibrosis in an animal model over time.

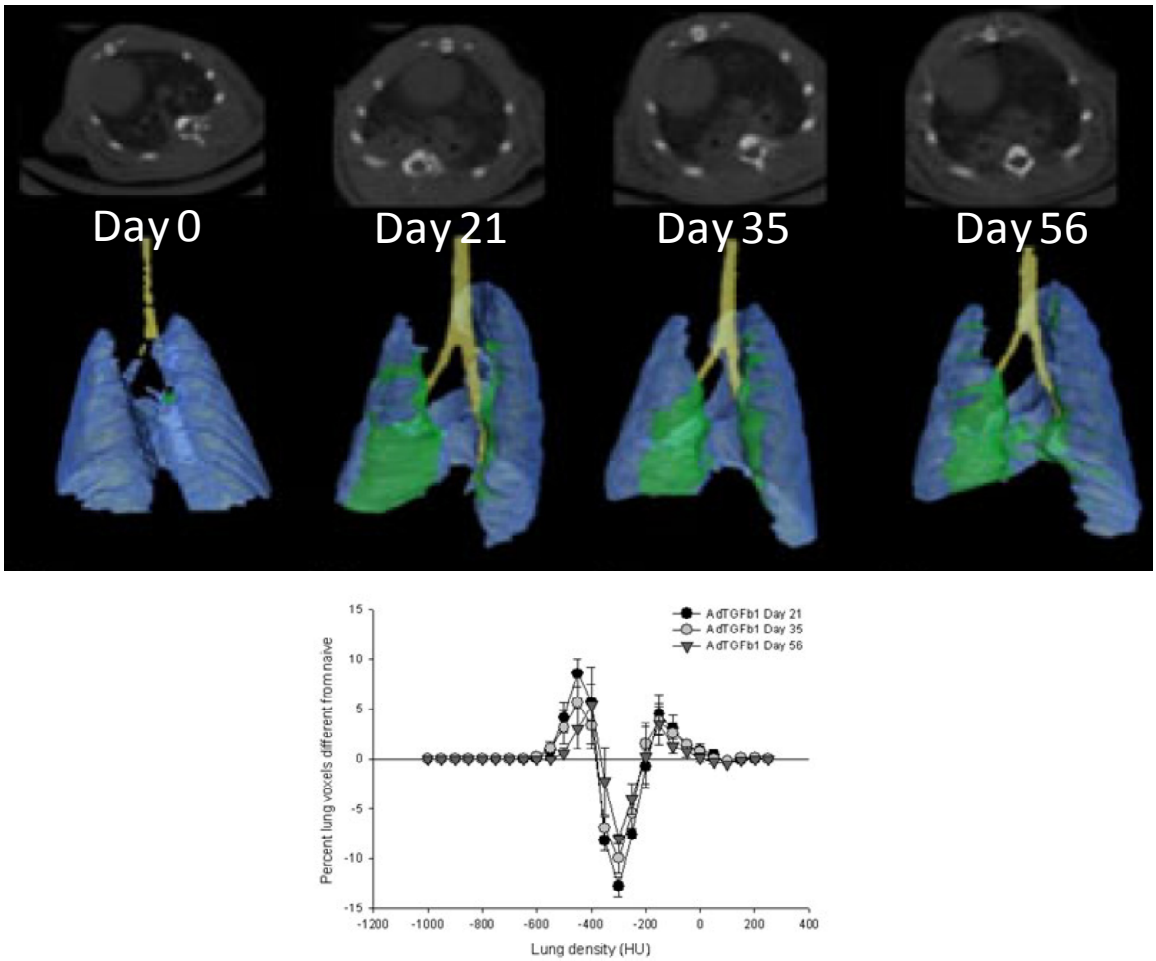

Figure 5.6. Representative 2D and 3D reconstructed CT images of a rat given Ad TGFβ_1(top). The blue indicates densities from –600 to -100 HU. Yellow indicates the trachea, and green indicates fibrotic areas with density between -100 and 200 HU. Images show the persistent nature of this lung fibrosis model without euthanasia. Percent lung density difference of fibrotic rats with respect to normal rat controls for days 21, 35 and 56 post viral instillation (bottom). A decrease in normal lung density was visible between -400 and -200 HU. The was an increase in lower densities between -600 and -400 HU and in higher densities between –200 and 100 HU. The high density increase corresponds to fibrogenesis and the lower density to airspace enlargement. N=4-6 per group. Graphs taken from Ask *et al.* 2008.

Exercise and Lung Physiology

The development of fibrosis leads to stiffening of the lungs and breathing difficulty. These clinical features are important indicators of fibrotic severity and also have some prognostic value for IPF (see Chapter 4.3). To define the physiologic characteristics of lung fibrosis we employed a rodent ventilator and a gas analyzing treadmill apparatus. Figure 5.8 describes these physiological observations. We observed that rats in the progressive stages of Ad TGFβ1 mediated lung fibrosis gradually gained lung stiffness.

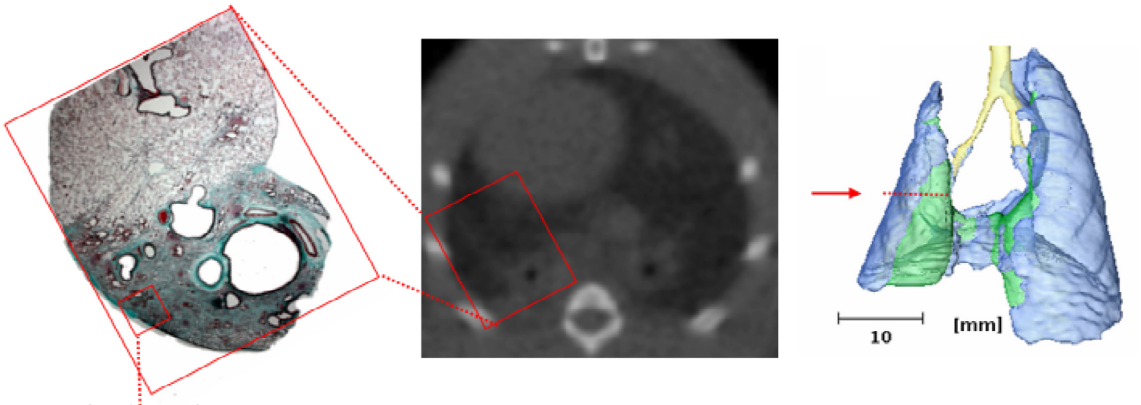

Figure 5.7. Representative example of the correlation between lung fibrosis in histology and high regional CT densities. Histological image of a lung lobe from a rat treated with Ad TGFβ1 at day 225 (left), 2D CT image at day 225 (center), 3D reconstructed image of the same data (right). Histological image is of Masson's Trichrome stained lungs. The 3D reconstructed data image represents blue as -600 to -200 HU and green as -200 to 100 HU densities. Yellow represents the trachea. Images taken from Ask *et al.* 2008.

We observed that stiffening lungs had a lengthening downward trend in the pressure volume-loops measured by the Flexivent rodent ventilator. The k-parameter which describes the shape of the pressure volume loop showed a significant decrease that was persistent to day 56. On day 21, the peak time point of fibrogenic severity as measured by Ashcroft scoring and pressure volume loops, the rats were placed in an enclosed treadmill with oxygen and carbon dioxide measuring apparatus to assess the maximal rate of oxygen consumption. We found that the rate of oxygen consumption and blood oxygen saturation measured by pulse oximetry decreased approximately 10% but was not significantly different from control animals (Figure 5.9).

Non-Invasive and Standard Assessment Correlations

Next we used linear regression to find correlations between histomorphometic Ashcroft scoring to lung function, exercise parameters, or high CT lung densities between -100 and 200HU. We also correlated high CT densities between -100 and 200HU with lung function parameters. This testing was crucial to prove that non-invasive assessments provide the same quality of data for the investigation of fibrosis as standard assessments. Figure 5.10 shows the data that supports non-invasive assessments as significantly correlated alternatives to standard assessments. Only maximal oxygen uptake rates did not correlate with Ashcroft scoring.

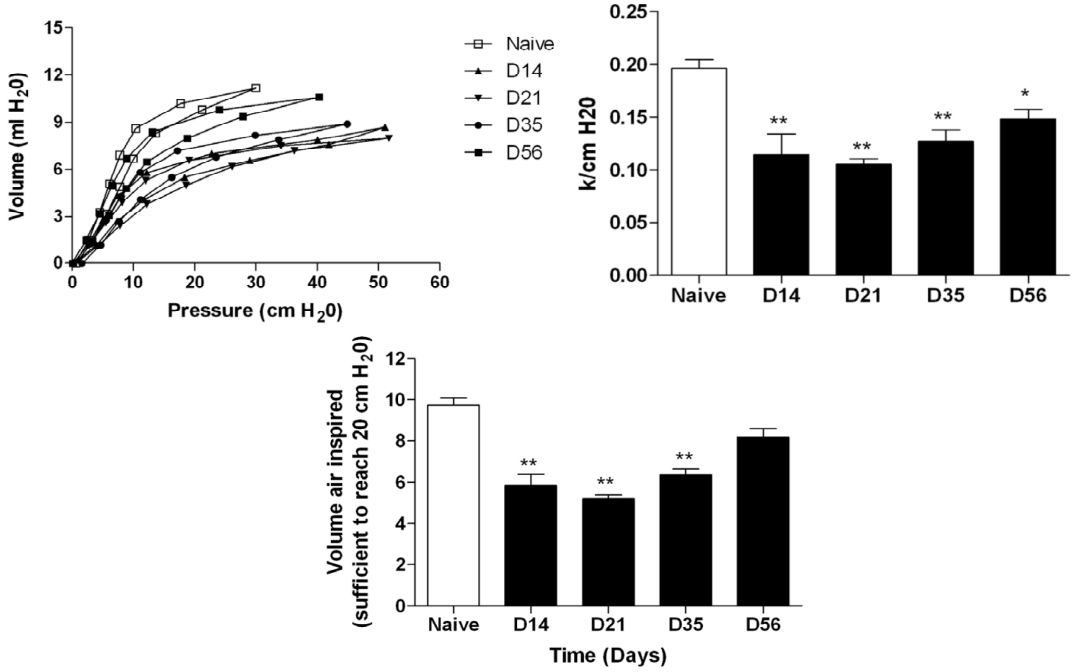

Figure 5.8. Pressure-volume loops of rats given Ad TGFβ_1 (left). As the fibrosis progresses, the stiffness of the lungs increases until the disease severity reverses between days 35 and 56.
Salazar Knowles factor k describing curvature of the pressure volume loop during the Ad TGFβ_1 fibrogenic rat lung process(right). Severity of curvature changes are most pronounce at day 21 which partially reverses afterward.
Lung stiffness with respect to time of progression of the Ad TGFβ_1 model (bottom). Volume value taken from the inspiratory phase of the pressure-volume loop at 20 cmH_20. Data indicates that lung stiffness increases till day 21 and then reverses afterward.
All bar chart statistics were performed by one-way ANOVA with Dunnett's multiple comparison analysis showing significant difference amounts groups. N= 4 to 6 per group with * $p < 0.05$, ** $p < 0.01$. All values are given as means +/- SE, n = 4–6 per group. Graphs and data taken from Ask *et al.* 2008.

5.4 Discussion of Non-Invasive Evaluations of Lung Fibrosis

Non-invasive evaluation methods of lung fibrosis have not played any significant role in the assessment of therapeutic drugs in preclinical trials. This has arguably lead to the situation today where, after roughly 30 years of research, only pirfenidone has shown very modest benefits IPF patients (277). This failure has lead groups to search for alternatives to classical assessments of disease to find more relevant markers. Intuitively, lung functional assessments seemed the most likely to provide the insight into the fibrotic disease process that could make a critical difference in discerning ineffective drugs from those that hold promise. We found that non-invasive lung functional assessments involving pressure volume loops gave information about the

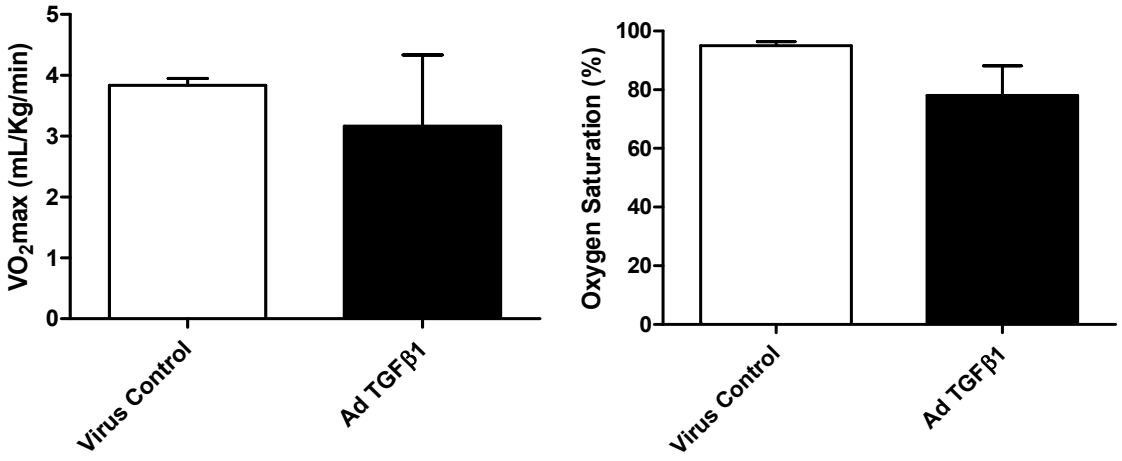

Figure 5.9. Maximal rate of oxygen consumption (VO_2max) during treadmill running exercise of fibrotic and control rats at day 21 post Ad TGFβ_1, p=0.3 (left). Pulse oximetry reading following treadmill exercise at day 21 post Ad TGFβ_1, p=0.2 (right). N= 3 per group. A non-parametric student's T-test was used to test statistical difference. This data was not part of the Ask *et al.* 2008 article.

health of the rats that would not be possible with euthanasia, allowing sequential analysis of the same animal. Fibrotic pressure volume loop Salazar-Knowles parameter k, provided data which correlated with both Ashcroft scoring and higher CT density lung volumes (Figure 5.10). Because of these highly significant correlations Ashcroft scoring can be replaced by a quick, more reliable, informative, quantitative method of lung function determination. The decision to move away from Ashcroft scoring may be best since it is quite labor intensive and because 20 tiny fields in a two dimensional medium cannot yield the same quality of data and might miss significant changes that a lung function test and 3D CT scan cannot.

As an alternative to histological investigation to follow and visualize fibrotic changes, we considered computed tomography imaging. Although expensive in comparison to histological procedures, CT imaging was validated and reproducible an animal followed through the fibrotic process for 7 months. One of the biggest issues involving anti-fibrotic experimental design is the large disparity between pre-clinical and clinical investigation. These disparities which were outlined by our group (115) present a consistent conundrum in which rodent fibrotic changes which take a couple of weeks to occur are modeled after fibrotic changes in the human which likely take years or even decades to occur. In light of the lengthy IPF progression, testing anti-fibrotic drugs for a few days in a rodent model and making a judgment based on the ability to reduce

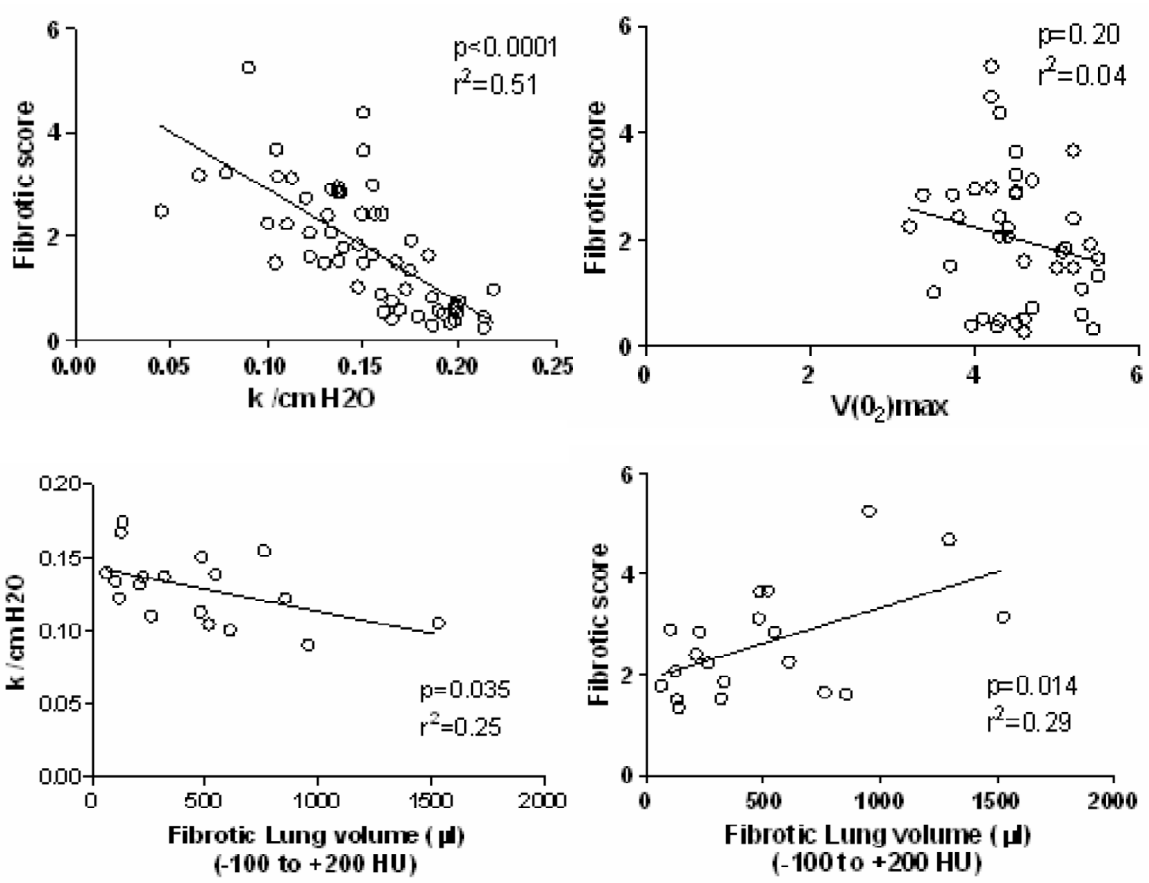

Figure 5.10. Linear regression and correlation of lung physiology, CT imaging densities parameters, exercise physiology, to standardized histomorphometric scoring. Ashcroft fibrotic histological scoring versus pressure-volume loop Salazar-Knowles k-parameter, p>0.001 (top left). Ashcroft fibrotic histological scoring versus maximal oxygen uptake rate during exercise, p=0.2 (top right). Salazar-Knowles k-parameter versus the number of lung CT voxels densities between -100 and -200 HU, p=0.035 (bottom left). The number of lung CT voxels densities between -100 and -200 HU versus Ashcroft fibrotic histological scoring, p=0.014 (bottom right). These data collectively assert that non-invasive lung physiology gives significantly equivalent information to the standard Ashcroft histology score. Graphs and data taken from Ask *et al.* 2008.

collagen production is a questionable approach. On top of this, the levels of collagen in fibrotic models rarely exceed two times the baseline level, and in the context of bleomycin models of lung fibrosis, can be highly variable (281). This greatly reduces the "therapeutic window" with respect to bleomycin induced rodent lung fibrosis. Because of these observations it may be important to define the longer term effects of anti-fibrotic therapeutics, since true reversion of disease will likely take months of time to occur. Here we describe that CT imaging is both significantly correlated with Ashcroft histomorphologic scoring and lung physiology parameters which would simplify longer

term investigation. These results also highlight the persistence of the Ad TGFβ_1 model of lung fibrosis which makes it uniquely suited to studying a longer term process.

Although human trials find significant indications of disease severity with the use of exercise tests including the six minute walk (254), our own analysis of rodent treadmill systems was less encouraging. We found there was a trend toward lower maximal consumption of oxygen during exercise in fibrotic rats than in control animals. This may be because the functional severity of the rodent model can be highly variable from rodent to rodent depending on the distribution of the disease. We've observed in our animals that if obliterating fibrosis is limited to one side of the lungs, the individual often appears outwardly to be healthy. We rationalize that this is because sufficient fully functional lungs still remain to support normal respiration for the whole rat. We also observed that rats in which some fibrosis is divided evenly amongst all lung lobes appear outwardly to be much less healthy. In humans, the diffuse lung disease IPF is patchy and often dispersed throughout all lobes (23). It may be that this dispersal of disease has more impact on overall patient health then a more focused phenomena confined to a smaller area. We believe that the exercise testing of rodent models of lung fibrosis still has promise but is limited to defining disease in more advanced cases. It could be that simply using older rats, which are less fit at the start of the experiment, would lead to reproducible differences in exercise capability during lung fibrosis.

In conclusion, a regime of non-invasive assessment tools similar those used in a clinical setting has been evaluated. We show significant correlation of lung function parameters and CT imaging densities with standard fibrotic analysis of hydroxyproline quantification and Ashcroft scoring techniques. The added advantage of repeated use of these methods with single animal over time adds to the impact and relevance for future anti-fibrotic therapeutic studies.

6.0 Introduction to Collagen Turnover

The extracellular matrix is a highly organized mixture of proteins, glycoprotein, oligo- and polysaccharides. This mixture serves numerous functions, the most important of which is the maintenance of elasticity and rigidity of tissue architecture (282). Second to this architecture function is its hydrating property. ECM components are often highly post-translationally modified with sugar side chains. These glycoproteins and glycosaminoglycans hold onto water through hydrogen bonding and ionic interactions to help safeguard the hydration of resident cells (283). The third most important aspect of the ECM is its adherence points for cell surface receptors (284). All of the above are vital aspects of ECM biology which are required for basic cell homeostasis. The ECM also functions to release danger signals which draw in immune cells and help prepare resident cells for bacterial, fungal, and parasitic attack. These danger signals are fragments of the ECM proteins and polysaccharides that are produced when microorganisms release their digest enzymes. These fragments bind to pathogen molecular pattern receptors such as Toll like receptors on the surface of immune and resident cells to prepare and maintain a protective response (285).

6.1 Collagen Biology

Types 1, 2 and 3 fibrillar collagens are large left handed triple helical proteins excreted primarily by fibroblasts into the extracellular matrix. Collagen is principally a structural protein and forms long scaffolds with other collagen molecules to form the tissue ultrastructure. It was estimated that 10% of all collagen in the body is synthesized and broken down each day to maintain tissue architectural homeostasis (286-288). Research by Jerry Last's group has called this turnover rate into question, indicating, for the lungs at least, turnover of collagen is very low or negligible (289). A disease such as fibrosis, involving greatly enhanced collagen production and retention, must also impact the turnover of collagen in that system. As collagen matures and condenses, its chemical nature changes, allowing investigation of the turnover rate by quantification of various bridging crosslink molecules (290). Fibrillar collagen propeptides, including types 1-3, are produced in large vesicle compartments which allow for triple helical formation prior to the removal of the both N and C terminus domains and cellular exocytosis. Prolyl-4-hydroxylase catalyzes the conversion of proline to 4-hydroxyproline

which is required to maintain the characteristic left handed triple helix structure (291). Since hydroxyproline is mostly found in collagen, its tissue content is generally considered a good surrogate marker for total collagen content (279, 292).

Lysine groups are oxidized to aldehyde products by the extracellular action of lysyl oxidase (293). Prolyl-4-hydroxylase and Lysyl oxidase expression were found to be regulated in response to TGFβ and PDGF in rat lung fibroblasts cultures (291). All of the main fibril forming collagens types I, II, and III have four main crosslinking points. One within each telopeptide, and one at around residue 87 and 930 within the triple helical domain (294). Collagen lysine residues are further processed by hydroxylation catalyzed by lysyl hydroxylase. There are three lysyl hydroxylases in humans with telopeptide hydroxylase 2 being subject to alternative gene splicing into two different subtypes: alpha and beta (295). The tissue distribution of isoforms varies, with lysyl hydroxylase 2b being upregulated by TGFβ during to skin fibrogenesis (296), ILD (297), and bleomycin-induced lung fibrosis (298). Also named PLOD2, lysyl hydroxylase 2b preferentially adds hydroxyl groups to lysine side chains at the ends of type 1 and 3 collagen fibrils. Bruck syndrome is characterized by chronic deficiency of pyridinolines in collagen of the bone which were mapped to missense mutations in exons of the PLOD2 gene (299). Due to the activity of lysyl oxidase, the aldehyde of the lysyl group on one collagen helix combines with the lysine on another helix to form a reducible di-functional crosslink termed dihydroxylysinenorleucine (DHLNL) or hydroxylysinenorleucine (HLNL) for crosslinks without prior hydroxylation (300). The ratio between DHLNL and HLNL in a collagen hydrolysate is a direct measurement of the activity of lysyl hydroxylase 2b in that tissue. After collagen forms its di-functional crosslinks DHLNL/HLNL, a slow but spontaneous maturation event occurs with the addition of another collagen helix. These tri-functional crosslinks are called pyridinoline (Pyd) and deoxypyridinoline (Dyd) (298). The ratio between Pyd and Dyd in normal bone tissue is 3.5 to 1 and is also a marker of the activity of lysyl hydroxylase 2b. Bone, tendons and cartilage contain more Pyd than Dyd and all other organs contain more Dyd than Pyd (301). The group lead by David Eyre that discovered pyridinolines in 1973 recently discovered additional crosslinks that form by the lysyl oxidase mechanism (302, 303). They discovered that HLNL and DHLNL disappear from mature tissues. These additional crosslinks are not fluorescent like pyridinolines and non-reducible. These crosslinks are considered to be adducts between HLNL or DHLNL with arginine instead of

another lysine residue. The authors called these crosslinks arginolines and noted that they were present in equivalent concentrations to pyridinolines in bone tissue (303). No groups have yet looked into presence of arginolines in any fibrotic disease process.

Pyridinolines are thought to denote a collagen that is more resistant to metabolic turnover as the hydroxylated crosslinks are more stable than their unhydroxylated analogues (300, 304, 305). As the rate of matrix breakdown of collagen decreases, the amount of pyridinolines in a given fibrotic tissue increases (298). Pyridinolines have been shown to be elevated in bleomycin induced fibrosis, serum, urine and skin biopsies from systemic sclerosis but have not been tested in IPF or for emphysema which also may contain elevated collagen levels (306-308). Condensation of collagen fibrils adds rigidity to the ultrastructure and resistance to MMP-1 mediated breakdown (309). Therefore, the concentrations and ratios of collagen crosslink bridge molecules are of value during the investigation of overall collagen turnover. In order to analyze collagen crosslinks, the entire collagen structure must be denatured and acid hydrolyzed to its constituent amino acids. However, DHLNL and HLNL bridges must be reduced with sodium borohydride to stabilize the linkage prior to acid hydrolysis. Assay of collagen bridge molecules including di- and tri-function crosslinks is performed using HPLC analysis.

6.2 Radiolabelled Lysine Experiments on Collagen Turnover

In 1989, Jerry Last and Karen Reiser published a ground breaking article underscoring the stability of collagen turnover *in vivo* (289). The authors gave 11 day old rats radiolabelled ^{3}H-lysine which would be incorporated into the collagen of the developing lungs. Several weeks later, after lung development had finished, the rats were given an IT bleomycin injection. Bleomycin is known to yield fibrosis which is mostly reversible in the rats, indicating that collagen is being built up in the lungs and then broken down (115). What the authors expected to see was changes in the quantity of radiolabelled lysine in the lung during the remission period in which collagen was broken down in the lungs. Instead, the authors failed to see any changes in lung radioactivity and no traces of radiolabelled lysine in the urine during the remission period using highly sensitive radioactive detection following HPLC. This startling discovery indicates that the collagen created during development is different than the collagen created during the fibrogenesis model. There was a lung collagen back bone template underneath the

"fibrosis collagen" which resisted proteolysis during the reversion period. IPF generates markedly elevated levels of collagen turnover products in serum and urine, and the disease is generally progressive (310). One could hypothesize that the primary collagen of the lungs formed during development and the collagen formed as a result of IPF fibrogenesis have become indistinguishable. If they were distinguishable, the IPF disease would be as reversible as the rodent IT bleomycin model. It follows that no treatment involving the same enzymes responsible for collagen proteolysis in the bleomycin model will be able to restore the original architecture in IPF lungs. Consequently, it is predicted that novel treatments for IPF will be limited to halting progression of the disease and perfecting transplantation of tissue engineered or donated lungs.

6.3 Collagen Turnover in Lung Fibrosis

A hallmark of IPF is the increase in types one and three fibrillar collagen content in the lungs. In the field, collagen is overwhelmingly quantified by tissue homogenization, acid hydrolysis, and subsequent colorimetric hydroxyproline quantification (279). Some researchers use a semi-quantitative Picrosirius Red staining method to analyze collagen content in histological tissue sections (311). When used with homogenized tissue, the Picrosirius Red method does not produce additional data above the method developed by Woessner in 1961. Highly sensitive HPLC methods for analyzing hydroxyproline have been reported (292). However, HPLC is seldom used in fibrosis research largely due to the high capital costs HPLC equipment in comparison to the inexpense of the time tested Woessner's colorimetric method. Collectively, these methods work well for the analysis of animal models of lung fibrosis but have no human equivalence. The patchy nature of IPF indicates that one or two biopsy samples are an insufficient polling of total organ collagen content. Methods to find better antifibrotic drugs continue to be marred by a lack of good metabolic readouts for fibrotic disease progression and reversion.

Since procollagen is processed to remove telo- and pro-peptides from the primary translation product, serum peptide markers do exist for the breakdown and synthesis of collagen. The N-terminal propeptide fragment of collagen III (PIIINP) marks collagen III synthesis which is elevated in IPF (310, 312). Another marker, the C-terminal terminus of collagen I telopeptide (ICTP) marks collagen I breakdown in scleroderma with pulmonary involvement (313) and in IPF serum (see data in Chapter 7). That these

molecules are elevated indicates enough to clinicians that there may be ECM turnover problems. It is counterintuitive that both collagen breakdown and synthesis products are elevated in a matrix accumulating disease. Another way to interpret this data is that there is an increase in the normal turnover rate of collagen within the fibrotic tissue, but the prevailing accumulation is too subtle to detect.

Pyd and Dyd are elevated in urine and serum of soft tissue fibrosis such as the skin of those afflicted with systemic sclerosis, a fibrosing disease involving the whole body. Urinary Pyd also correlated with severity in skin score (314). Systemic sclerosis and IPF, which is limited to the lungs, share similar disease phenotypic features, namely the appearance of widespread interstitial accumulation of collagen scars. Early efforts in the investigation of pyridinolines in IPF showed these methods to be irreproducible in our hands (315). Common protocols used to analyze pyridinolines include cellulose partition chromatography and C18 HPLC columns, caustic ion pairing detergents, and fluorescence detection (316-321). Because of these difficulties a new and far simpler method for quantification of pyridinoline crosslinks was developed. Chapter 7 demonstrates a new facile method for the detection of pyridinoline crosslinks and the analysis of PIIINP and ICTP from urine and serum of IPF patients.

7.0 Collagen Turnover in Lung Fibrosis

7.1 Preamble

In the field of tissue fibrogenesis study, researchers have neglected earlier findings of abnormalities in matrix composition and turnover. These findings indicate that lung collagen is produced during development and matures to an important original scaffold state. Although earlier estimates indicated that 10% of total body collagen was being created and degraded at a time (286-288), work by Jerry Last's group showed that only 0.5% of total lung collagen was in turnover (289). Last's results are more logical since a 10% total body collagen turnover would represent a major biophysical investment toward basic organ architecture. As organs develop the turnover of collagen should be higher as the tissue grows. Some collagen is broken down to give architectural characteristic aspects of each organ. When organ development completes in the lungs, the collagen "hardens" by becoming tighter bound to resist MMP activity (309). This "hardening" of collagen is thought to occur spontaneously in part through the formation of tri-functional pyridinoline crosslinks. The synthesis and breakdown of collagen protein can also be followed during fibrotic disease by monitoring serum metabolic products. PIIINP, which is a peptide of newly synthesized type III collagen and ICTP, which is a breakdown peptide catabolized from type I collagen are readily available assays which are known to detect abnormalities in bone metabolism. Collagen metabolism in IPF, which has no bone involvement, could potentially be monitored using PIIINP and ICTP. In this chapter we demonstrate a novel method for pyridinoline detection by HPLC, an adapted method for hydroxyproline detection by HPLC, and the analysis for collagen metabolic products in lung fibrotic fluids. All of the method development and sample experimentation presented in this chapter was performed primarily by Aaron Froese.

7.2 Methods Pertaining to Collagen Turnover

Sample Hydrolysis for Pyridinoline Analysis

Urine and serum samples were obtained from Dr. Eva Baroke's lab at Medizinische Hochschule of Hannover, Germany. All samples of urine and serum were stored in a -70˚C freezer. Serum samples were warmed slowly on ice for 2 hours and then moved to room temperature for 20 minutes and finally placed into a 37˚C water bath (Model 1212, Sheldon Lab Manufacturing Inc., VWR) with gentle periodic agitation for 20 minutes. Slowly warming frozen serum samples helped to keep blood proteins in solution. Serum samples of >7mL were filtered through an Amicon Centrifugal filter with molecular mass cutoff of 30 KDa (Millipore, Inc.) for 20 minutes at 7000 rpm in a Sorvall RC-5B High Speed Ultracentrifuge (Thermo Scientific Inc.) using a Sorvall SS-34 Centrifuge Rotor. The use of this centrifugal filter removes the bulk of blood proteins, which interfere with the HPLC analysis. Lower molecular weight breakdown products of collagen are retained with the 30kDa cutoff. Serum filtrate was freeze dried (FreeZone Freeze Drier, Labconco Inc.) overnight and then resuspended with 1mL of 3 M HCl (Fisher Scientific, Inc.). Serum was hydrolyzed in Teflon®-lined screw cap test tubes in acid overnight at 110˚C. Hydrolysis in hot acid breaks down the peptide bonds within all protein amino acid chains, including partially degraded collagen. This makes all pyridinolines in the sample free to enter the solution. Urine samples in 750uL aliquots were hydrolyzed overnight at 110˚C by mixing with a 250uL aliquot of concentrated HCl (Fisher Scientific, Inc). Urine hydrolysates were centrifuged to remove char solids at 14000 rpm on a table top centrifuge (Eppendorf 5417C, Hamburg, Germany) for 4 minutes.

Solid phase extraction of Pyridinolines

The solid phase consisted of a 50 mg Varian PRS strong cation exchange tubes and a Supelco Visiprep DL vacuum manifold. The solid phase was wet with 500uL methanol (Caledon Laboratories Inc.) followed by 1.5mL of a wash phase containing 5mM sodium formate (Sigma Aldrich Inc.), pH 2.5 with HCl. All acid hydrolyzed samples were diluted 10X with 25mM sodium tetraborate (Sigma Aldrich Inc.), pH 9.5, solution. The diluted samples were then loaded onto the PRS column at approximately 1 mL/min. The tubes were then washed with 500uL of wash phase followed by 2mL of wash phase containing

40% methanol followed by 2mL wash phase and allowed to dry all at 1 mL/min. The samples were then eluted using 100mM sodium formate solution, pH 5.0, (400uL) at 1 mL/min. Collected samples were then acidified with 6 M HCL to a final pH of 2.0. The samples were then passed through a 0.45um syringe filter (Chromatography Specialties, Inc.) and frozen at –20˚C until analysis. Pyridinolines frozen under these purified conditions saw little negligible degradation over a period of at least 3 months.

HPLC quantification of Pyridinoline and Deoxypyridinoline

All HPLC mobile phase solutions were passed through a 0.45um filter (Pall Corp.) and initially degassed with vacuum pressure. Subsequent degassing during HPLC analysis was performed by periodic sparging with helium gas using the Waters 600 Multisolvent Fluid Delivery System Unit (Waters Corp.). Since helium is highly insoluble, soluble gases become attracted to the gas phase helium and exit the solution with it. The serum or urine samples were injected in 300uL and 150uL aliquots respectively with an autosampler (WISP 712, Waters Corp.) and trapped on a Polysulfoethyl A guard column (2.1 x 10 mm, 5um particle size, Nest Group Inc.) with the trapping phase driven by a Waters HPLC Pump 515 (Waters Corp.). The trapping phase was 5mM Sodium Formate, pH 2.2, with HCl and a flow rate of 0.5 mL/min. Pyridinolines were eluted from the ion exchange column trap by a column switching mechanism which back flushed the isocratic analytical phase containing 100mM Sodium Formate, pH 5.0, with HCl using a Waters 600 Multisolvent Fluid Delivery System Unit. Analytical phase carrying pyridinolines were then separated on a 2.1 x 250 mm, 5um particle size, mixed mode HPLC column containing both C18 and sulfonic acid surface groups (Primesep 100, Sielc Technologies Inc.) at 0.4mL/min. The pyridinolines were detected using a Waters 474 Scanning Fluorescence Detector set to excitation wavelength of 295nm and emission wavelength of 400nm. Figure 7.0 illustrates how the column switching mechanism functioned to traffic mobile phases. Finally the analytical and trapping column systems were washed at 1 mL/min for 3 minutes using the wash phase containing 100mM Sodium Formate, pH=5.0, and 70% Acetonitrile (Fisher Scientific, Inc.). The column switch mechanism was then reset for sample loading and the analytical column and trap are washed again for 9 minutes at 1 mL/min with the analytical and trapping phase respectively. Using these settings pyridinolines and deoxypyridinolines were detected at 6.0 and 6.5 minutes post injection respectively. The entire procedure analysis of one sample took 20 minutes including column washing and equilibration.

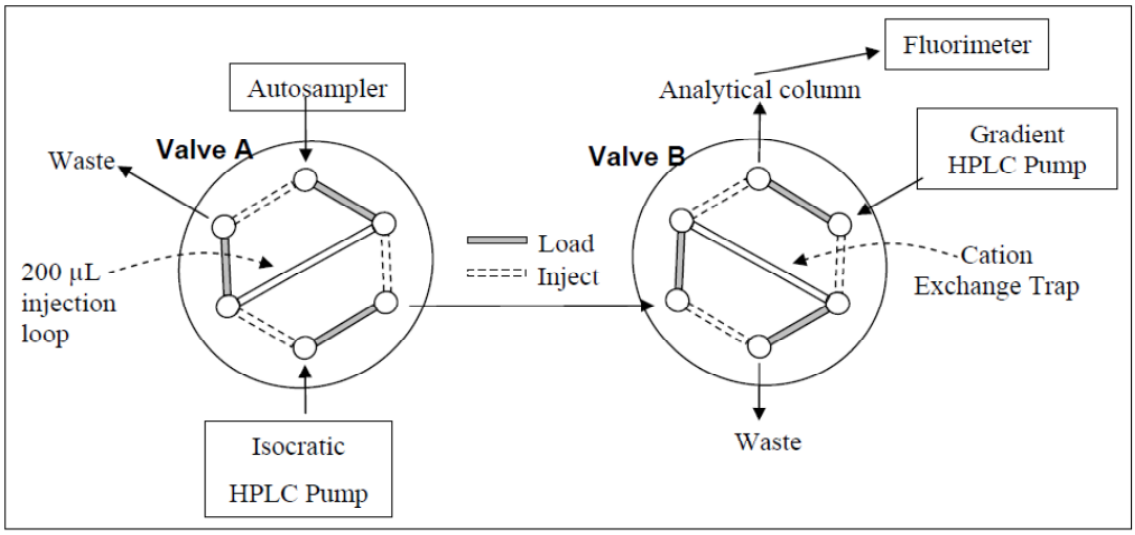

Figure 7.0. Diagram describing the column switching mechanism involved in loading and eluting pyridinolines using HPLC fluorimetric analysis. The autosampler first takes injects the sample into the injection loop. Valve A switches to allow the injected sample to collect on the cation exchange trap. Valve B then switches and the gradient pump back flushes the trap into the analytical column. The analytical column then separates the pyridinolines and allows them to be read in the fluorimeter. The columns are then washed with a mobile phase containing acetonitrile followed by equilibration with the original analytical mobile phase. The valves are then switched back to the original setting for another sample injection.

Preparation of Pyridinoline Standards

Pyridinoline and deoxypyridinoline standards were produced from mouse femurs. C57/Blk6 mice were sacrificed by CO_2 cull and femurs removed. Several femurs were first decalcified in 10% formic acid for 48 hours, rinsed in water, cut into small pieces and homogenized in 5mL of phosphate buffered saline using an Ultra Turrax T25 homogenizer (Staufen, Germany). The bone homogenate (750uL per sample) was then hydrolyzed and extracted using the solid PRS phase as described above. Concentrations of prepared pyridinolines standards were measured against purified standards obtained from Quidel Inc., San Diego, CA.

Mass Spectrometry of Pyridinolines

Samples were separated using the same chromatographic method used above but instead detected in a Micromass Ultima LC-ESI/APCI Triple Quadrupole Mass Spectrometer (Waters Corp.) with electrospray ionization capillary setting of 4.0 kiloVolts, collision energy 28 Volts, desolvation temperature 450˚C, cone gas flow 100L/hr, desolvation gas flow 1036L/hr. Mass Spectrograms were analyzed with MassLynx Mass Spectrometry software (Waters Corp.).

Analysis of Hydroxyproline from Rat Lung Homogenates

The hydroxyproline quantification method was adapted from Kakinuma *et al.* to function with small sample rat lung homogenates (322). Rat lung samples were homogenized in X mL RIPA buffer using a TH homogenizer (OMNI International, Kennesaw GA). The volume of buffer varied depending on the size of the lung sample with 100mg samples requiring 500uL of RIPA buffer. Smaller sized samples down to 25mg of wet weight lung tissue were homogenized in 200uL of RIPA buffer. Of the homogenate solution, a 100uL aliquot was freeze-dried (FreeZone Freeze Drier, Labconco Inc.) in pre-weighed bottles. The rest of the homogenate was used for mRNA and protein western quantification. The dried samples are then weighed again to determine dry sample weight. Lyophilized lung homogenate was then resuspended in 200uL of phosphate buffered saline and 20uL of 50% trichloroacetic acid (Sigma Aldrich, Inc.) was mixed in. The trichloroacetic acid precipitates all proteins from solution allowing many compounds that interfere with HPLC analysis to be removed. The samples were then frozen at -20˚C for 30 minutes and then centrifuged at 1800 rpm in a Sorvall RC-5B High Speed Ultracentrifuge (Thermo Scientific Inc.) using a Sorvall SS-34 Centrifuge Rotor. The supernatant was then removed carefully and the pellet was resuspended in 50uL of 3 M HCl (Fisher Scientific, Inc.) and hydrolyzed overnight in 2 mL Teflon®-lined screw cap test tubes at 110˚C. Hydrolysis frees hydroxyproline into a single amino acid form from soluble and insoluble mature collagen. The acid in the samples was then neutralized by addition of 15uL of 10 M Sodium Hydroxide (Fisher Scientific Inc.). Of the neutralized hydrolysate 25uL was diluted in 175uL of internal standard buffer solution. The internal standard contained 7.5uM L-Homoserine, 20mM Sodium Ethylenediaminetetraacetate (EDTA), 50 mM Sodium Tetraborate, pH 8.0 (Sigma Aldrich, Inc.). Of the internal standard diluted sample, 30uL was added to 10 uL of 10 mM 4-fluoro-7-nitrobenzofurazan in acetonitrile (Sigma Aldrich, Inc.). The derivatizing reaction is heated to 60˚C for 1 minute and then placed on ice and quenched with the addition of 40uL of 0.05 M HCl. This derivatizes the amino acids with a fluorophore that is easily detected.

Of the derivatized amino acid solution, 10uL is injected by an autosampler (WISP 712, Waters Corp.) with an isocratic mobile phase of 25 mM KH_2PO_4, 8% acetonitrile, pH 5.0, which is driven at 0.8mL/min by a Waters HPLC Pump 515 (Waters Corp.). A Waters Sunfire C8 guard column with dimensions 3x2mm, 3.5um particle size was placed in

front of the separating column. The sample was separated in a Waters Sunfire C18 HPLC column with dimensions 20cmx4mm, 5um particle size (Waters Corp.). The retention time for derivatized hydroxyproline and homoserine was 9.8 and 14.8 minutes respectively detected with a Waters 474 Scanning Fluorescence Detector (Waters Corp.) set to excitation wavelength of 470nm and emission wavelength of 540nm. The amount of dry lung tissue used in this analysis is between 1 and 2 mg. Quantification of hydroxyproline performed based on standards of pure hydroxyproline purchased from Sigma-Aldrich Inc.

Analysis of Serum ICTP and PIIINP

Human serum samples stored in a -70˚C freezer were warmed as noted above. PIIINP and ICTP collagen peptides were analyzed by UniQ PIIINP and UniQ ICTP radioimmunoassays (Orion Diagnostica Oy., Espoo, Finland) respectively. The radioimmunoassay uses two different antibodies. Antibody A, which is specific for the protein peptide and the second radioactive labeled antibody B that is specific for the variable domains of the antibody A. In the first step, the antibody A binds to the protein peptide in the sample. The excess antibody A is then bound to the antibody B. The large complex formed by binding antibody A to radiolabelled antibody B is then precipitated, leaving the soluble antibody A and B to be washed away. The amount of radioactivity is then read using a D5005 Cobra II automatic gamma counter (Packard Inc.). Since the radioactivity of the antibody B is known, the amount of protein peptide is calculated by subtracting total antibody B used in the first step from the final counted antibody B.

Statistical Analysis

All data was reported in means plus standard deviations except for the intra-assay variation which shows the same sample repeated 9 times as a bar plot. Statistical significant difference between groups was performed by one way ANOVA with Tukey's post hoc analysis. In all cases, p values less than 0.05 were considered significant.

7.3 Results of Collagen Turnover Markers in Lung Fibrosis

A facile experimental method for pyridinoline quantification

Although collagen crosslink pyridinolines can be detected by an enzyme linked immunosorbent assay, this assay only yields the total quantity of Pyd and Dyd. Because of this difficulty, HPLC analysis is the gold standard for the quantification of collagen crosslinks from any solution. We set out to analyze collagen crosslinks as markers of mature collagen breakdown during the resolution of an established fibrotic scar. The resolution of a mature scar would be one of the most important outcomes determining clinical efficacy of an antifibrotic therapeutic. As we began working out a quantitative HPLC method for pyridinolines we noted that the published and established methods being used were irreproducible in our hands. We then formulated a novel method for pyridinoline quantification taking advantage of two important aspects of these molecules. Pyridinolines are positively charged and strongly fluorescent. Another complication of pyridinoline analysis is the interference of large quantities of interfering compounds in blood serum. In order to remove the majority of the unwanted proteins and compounds from serum we used an ultracentrifugation filter with a molecular weight cutoff of 30 kDa. This removes most blood proteins, especially albumin leaving the collagen fragments and pyridinolines in the filtrate. Serum is has especially trace quantities of pyridinolines which on average in normal individuals are 3.2 pmol/mL and 0.61 pmol/mL for Pyd and Dyd respectively (323). Urine concentrations of pyridinolines are on the level of 50 and 8 pmol/umol creatine for Pyd and Dyd respectively (323). In practical terms, 750uL of even highly dilute urine contains sufficient pyridinolines for quantification our method. In the case of serum, between 8-10 mL volumes are often needed for quantification. High quality ultracentrifugation filters can also be costly for large quantities of samples, making serum pyridinoline analysis less practical. Sinigaglia *et al.* noted however that urine and serum pyridinoline concentrations mirrored each on distribution, making urine analysis a preferable choice (323).

We noted that the quantity of hydrochloric acid needed to break down peptide bonds did not need to be at the high 6 Molar concentration. Hydrochloric acid concentration of 3M had the same efficiency of acid hydrolysis. This allowed for less reagent use and less dilution upon neutralization with sodium tetraborate buffer. Following hydrolysis, urine samples yielded insoluble char fragments which flowed freely or adhered to the

sides of the glass vessels. These char fragments were removed by centrifugation of the hydrolysate in a microcentrifuge. Following neutralization with sodium tetraborate solution, the samples had a pH of 2.5 were loaded in into a pretreated cation exchanging solid phase extraction column. This step is essential to remove the bulk of unwanted and potentially reactive chemicals that could plug or damage the HPLC column or instrumentation. Since pyridinolines are positively charged they were retained on the cation exchanging resin at pH 2.5. The column was then washed with mild wash phase of sodium formate at pH 2.5 with HCl, followed by wash phase with 40% methanol, and finally equilibrating with the original wash solution. This removed most of the colour from the column and all of the strongly interfering compounds. The

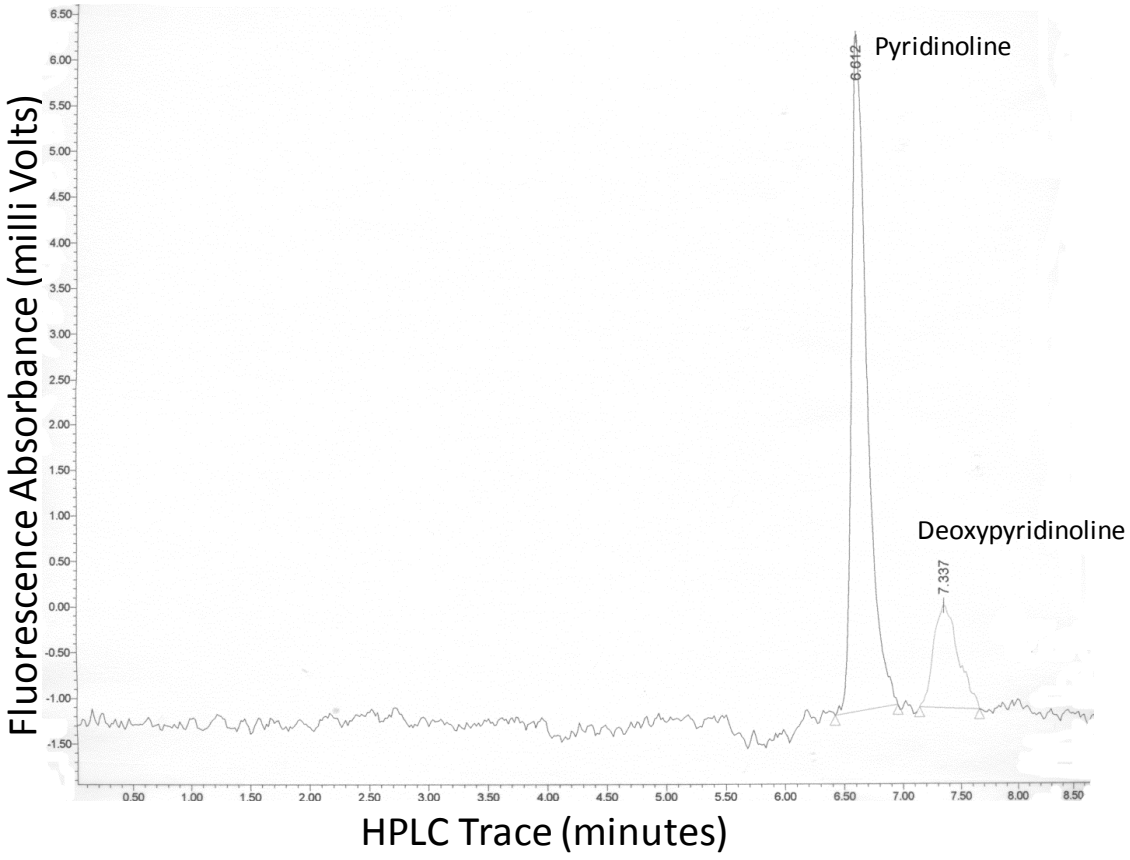

Figure 7.1. Typical fluorimetric absorbance trace of HPLC for pyridinolines from a human IPF serum sample. The fluorimeter detects pyridinolines with an excitation light wavelength of 295nm and emission reading wavelength of 400nm. Pyridinoline and deoxypyridinoline retention time on the column was 6.6 and 7.3 minutes respectively. The area under the chromatogram curve is directly proportional the amount of chemical in the original sample.

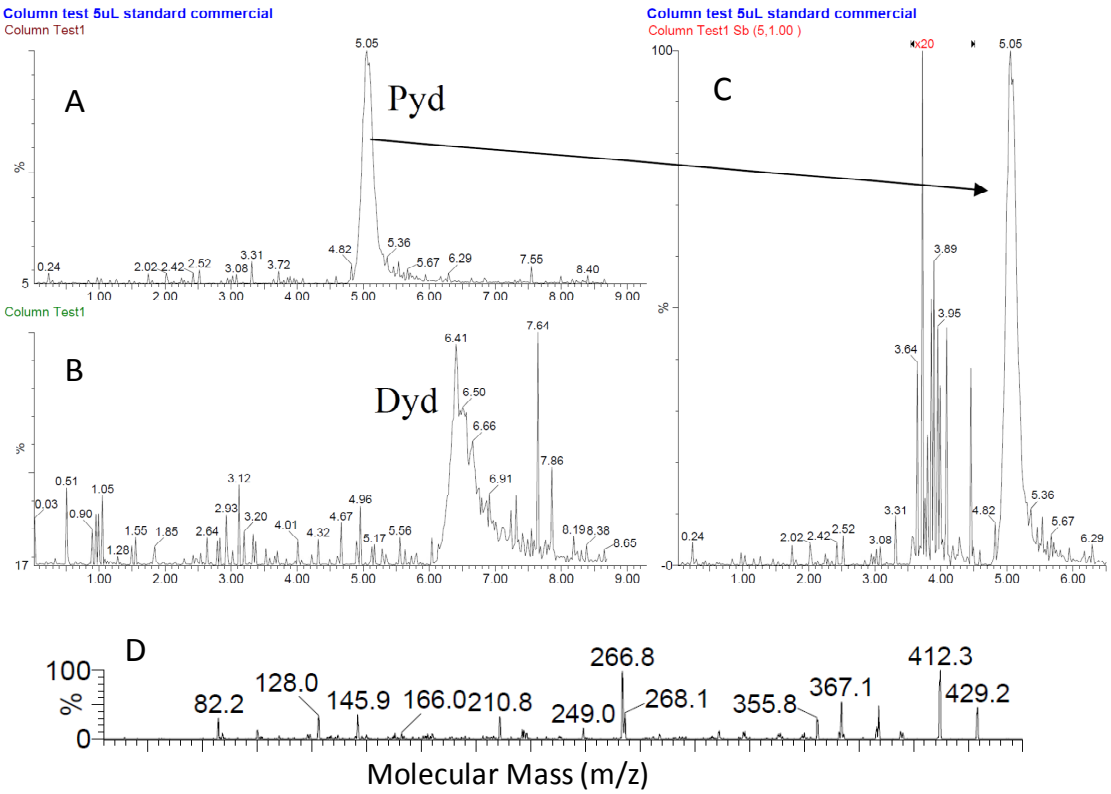

Figure 7.2. Liquid chromatography of Pyd/Dyd mouse bone standard with a mass spectrometer signal detector (LC-MS). Panel A and B: The mass spectrometer was set to detect only two masses: the 267 m/z fragment of Pyd (molecular mass 429.2 g/mol) and the 267 m/z fragment of Dyd (413 g/mol). Panel C: Part of the background of chromatogram from panel A was multiplied by 20 to assess the signal to noise ratio for the Pyd peak which was approximately 20 to 1. Panel D: MS-MS spectrum of Pyd/Dyd commercial standard. Note the 429.2 m/z represents the Pyd parent compound and the rest are the breakdown products. The most prominent fragment was at 266.7 m/z. Dyd at 413 m/z was not detectable by this mass spectrometric method.

column was then air dried by vacuum followed by elution with 400uL of sodium formate solution at pH 5.0. At this pH the column releases the pyridinolines. The volume of eluant from the solid phase extraction varied and needed to be recorded for final correction. At pH 5.0, the sample is too basic and needed to be re-acidified with a small aliquot of HCl. After this the sample wash filtered through a non-binding 0.45um syringe filter. This filter is an important step which removes any particles from the samples which may begin to build up in the HPLC instrumentation. Finally, the complete sample was loaded as a 300uL injection into the HPLC column using an auto-sampler.

The sample transits first to the ion exchange trap were it is bound during the large volume injection. After sample is bound the mobile phase is switched to allow the analytical phase through the back of the trapping column (Figure 7.0). The analytical

column separates the pyridinolines which are detected by fluorimetry. Figure 7.1 shows a HPLC fluorimetry trace of a sample of human serum. The signal to noise ratio for typical detection of pyridinolines was 120 to 1. The identity of the pyridinolines analyzed by this method was verified by mass spectrometric analysis. Figure 7.2 illustrates that the peaks in Figure 7.1 correspond to the correct molecular weight of pyridinoline and deoxypyridinoline major fragment with m/z 267. Further analysis of

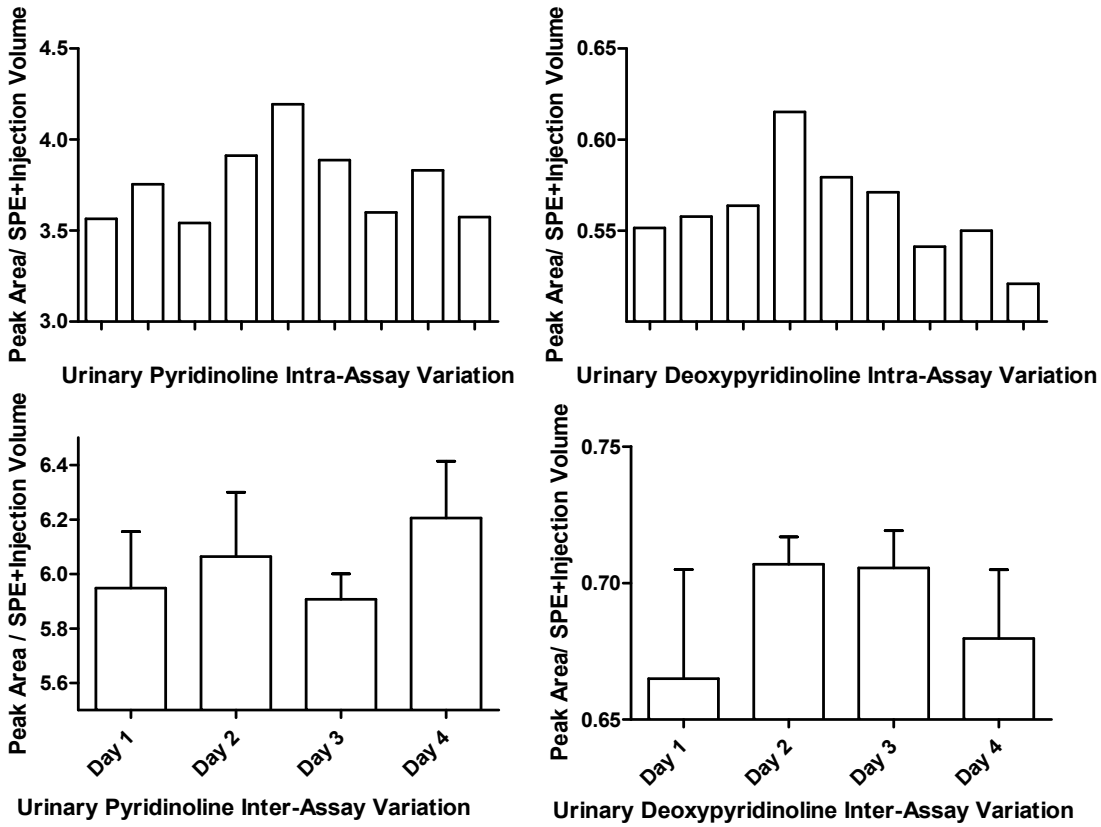

Figure 7.3. Intra and inter-assay variation for urinary pyridinolines measured by HPLC analysis. The intra-assay coefficient of variation was 5.7% and 4.7% for Pyd and Dyd respectively. In the urinary inter-assay variation experiment, the means of groups did not reach statistic significant difference for either Pyd or Dyd by one way ANOVA analysis. Percent recovery of a standard added to a urine sample was 97.8% and 95.8% for Pyd and Dyd respectively.

the pyridinoline peak indicated that mass spectrometric spectrum corresponded to the fragment spectrum reported previously (324). Intra-assay variation in a urine sample analyzed for Pyd and Dyd nine times indicated that there was a 5.7% and 4.7% coefficient of variation respectively. Inter-assay variation of a urine sample analyzed five times on four separate days indicated that there was no statistical difference

between the means by one way ANOVA. Figure 7.3 describes the data from the variation analysis. Of a pyridinoline standard spiked into a urine sample, 97.8 and 95.8 percent recovery were achieved for pyridinoline and deoxypyridinoline respectively. In order to quantify pyridinolines in samples, a standard line needed to be drawn. Figure 7.4 illustrates standard lines for pico mole quantities of pyridinolines analyzed by either constant volume or variable volume injections. That variable injections yielded similar values to constant volume injections indicates that the trapping column collects all of the pyridinolines regardless of the injection method used.

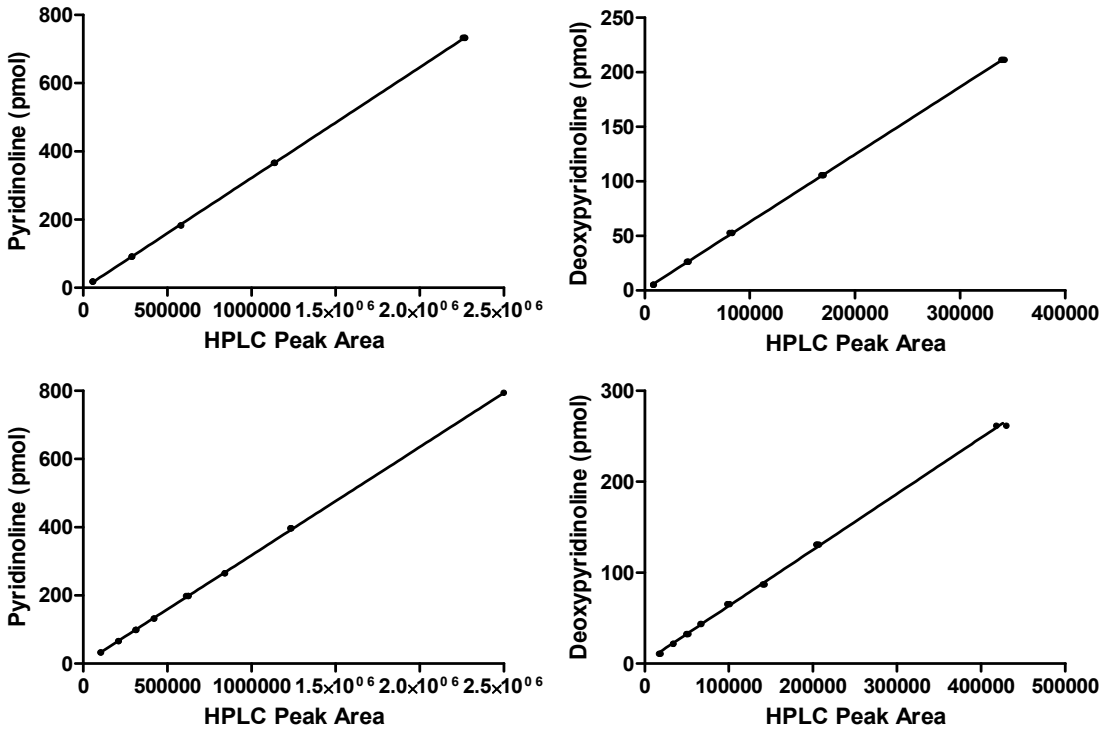

Figure 7.4. Pyridinolines and Deoxypyridinolines standard lines by HPLC analysis. The top and bottom represent constant and variable volume standard injections respectively. Linear regression fit to all of the above lines (R^2) was 0.999.

With a method for pyridinoline analysis established we then set out to investigate the concentrations of pyridinolines in IPF serum. We analyzed serum of 8 IPF patients and 4 age matched healthy controls. Figure 7.5 shows that there is a significant increase deoxypyridinoline but not in pyridinolines. The ratio of pyridinolines to deoxypyridinolines was also significantly decreased in IPF serum. This is interesting

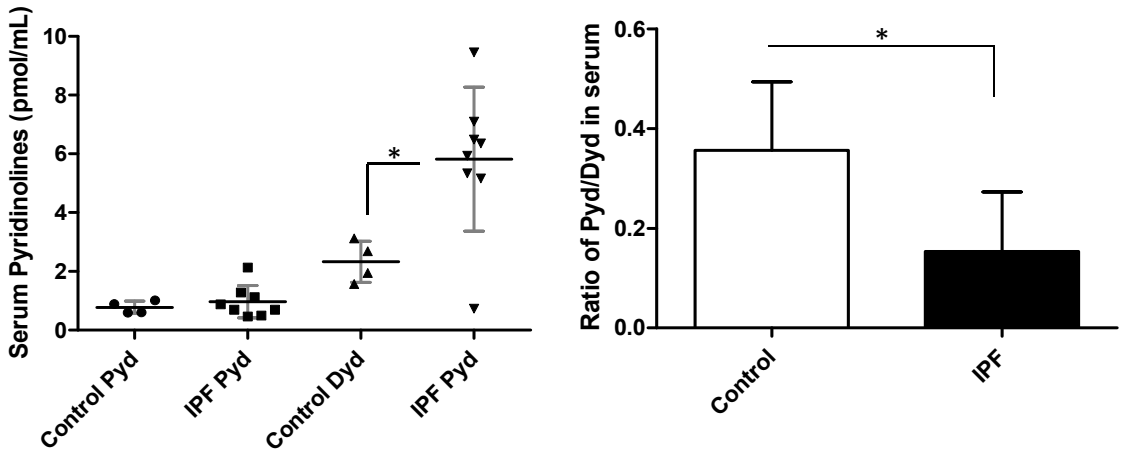

Figure 7.5. Serum Pyridinolines from healthy human controls and stable IPF patients by HPLC analysis (left). There was significantly more Dyd in IPF serum than in healthy controls, * $p<0.05$. The ratio between serum Pyd and Dyd in healthy controls and IPF patients (right). There was a significant decrease in the ratio of Pyd to Dyd in IPF patients, * $p<0.05$.

since logically both types of pyridinoline crosslinks should be upregulated during in the conditions of progressive fibrotic scarring.

In order to understand how collagen accumulation and maturation affect the fibrotic process we sought out to reproduce and adapt a method for analyzing hydroxyproline accumulation from small tissue samples (322). This method involves HPLC and derivatization of hydroxyproline with 4-fluoro-7-nitrobenzofurazan. The 4-fluoro-7-nitrobenzofurazan reaction creates fluorophore containing adducts with primary amines groups. These fluorophore adducts are then read easily following HPLC separation on a C18 column via fluorescence detection. The method described by Kakinuma et al. was changed to simplify its use with rat or human lung biopsy samples. Lyophilized tissue samples were resuspended in trichloroacetic acid to precipitate all proteins from the solution followed by freezing and ultracentrifugation. This allows the removal of all left over interfering sample components while minimizing any hydroxyproline loss. This method analyzes only hydroxyproline incorporated into a protein. This precipitation step also minimizes the volume of acid required for hydrolysis and subsequent neutralization. The acid hydrolysis step was changed to 3 M HCl from 6 M and the removal of acids following hydrolysis was achieved by neutralization with sodium hydroxide. Using 3 M HCl was sufficient to break down all peptide bonds after overnight boiling. Figure 7.6 shows an HPLC trace of a hydrolyzed rat lung sample and another identical sample spiked with pure hydroxyproline. Derivatized homoserine was to be

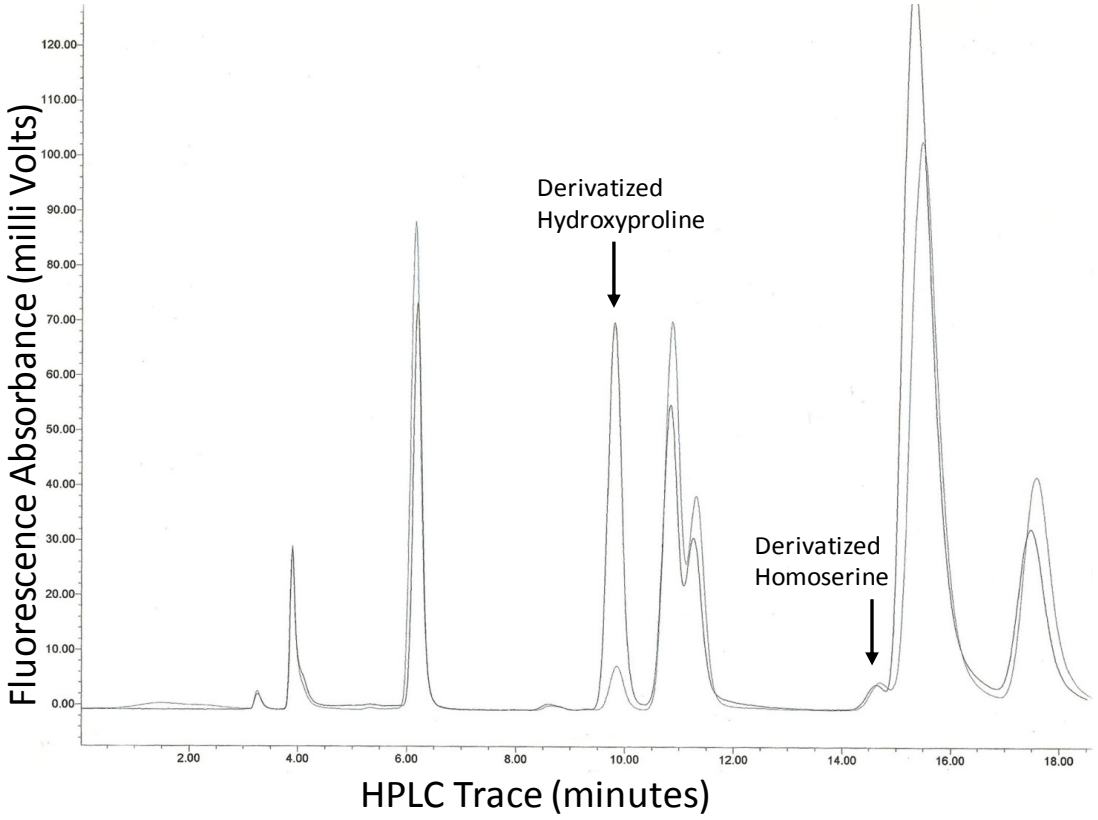

Figure 7.6. HPLC analysis of hydroxyproline in a rat lung homogenate sample and the same sample spiked with pure hydroxyproline standard. Retention time for hydroxyproline and homoserine was 9.8 and 14.7 minutes respectively. Samples were derivatized with 4-fluoro-7-nitrobenzofurazan which yields fluorophore containing adducts with excitation at 470nm and emission at 540nm. Homoserine was used as the internal standard. In this figure, more homoserine was needed to produce a stronger signal for reproducible quantification.

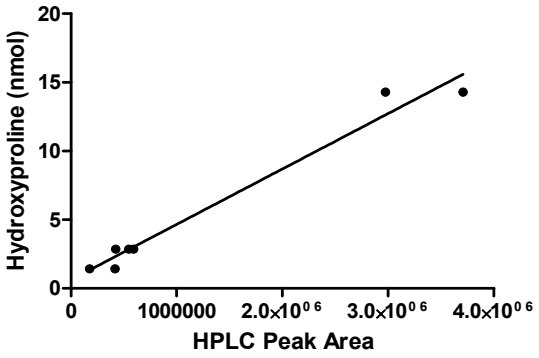

Figure 7.7. Derivatized hydroxyproline standard line by HPLC analysis. Linear regression fit (R^2) was 0.973. This standard run was incomplete since the fluorimeter light broke near the end of the sample list.

used as an internal control but was in lower than desired quantity in this trace. Standard line analysis of this hydroxyproline HPLC analysis revealed a good fit with linear regression analysis (Figure 7.7).

Next we quantified the synthesis of collagen III and the breakdown of collagen I in human serum samples. This was accomplished by radioimmunoassay of procollagen III N-terminal propeptides and collagen I telopeptide. The portion of procollagen III that is analyzed by this method is a portion that is released following synthesis of the protein. The telopeptide is released from the collagen type I molecule following its tissue proteolysis. We looked at the serum of 7 healthy controls, 4 patients with rheumatoid arthritis, 4 patients with non-specific interstitial pneumonia, 21 stable IPF patients, 4 patients with acute exacerbations of IPF, and finally 3 patients with scleroderma. Figure 7.8 shows that there was no significant difference amongst groups in PIIINP analysis. Figure 7.8 also shows a marked upregulation of ICTP in the serum of IPF and scleroderma patients. This analysis suggests that it is not the synthesis of collagen but the breakdown that is disordered in the context of advanced tissue fibrosis.

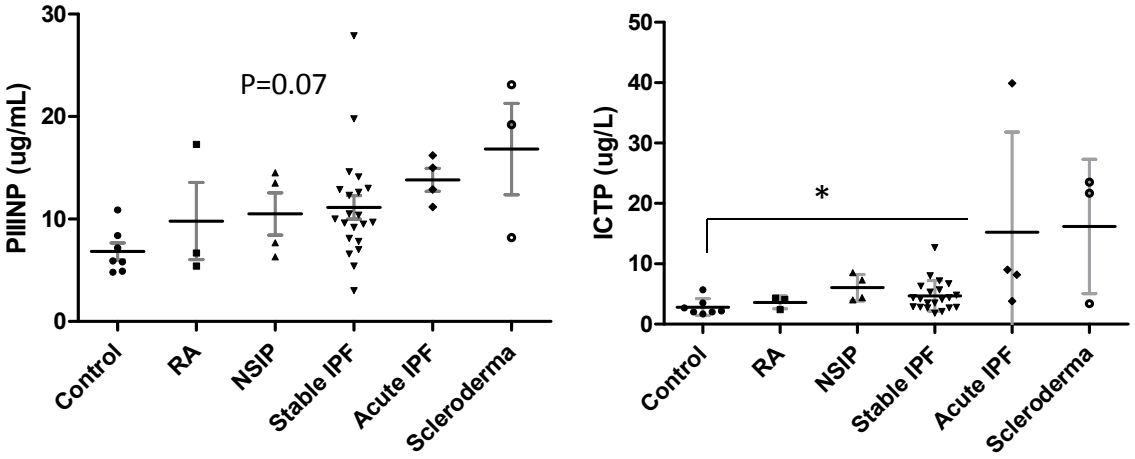

Figure 7.8. Human serum PIIINP(left) and ICTP(right) from various patient groups assayed by radioimmunoassay. The means in ICTP but not the PIIINP graph were significantly different when analyzed by one way ANOVA, $p<0.05$. Tukey's post hoc analysis showed significant difference between the control and both acute IPF and scleroderma groups, and between stable IPF and acute IPF groups, * $p<0.05$.

7.4 Discussion of Collagen Turnover in Lung Fibrosis

This chapter endeavors to ask how collagen is produced and removed from lung tissue and the nature of collagen turnover. To answer these questions we first produced a novel method for the quantification of pyridinolines from urine and serum samples. This method proved useful for the analysis of IPF patient samples. Pyridinolines in IPF serum revealed a marked increase in deoxypyridinoline instead of pyridinoline. This was unexpected since regular pyridinoline crosslinks predominate over deoxypyridinolines in normal non-bone soft tissue (323). How and why deoxypyridinoline is upregulated in IPF serum is not known but this effect could be important to the overall turnover of collagen in advanced fibrotic disease. To our knowledge our data is the first to show serum deoxypyridinoline increases and a discrepancy in pyridinolines ratios in IPF.

The method we produced to analyze pyridinolines could easily be modified to look at tissue crosslink content. The equipment used in this method is fairly universal and easy to use. One drawback of this method was the quantity of serum needed to detect pyridinolines. Some control serum samples had vanishingly low levels of pyridinolines in a 10mL volume. Hydrolysis of larger volume samples was a practical difficulty. Also, ultracentrifugation filtration of larger serum samples was problematic. Amicon centrifugation filters often plugged up and were later replaced with Centricon ultracentrifugation filters from Millipore Inc. These Centricon filters are angled with respect to the force of centrifugation which allows for sideways filtration when the lowest areas of the filters become plugged. Altogether, this method could not be used to monitor serum pyridinolines in animals due their lower blood volumes. However, human serum and rodent and human urinary pyridinolines are readily detected by this method. Modern equivalent HPLC analysis with narrow bore capillary columns could be easily adapted to use our proposed method and would further increase sensitivity and sample throughput speed. It is likely that narrow bore columns would produce the needed sensitivity for detection of serum pyridinolines. Urinary pyridinolines also need to be measured against urinary creatine levels to account for kidney filtration function (323).

Hydroxyproline content in lung tissue samples is also an important measurement for understanding collagen metabolism. To analyze IPF biopsies and small rodent lung slice samples we looked at the use of HPLC methods in hydroxyproline quantification. We

found and successfully adapted a method first described by Kakinuma *et al*. in 1997. This method, uses 4-fluoro-7-nitrobenzofurazan to create adducts with primary amine groups and allowed for hydroxyproline quantification in 1 milligram samples. Smaller samples could have been analyzed as well since the homoserine standard dilution prior to fluorophore derivatization could have been reduced.

For the detection of serum collagen peptides in fibrotic disease patients we used a radioimmunoassay. Assaying various fibrosing patient populations showed an increase in ICTP, a collagen type I breakdown product. PIIINP which corresponds to type III collagen products released during synthesis were not upregulated. These data and data from serum pyridinolines in IPF patients paint an interesting picture in which the breakdown of collagen, not its synthesis is abnormally increased. This is counter intuitive since it is generally held that collagen synthesis is increased during lung fibrosis. While this may be true we extrapolated that lung collagen turnover may be maintained more by its breakdown then its production. More detailed analysis of collagen turnover in animal models of lung fibrosis is warranted to better understand what role collagen breakdown plays in collagen metabolism.

8.0 Thesis Discussion

8.1 Preamble

The main focus of this thesis has been on the activation of transforming growth factor beta in relation to fibrotic processes in the lung of experimental animal models and in human IPF tissue. This single cytokine protein is so important to organ development (36, 37), immune tolerance regulation (35), and the pathogenesis and persistence of tissue fibrosis (30), that many have devoted their lives to studying its biology. Here we focus on one aspect of its activation in the context of pulmonary fibrosis. Knowledge described here about the mechanical or ventilation induced activation of TGFβ involving integrins, serine proteases, and MMPs provides data that will be important to the establishment of an anti-fibrotic drug. Our experience with the rodent lung strip tissue bath model has lead to many conclusions about the nature of mechanical TGFβ activation and its possible impact on tissue fibrosis biology.

In order to focus on the bigger picture of the pathobiology of pulmonary fibrosis, our laboratories devoted a great deal of effort into making our analysis of anti-fibrotic drug regimes more relevant to clinical outcomes. It is our belief that the data from non-invasive evaluations of lung fibrogenesis involving small animal CT imaging, PET imaging with metabolically active radioactive proline probes, lung functional testing with rodent ventilators, and exercise testing will lead to higher quality interpretation of intervention studies. Our experience with these non-invasive tools has lead to the conclusion that an anti-fibrotic drug will need to do much more than correct the mismanaged accumulation of collagen. A concerted effort is now needed in the lung fibrosis field to use the enhanced tools and models we've described to address the pathobiology of TGFβ, including its mechanical activation, and other IPF relevant systems identified by others. Although our laboratory has excelled in the development of lung fibrosis modeling and intervention analysis, our focused efforts have required others to fill in the important gaps involving mechanisms, drug design, and production. Together, we believe a drug regime can be produced to have significant clinical applicability.

Although collagen turnover markers have attracted little attention over the past 25 years, their importance is now becoming clearer. We found that collagen breakdown products were elevated in IPF serum while synthesis products were unchanged. These

observations do not conform to conventional understanding of IPF disease and provided evidence revealing that IPF could be a disease more involved in collagen breakdown rather than collagen accumulation. These results, and the methods developed for urine and serum pyridinoline quantifications tie together with the rest of this thesis as an added tool to identify, at the molecular level, whether or not mature collagen breakdown is occurring in an anti-fibrotic therapeutic drug invention study. We believe that for any drug to have the desired effect in reducing lung stiffness in a lung functional test, it must first loosen the tight knit collagen crosslinking. Pyridinolines could also be evident in the urine of IPF patients and could provide a higher quality interpretation of clinical or pre-clinical data.

8.2 Thesis Discussion on Mechanical TGFβ Activation

TGFβ activation, as noted before, is a complex topic involving all aspect of biological regulation from the level of promoter control to the level of post-translation modification. We found that in the context of lung tissue fibrosis, TGFβ can be mechanically activated by placing physical tension on the tissue. This tension not only liberated the small TGFβ cytokine from its latency associated complex in the extracellular matrix as suggested by Hinz *et al.*, but allowed the cytokine access to its cell surface receptor (50). The mechanical stimulus released active TGFβ in the tissue and caused the accumulation of the downstream signaling molecule phospho-Smad2 in the nucleus of fibrotic lung cells. We found that TGFβ activation was dependent on time and intensity of mechanical stimulus, as would be expected in a biological signaling process. Protease inhibition during mechanical stimulus of fibrotic tissue yielded the same amount of active TGFβ as uninhibited mechanical stimulus. To understand the impact of TGFβ mechanical activation on intact lungs we designed an *ex vivo* lung ventilation model. Following a significant increase in ventilation pressure, fibrotic lungs responded by the accumulation of downstream phospho-Smad2. These data illustrate how mechanical TGFβ activation could contribute to stimulating the fibrotic process. We analyzed lung biopsies from normal and fibrotic patients and found that the same post-translation activation of TGFβ and subsequent downstream phospho-Smad2 signaling events occurred as in the rodent models. At all levels of experimentation, control lungs did not produce detectable quantities of TGFβ protein nor had a significant

impact on nuclear phospho-Smad2 accumulation. These observations indicate that mechanical TGFβ activation is likely confined to an abnormal wound healing process.

ECM adhesion receptors are a large diverse group including integrins, selectins, and cadherins which link themselves with the cytoskeleton. During the fibrotic process, cell surface αV integrins receptors are required to release active TGFβ by binding to the LAP peptide in the ECM (48, 50). Integrin associated Src and focal adhesion kinases function to send force related signals from the ECM to the nucleus (325). Integrin signaling can lead to nuclear factor-κβ (NF-κβ) nuclear accumulation through the breakdown of the inhibitor of kinases of NF-κβ (IKK). NF-κβ signals to increase expression of pro-inflammatory molecules such as IL-8 and IL-6 and is thought to be an important stimulus in ventilator induced lung injury (326).

It is likely that the rhythmic motion of the tidal pressure acting on the lungs translates into a cell stimulating response as the organ strives to maintain elasticity. Cells are known to respond to outside stimuli by activating stretch dependent Ca^{2+} ion channels (202). The cytoskeleton itself is capable of detecting cell wide mechanical tension which is translated in to intracellular calcium ion concentration cycles through TGFβ signaling (205). Smad2, the prototypical TGFβ signaling molecule links itself to the actin cytoskeleton. Disruptions in cytoskeletal structure release Smad2 allowing it to be phosphorylated by the TGFβ receptor (61). TGFβ can also directly affect calcium cytoplasmic concentration cycles directly through activation of the inositol triphosphate pathway (79). It is likely that other yet to be discovered cytokines and pathways exist with unique but opposing effects to the TGFβ mechanotransduction signal. Other cytokine pathways that have been implicated in mechanotransduction are the Wnt/β-catenin pathway. The Wnt/β-catenin pathway has been shown to be activated by mechanical tension in the context of acid induced ARDS rodent models (219). It is unclear whether cross-talk between the TGFβ and Wnt pathways is responsible for mechanical induced β-catenin response or if this response functions independently.

The model we developed held certain drawbacks that became evident earlier on. We found that repetitive stimulation of an individual *ex vivo* fibrotic lung strip produced highly variable results. This made serial analysis under intervening conditions problematic at best. It would seem from our observations that TGFβ activation from the tissue following mechanical stimulus continues for a prolonged period. This made

simply washing the tissue and re-probing with intervention drugs next to impossible, since the TGFβ continues to come out of the tissue. We found that using protease inhibitors was one example that limited further continuous activation of TGFβ after an initial stimulus. We can only surmise that acute mediator proteases involved in wound healing are activated following initial mechanical stretch, which perpetuate further TGFβ activation.

The use of contractile agonists for *ex vivo* fibrotic lung strips was another example of the difficulty of interpreting serial stimulation results. Endothelin-1 and Angiotensin-2 both seem to activate TGFβ from fibrotic tissue strips. ET-1 produced far more reproducible results than AT-2. AT-2 has been noted by others to produce lower amplitude contraction forces than ET-1 in skin granulation tissue (327). It may be that AT-2 mediated contraction simply lacks the strength to elicit a robust response that could be identified using our readouts. If this is true, analysis of smaller tissue samples with a more sensitive force transducer could illuminate slight contraction mediated by AT-2. Such experiments with narrower ~100 micrometer width tissue would involve first inflating lung tissue with agarose for it to be cut using a vibrotome. Also, placing delicate 100 micrometer wide strips into a tissue bath without tearing it would be impossible. At this level of width, any force exerted would have a more profound effect on the resident cells since there is less mass in the specimen to dissipate the force of adjustments during bath positioning. ET-1 however produced a pronounced effect that could be followed more robustly at the millimeter tissue width level. As noted earlier, ET-1 caused the tissue contraction and subsequent release of active TGFβ. Even after many attempts, we could not show reproducible downstream accumulation of nuclear phospho-Smad2. In order to improve our understanding of the tissue contraction model, we tried to find a way of reducing the ET-1 mediated contraction amplitude following Y-27632 mediated Rho kinase inhibition. We were able to reduce the average contraction of tissue strips by approximately 40-50% inconsistently. We discovered that lung parenchymal tissue contraction by ET-1 could not be readily relaxed by washing the tissue and continued for at least 2 hours. A second administration with ET-1 causes inconsistent contraction events and even more inconsistent TGFβ release. This made past contraction intervention studies not interpretable. After much trial and error, intervention studies are now being addressed by increasing the study lung strip n

number to overcome issues with robustness and assessing only one stimulus or stimulus plus inhibitor per lung strip specimen.

Reactive oxygen species have been shown to be important activators of TGFβ in human lung fibroblast cells (149, 150, 328). An IPF drug trial involving anti-oxidant N-acetyl cysteine showed that there may be some benefit in delaying progression of the disease and preserving lung function (152). We tried testing N-acetyl cysteine's effects on the activation of TGFβ in the context of the ex vivo lung strip bath. Instead we found that mechanical activation could not reproduce a similar TGFβ response twice in the same fibrotic lung strip. Our data with N-acetyl cysteine was thus inconclusive. However, we did not note any sudden changes in TGFβ released from the tissues. If N-acetyl cysteine has an effect on mechanical TGFβ activation it will be slight and difficult to ascertain.

In order to test whether latent TGFβ stores could be activated mechanically in lungs from a "quiescent" state, we delivered Ad latent $TGF\beta_1$ by intratracheal administration into the rat (30). We found that even though latent TGFβ was expressed in large quantities, a least some of this protein could be activated by mechanical stimulus in the tissue bath. This latent TGFβ also caused the nuclear accumulation of phospho-Smad2 in the lung cells. Nuclear accumulation of phospho-Smad2 caused a trend toward increasing early TGFβ responder genes PAI1 and CTGF without reaching statistical significance, likely the result of tissue mRNA degradation. We chose this model to test early responder genes since we knew that PAI1 and CTGF are already upregulated in the context of the Ad active $TGF\beta_1$ model at this time point. We hoped that a lower baseline signal for PAI1 and CTGF in the Ad latent TGFβ model would allow us to better see changes upon mechanical stimulation. It is important to note that this model is not associated with hallmark fibrotic histomorphologic changes which lead to collagen accumulation. We did however note that there was a slight but significant increase in tissue stiffness in this model. This indicates that at some lower level, latent TGFβ was impacting tissue architecture. These results point to the availability of latent TGFβ as being sufficient for the induction of mechanical activation events, which might be a model for early phase TGFβ activation in the pathogenesis of IPF.

In conclusion, mechanical TGFβ activation works via ventilation forces, and possibly though cell contractile agonists, during strong inhibition of serine proteases and signals through phospho-Smad2 to the nucleus of fibrotic lung cells. In the context of other

known methods of TGFβ activation, mechanical activation stands apart. We know that this method is limited to the context of a fibrotic disease process, unlike other methods which are also present in normal tissue biological functions. This finding could be highly significant for therapeutic design as mechanical activation represents a method of TGFβ biology that could be modulated without affecting normal and protective TGFβ function elsewhere in the body.

8.3 Thesis Discussion on Non-Invasive Evaluations of Lung Fibrosis

We have observed that preclinical trials for lung fibrosis have yielded improper conclusions based on standardized readouts. The normal model used for studying lung fibrosis, bleomycin instillation, adds yet another confounding factor to the disconnection between pre-clinical and clinical trial findings. The bleomycin intratracheal instillation model is foremost an inflammatory response, which may or may not exist in IPF pathogenesis, which results in tissue injury and subsequent fibrosis (115, 171). Bleomycin modeled lung fibrosis is also more variable in severity among animals and is reversible over time (281). When the inflammatory phase of bleomycin fibrosis is inhibited, the subsequent fibrotic phase is curtailed (115). When the fibrotic phase of bleomycin fibrosis is targeted, the results are invariably read by differences in collagen deposition. Collagen deposition rates, although important, have no clinical correlative counterpart. The disparity between clinical and pre-clinical trials is very likely due to this difference in readouts. We have observed that total lung collagen deposition tells one little of the overall lung health of the animal. In order to power studies with high quality interpretations for pre-clinical trials, we sought out a new approach to bridge the gap from the rat to the human. Human lung fibrosis trials investigate changes in lung function as a primary indicator for health improvement along with CT scanning and exercise testing (23, 250, 253, 254).

We found that rats given Ad TGFβ_1 modeled lung fibrosis could be followed by lung function parameters, CT imaging, and possibly exercise testing in a manner that correlated with histomorphometric scoring. These tests were superior to classical analysis since they could be repeated within the same animal over the course of the disease. The non-invasive nature of these measurements allows the researcher to analyze the appropriate onset of fibrogenesis during model progression before adding a

drug, ensuring that a fibrogenic response is occurring before treatment. This is important because the variability in lung fibrosis models can lead to errors, especially when depending on total collagen quantification at the end of a therapeutic pre-clinical trial. We found that lung functional parameters were good indicators of the overall health of the rodent during the fibrogenic process. Although maximal oxygen consumption during exercise did not correlate with histological Ashcroft scoring, we still consider this tool of great importance for indicating the health of the rodents. Young adult rats used in this model may have been too fit at the beginning of the experiment. Older animals are known to be more susceptible to lung fibrotic models than younger adults (329, 330). It may be that exercise testing will be able to show significant differences in lung health improvement if the fibrotic model were changed to focus on older, less fit animals.

The use of radiolabelled proline metabolic PET imaging could also yield higher quality investigative information for lung fibrosis research. Since the intensity of proline incorporation into the lungs is dependent on the rate of collagen synthesis, the metabolic effects of an anti-fibrotic therapeutic can be measured in real time (266, 267). These markers have shown enhanced uptake in the lungs during the fibrogenic process in animal models (268, 269).

Collagen promoter reporter mice similar to those employed by Fragiadaki *et al.* could very easily be adapted for use in studying lung fibrogenesis (256). Using LacZ as a reporter gene is not well adapted to non-invasive evaluation of fibrogenesis since assays of beta-galactosidase activity all require euthanasia. A better approach would be to engineer a mouse with a collagen promoter expressing an easily traceable surface antigen such as DYKDDDDK with a cell surface transmembrane domain and location signal. The collagen promoter could also be replaced with the TGFβ responsive elements of the PAI1 promoter as a marker of direct TGFβ signaling activity (208). A PET isotope labeled antibody specific to DYKDDDDK would then injected into the blood stream of the mouse during a fibrogenesis model and subsequently imaged upon binding to the surface of collagen or PAI1 expressing cells. Under these conditions, a drug efficacy trial could monitor the amount of collagen or PAI1 expressing cells in the lung in real time.

Even if these mice are not PET imaged, the reporter activity would make the quantification of fibrogenesis process more standardized for objective analysis during a drug treatment trial. For example, collagen content is most often used as a marker of fibrosis severity and a primary outcome of any anti-fibrotic pre-clinical trial is to indicate the remission of collagen production. However, tissue collagen content alone cannot indicate if the tissue is currently going into disease remission or if more collagen is being expressed. A fibrogenesis reporter animal would indicate the extent of disease severity from an easily measured outcome with the added benefit of a non-invasive approach.

In conclusion, a non-invasive evaluation approach is vital to the effort of finding an effective anti-fibrotic drug. This is due to the increase in the quality of interpretation of experimental results over those produced by classical assessment tools.

8.4 Thesis Discussion on Collagen Turnover in Lung Fibrosis

Collagen turnover is an important but largely ignored component of the lung fibrotic process. As lungs accumulate collagen, the fibrils eventually "harden", becoming resistant to proteolysis by MMPs (309). As collagen becomes denser it forms crosslinks via pyridinolines. The rate of mature collagen turnover can be identified by assaying the release of pyridinolines as they exit the tissue. In order to assay pyridinolines, we reviewed and experimented with various HPLC dependent methods of quantification. We found that these methods were overly complex and not reproducible in our hands. We set out to design our own method by gleaning the strengths of other methods to from a facile method for the detection of pyridinolines in urine and serum. We confirmed that this method quantified pyridinolines by mass spectrometric analysis. We found that low concentrations pyridinolines in serum presented a problem for experiments involving rats as they have only ~7-11 mL of blood, too little to work with. It is likely that a narrow bore capillary HPLC column format would make it possible to adequately resolve serum pyridinolines in volumes less than 1 mL. We analyzed the concentrations of pyridinolines from serum of IPF and control patients and found that deoxypyridinolines, but not pyridinolines, were significantly upregulated above controls. This difference would likely not have been detected had we assayed total pyridinolines via commercial ELISA assay. Higher production of deoxypyridinolines in IPF serum is indicative of collagen breakdown abnormalities. Deoxypyridinolines are more often found in skin and soft tissues like the lungs, which our findings corroborate (323). The

lungs should be the major source of collagen breakdown in the body in the context of IPF, which has no other significant organ involvement. Urine samples yielded a higher concentration of pyridinolines sufficient for routine analysis in rats with 750 uL volumes or less. Our observations also indicated that pyridoxine (vitamin B6) could perform adequately as an internal control since its structure bares significant resemblance to pyridinoline.

In order to identify hydroxyproline in smaller lung samples such as those used in our 1D tissue bath (see Figure 3.1.1), we devised and adapted the method of Kakinuma *et al.* 2005 (322). We modified the extraction of collagen from the tissue homogenate by precipitation with trichloroacetic acid which greatly simplified subsequent derivatization of hydroxyproline with a fluorophore and HPLC analysis. This ultra sensitive method was confirmed by spiking rat homogenate samples with purified hydroxyproline. Future investigation of lung fibrosis collagen content, especially for smaller 1 mg samples, will greatly benefit from these simplifying methodological improvements.

Collagen breakdown and synthesis can also be followed by assaying for release of associated pro- and telo- peptides. Our analysis of serum breakdown peptides using commercially available radioimmunoassays discovered that it was collagen breakdown via ICTP, not its synthesis via PIIINP, which was increased in the serum of IPF patients. These data, and observations from IPF serum deoxypyridinolines, suggest that closer attention should be paid to why breakdown products are upregulated in a disease that is classically defined by collagen accumulation (23).

In conclusion, our methods development for pyridinoline detection and subsequent analyses of IPF samples has uncovered significant findings. If the fibrotic disease IPF is classically known as a disease of collagen synthesis and accumulation, then why are collagen breakdown products and not synthesis products upregulated? A more detailed investigation of these findings in the context of a persistent fibrotic model, such as Ad TGFβ_1, and IPF patient serum is warranted. It may be that the TGFβ activation that spurs additional accumulation in IPF lungs is sporadic and confined to short episodes, which were not detected by our radioimmunoassay findings. If TGFβ activation in IPF is confined to short bursts, then this will have strong bearing on intervention focused on anti-TGFβ therapeutics in clinical trials. IPF patients would need to be monitored closely to watch for “flair up’s” of fibrotic disease activity and treated accordingly.

Concluding Comments

As we bring this thesis to a close, we would like to offer our thoughts about the future of lung fibrosis research. We foresee a treatment that will limit the progression of lung fibrosis on the horizon, as drug companies gain interest in all levels TGFβ activation and signaling inhibition. Mechanical TGFβ activation described in this thesis will likely play an important role in this intervention. However, the destructive nature of fibrosis to the underlying collagen architecture of the lungs makes it unlikely that a drug will be found to restore IPF lungs back to a healthy state. In order to completely remove IPF from an individual, lung transplantation must become the focus of the future. More progress must be made in tissue engineering to grow new lungs for those that need them. Genetic modification of donated lungs must also be pursued to negate tissue rejection. Once it is relatively easy to replace lungs, pulmonary fibrosis will finally be conquered.

9.0 References

1. Renvall, S., Lehto, M., and Penttinen, R. 1987. Development of peritoneal fibrosis occurs under the mesothelial cell layer. *J. Surg. Res.* **43**:407-412.

2. Muro, A.F., Moretti, F.A., Moore, B.B., Yan, M., Atrasz, R.G., Wilke, C.A., Flaherty, K.R., Martinez, F.J., Tsui, J.L., Sheppard, D. et al. 2008. An essential role for fibronectin extra type III domain A in pulmonary fibrosis. *Am. J. Respir. Crit. Care Med.* **177**:638-645.

3. Tarantal, A.F., Chen, H., Shi, T.T., Lu, C.H., Fang, A.B., Buckley, S., Kolb, M., Gauldie, J., Warburton, D., and Shi, W. 2010. Overexpression of transforming growth factor-beta1 in fetal monkey lung results in prenatal pulmonary fibrosis. *Eur. Respir. J.* **36**:907-914.

4. Venkatesan, N., Ouzzine, M., Kolb, M., Netter, P., and Ludwig, M.S. 2011. Increased deposition of chondroitin/dermatan sulfate glycosaminoglycan and upregulation of beta1,3-glucuronosyltransferase I in pulmonary fibrosis. *Am. J. Physiol. Lung Cell. Mol. Physiol.* **300**:L191-203.

5. Aiba, M. 1976. Enzyme histochemical observations of diffuse pulmonary fibrosis of rats experimentally induced by ionizing irradiation. *Acta Pathol. Jpn.* **26**:205-222.

6. Heppleston, A.G. 1969. The fibrogenic action of silica. *Br. Med. Bull.* **25**:282-287.

7. Begin, R., Masse, S., Sebastien, P., Bosse, J., Rola-Pleszczynski, M., Boctor, M., Cote, Y., Fabi, D., and Dalle, D. 1986. Asbestos exposure and retention as determinants of airway disease and asbestos alveolitis. *Am. Rev. Respir. Dis.* **134**:1176-1181.

8. Manabe, J., and Ogata, T. 1987. Lung fibrosis induced by diquat after intratracheal administration. *Arch. Toxicol.* **60**:427-431.

9. Bedrossian, C.W., Greenberg, S.D., Yawn, D.H., and O'Neal, R.M. 1977. Experimentally induced bleomycin sulfate pulmonary toxicity: histopathologic and ultrastructural study in the pheasant. *Arch. Pathol. Lab. Med.* **101**:248-254.

10. Zhao, J., Shi, W., Wang, Y.L., Chen, H., Bringas, P.,Jr, Datto, M.B., Frederick, J.P., Wang, X.F., and Warburton, D. 2002. Smad3 deficiency attenuates bleomycin-induced pulmonary fibrosis in mice. *Am. J. Physiol. Lung Cell. Mol. Physiol.* **282**:L585-93.

11. Epperly, M.W., Franicola, D., Zhang, X., Nie, S., Wang, H., Bahnson, A.B., Shields, D.S., Goff, J.P., Shen, H., and Greenberger, J.S. 2006. Reduced irradiation pulmonary fibrosis and stromal cell migration in Smad3-/- marrow chimeric mice. *In Vivo* **20**:573-582.

12. Dong, X.S., Hu, X.B., Liu, W., Sun, Y.Q., and Liu, Z. 2012. Effects of RNA interference-induced Smad3 gene silencing on pulmonary fibrosis caused by paraquat in mice. *Exp. Biol. Med. (Maywood)*.

13. Mariani, T.J., Roby, J.D., Mecham, R.P., Parks, W.C., Crouch, E., and Pierce, R.A. 1996. Localization of type I procollagen gene expression in silica-induced granulomatous lung disease and implication of transforming growth factor-beta as a mediator of fibrosis. *Am. J. Pathol.* **148**:151-164.

14. Tsukada, T., Fushida, S., Harada, S., Yagi, Y., Kinoshita, J., Oyama, K., Tajima, H., Fujita, H., Ninomiya, I., Fujimura, T. et al. 2012. The role of human peritoneal mesothelial cells in the fibrosis and progression of gastric cancer. *Int. J. Oncol.*

15. Rancoule, C., Pradere, J.P., Gonzalez, J., Klein, J., Valet, P., Bascands, J.L., Schanstra, J.P., and Saulnier-Blache, J.S. 2011. Lysophosphatidic acid-1-receptor targeting agents for fibrosis. *Expert Opin. Investig. Drugs* **20**:657-667.

16. Royce, S.G., Miao, Y.R., Lee, M., Samuel, C.S., Tregear, G.W., and Tang, M.L. 2009. Relaxin reverses airway remodeling and airway dysfunction in allergic airways disease. *Endocrinology* **150**:2692-2699.

17. Ploss, A., and Dubuisson, J. 2012. New advances in the molecular biology of hepatitis C virus infection: towards the identification of new treatment targets. *Gut* **61 Suppl 1**:i25-35.

18. Ongali, B., Nicolakakis, N., Lecrux, C., Aboulkassim, T., Rosa-Neto, P., Papadopoulos, P., Tong, X.K., and Hamel, E. 2010. Transgenic mice overexpressing APP and transforming growth factor-beta1 feature cognitive and vascular hallmarks of Alzheimer's disease. *Am. J. Pathol.* **177**:3071-3080.

19. Bradley, B., Branley, H.M., Egan, J.J., Greaves, M.S., Hansell, D.M., Harrison, N.K., Hirani, N., Hubbard, R., Lake, F., Millar, A.B. et al. 2008. Interstitial lung disease guideline: the British Thoracic Society in collaboration with the Thoracic Society of Australia and New Zealand and the Irish Thoracic Society. *Thorax* **63 Suppl 5**:v1-58.

20. Maharaj, S.S., Baroke, E., Gauldie, J., and Kolb, M.R. 2011. Fibrocytes in chronic lung disease - Facts and controversies. *Pulm. Pharmacol. Ther.*

21. Wynn, T.A. 2011. Integrating mechanisms of pulmonary fibrosis. *J. Exp. Med.* **208**:1339-1350.

22. Cool, C.D., Groshong, S.D., Rai, P.R., Henson, P.M., Stewart, J.S., and Brown, K.K. 2006. Fibroblast foci are not discrete sites of lung injury or repair: the fibroblast reticulum. *Am. J. Respir. Crit. Care Med.* **174**:654-658.

23. Meltzer, E.B., and Noble, P.W. 2008. Idiopathic pulmonary fibrosis. *Orphanet J. Rare Dis.* **3**:8.

24. Anonymous 2000. American Thoracic Society. Idiopathic pulmonary fibrosis: diagnosis and treatment. International consensus statement. American Thoracic Society (ATS), and the European Respiratory Society (ERS). *Am. J. Respir. Crit. Care Med.* **161**:646-664.

25. Selman, M., and Pardo, A. 2006. Role of epithelial cells in idiopathic pulmonary fibrosis: from innocent targets to serial killers. *Proc. Am. Thorac. Soc.* **3**:364-372.

26. Trulock, E.P., Edwards, L.B., Taylor, D.O., Boucek, M.M., Keck, B.M., Hertz, M.I., and International Society for Heart and Lung Transplantation. 2006. Registry of the International Society for Heart and Lung Transplantation: twenty-third official adult lung and heart-lung transplantation report--2006. *J. Heart Lung Transplant.* **25**:880-892.

27. Li, X.X., Li, N., Ban, C.J., Zhu, M., Xiao, B., and Dai, H.P. 2011. Idiopathic pulmonary fibrosis in relation to gene polymorphisms of transforming growth factor-beta1 and plasminogen activator inhibitor 1. *Chin. Med. J. (Engl)* **124**:1923-1927.

28. Bonniaud, P., Margetts, P.J., Kolb, M., Schroeder, J.A., Kapoun, A.M., Damm, D., Murphy, A., Chakravarty, S., Dugar, S., Higgins, L. et al. 2005. Progressive transforming growth factor beta1-induced lung fibrosis is blocked by an orally active ALK5 kinase inhibitor. *Am. J. Respir. Crit. Care Med.* **171**:889-898.

29. Bonniaud, P., Kolb, M., Galt, T., Robertson, J., Robbins, C., Stampfli, M., Lavery, C., Margetts, P.J., Roberts, A.B., and Gauldie, J. 2004. Smad3 null mice develop airspace

enlargement and are resistant to TGF-beta-mediated pulmonary fibrosis. *J. Immunol.* **173**:2099-2108.

30. Sime, P.J., Xing, Z., Graham, F.L., Csaky, K.G., and Gauldie, J. 1997. Adenovector-mediated gene transfer of active transforming growth factor-beta1 induces prolonged severe fibrosis in rat lung. *J. Clin. Invest.* **100**:768-776.

31. Roberts, A.B., Anzano, M.A., Lamb, L.C., Smith, J.M., and Sporn, M.B. 1981. New class of transforming growth factors potentiated by epidermal growth factor: isolation from non-neoplastic tissues. *Proc. Natl. Acad. Sci. U. S. A.* **78**:5339-5343.

32. Roberts, A.B., Anzano, M.A., Meyers, C.A., Wideman, J., Blacher, R., Pan, Y.C., Stein, S., Lehrman, S.R., Smith, J.M., and Lamb, L.C. 1983. Purification and properties of a type beta transforming growth factor from bovine kidney. *Biochemistry* **22**:5692-5698.

33. Coward, W.R., Saini, G., and Jenkins, G. 2010. The pathogenesis of idiopathic pulmonary fibrosis. *Ther. Adv. Respir. Dis.* **4**:367-388.

34. Letterio, J.J., and Roberts, A.B. 1998. Regulation of immune responses by TGF-beta. *Annu. Rev. Immunol.* **16**:137-161.

35. Shull, M.M., Ormsby, I., Kier, A.B., Pawlowski, S., Diebold, R.J., Yin, M., Allen, R., Sidman, C., Proetzel, G., and Calvin, D. 1992. Targeted disruption of the mouse transforming growth factor-beta 1 gene results in multifocal inflammatory disease. *Nature* **359**:693-699.

36. Sanford, L.P., Ormsby, I., Gittenberger-de Groot, A.C., Sariola, H., Friedman, R., Boivin, G.P., Cardell, E.L., and Doetschman, T. 1997. TGFbeta2 knockout mice have multiple developmental defects that are non-overlapping with other TGFbeta knockout phenotypes. *Development* **124**:2659-2670.

37. Kaartinen, V., Voncken, J.W., Shuler, C., Warburton, D., Bu, D., Heisterkamp, N., and Groffen, J. 1995. Abnormal lung development and cleft palate in mice lacking TGF-beta 3 indicates defects of epithelial-mesenchymal interaction. *Nat. Genet.* **11**:415-421.

38. Kusakabe, M., Cheong, P.L., Nikfar, R., McLennan, I.S., and Koishi, K. 2008. The structure of the TGF-beta latency associated peptide region determines the ability of the proprotein convertase furin to cleave TGF-betas. *J. Cell. Biochem.* **103**:311-320.

39. Nunes, I., Gleizes, P.E., Metz, C.N., and Rifkin, D.B. 1997. Latent transforming growth factor-beta binding protein domains involved in activation and transglutaminase-dependent cross-linking of latent transforming growth factor-beta. *J. Cell Biol.* **136**:1151-1163.

40. Fontana, L., Chen, Y., Prijatelj, P., Sakai, T., Fassler, R., Sakai, L.Y., and Rifkin, D.B. 2005. Fibronectin is required for integrin alphavbeta6-mediated activation of latent TGF-beta complexes containing LTBP-1. *FASEB J.* **19**:1798-1808.

41. Lyons, R.M., Keski-Oja, J., and Moses, H.L. 1988. Proteolytic activation of latent transforming growth factor-beta from fibroblast-conditioned medium. *J. Cell Biol.* **106**:1659-1665.

42. Bellocq, A., Azoulay, E., Marullo, S., Flahault, A., Fouqueray, B., Philippe, C., Cadranel, J., and Baud, L. 1999. Reactive oxygen and nitrogen intermediates increase transforming growth factor-beta1 release from human epithelial alveolar cells through two different mechanisms. *Am. J. Respir. Cell Mol. Biol.* **21**:128-136.

43. Woessner, J.F.,Jr. 1991. Matrix metalloproteinases and their inhibitors in connective tissue remodeling. *FASEB J.* **5**:2145-2154.

44. Garcia-Alvarez, J., Ramirez, R., Sampieri, C.L., Nuttall, R.K., Edwards, D.R., Selman, M., and Pardo, A. 2006. Membrane type-matrix metalloproteinases in idiopathic pulmonary fibrosis. *Sarcoidosis Vasc. Diffuse Lung Dis.* **23**:13-21.

45. Sato, Y., and Rifkin, D.B. 1989. Inhibition of endothelial cell movement by pericytes and smooth muscle cells: activation of a latent transforming growth factor-beta 1-like molecule by plasmin during co-culture. *J. Cell Biol.* **109**:309-315.

46. Schultz-Cherry, S., and Murphy-Ullrich, J.E. 1993. Thrombospondin causes activation of latent transforming growth factor-beta secreted by endothelial cells by a novel mechanism. *J. Cell Biol.* **122**:923-932.

47. Blakytny, R., Ludlow, A., Martin, G.E., Ireland, G., Lund, L.R., Ferguson, M.W., and Brunner, G. 2004. Latent TGF-beta1 activation by platelets. *J. Cell. Physiol.* **199**:67-76.

48. Munger, J.S., Huang, X., Kawakatsu, H., Griffiths, M.J., Dalton, S.L., Wu, J., Pittet, J.F., Kaminski, N., Garat, C., Matthay, M.A. et al. 1999. The integrin alpha v beta 6 binds and activates latent TGF beta 1: a mechanism for regulating pulmonary inflammation and fibrosis. *Cell* **96**:319-328.

49. Tatler, A.L., John, A.E., Jolly, L., Habgood, A., Porte, J., Brightling, C., Knox, A.J., Pang, L., Sheppard, D., Huang, X. et al. 2011. Integrin alphavbeta5-mediated TGF-beta activation by airway smooth muscle cells in asthma. *J. Immunol.* **187**:6094-6107.

50. Wipff, P.J., Rifkin, D.B., Meister, J.J., and Hinz, B. 2007. Myofibroblast contraction activates latent TGF-beta1 from the extracellular matrix. *J. Cell Biol.* **179**:1311-1323.

51. Mu, D., Cambier, S., Fjellbirkeland, L., Baron, J.L., Munger, J.S., Kawakatsu, H., Sheppard, D., Broaddus, V.C., and Nishimura, S.L. 2002. The integrin alpha(v)beta8 mediates epithelial homeostasis through MT1-MMP-dependent activation of TGF-beta1. *J. Cell Biol.* **157**:493-507.

52. Souchelnytskyi, S., ten Dijke, P., Miyazono, K., and Heldin, C.H. 1996. Phosphorylation of Ser165 in TGF-beta type I receptor modulates TGF-beta1-induced cellular responses. *EMBO J.* **15**:6231-6240.

53. Chu, W., Li, X., Li, C., Wan, L., Shi, H., Song, X., Liu, X., Chen, X., Zhang, C., Shan, H. et al. 2011. TGFBR3, a potential negative regulator of TGF-beta signaling, protects cardiac fibroblasts from hypoxia-induced apoptosis. *J. Cell. Physiol.* **226**:2586-2594.

54. Rajagopal, R., Ishii, S., and Beebe, D.C. 2007. Intracellular mediators of transforming growth factor beta superfamily signaling localize to endosomes in chicken embryo and mouse lenses in vivo. *BMC Cell Biol.* **8**:25.

55. Penheiter, S.G., Mitchell, H., Garamszegi, N., Edens, M., Dore, J.J.,Jr, and Leof, E.B. 2002. Internalization-dependent and -independent requirements for transforming growth factor beta receptor signaling via the Smad pathway. *Mol. Cell. Biol.* **22**:4750-4759.

56. Ehrlich, M., Shmuely, A., and Henis, Y.I. 2001. A single internalization signal from the di-leucine family is critical for constitutive endocytosis of the type II TGF-beta receptor. *J. Cell. Sci.* **114**:1777-1786.

57. Tsukazaki T. 1998. SARA, a FYVE domain protein that recruits Smad2 to the TGFβ receptor. *Cell* **95**:779.

58. Di Guglielmo, G.M., Le Roy, C., Goodfellow, A.F., and Wrana, J.L. 2003. Distinct endocytic pathways regulate TGF-beta receptor signalling and turnover. *Nat. Cell Biol.* **5**:410-421.

59. Kang, J.S., Saunier, E.F., Akhurst, R.J., and Derynck, R. 2008. The type I TGF-beta receptor is covalently modified and regulated by sumoylation. *Nat. Cell Biol.* **10**:654-664.

60. Kang, J.S., Liu, C., and Derynck, R. 2009. New regulatory mechanisms of TGF-beta receptor function. *Trends Cell Biol.* **19**:385-394.

61. Dong, C., Li, Z., Alvarez, R.,Jr, Feng, X.H., and Goldschmidt-Clermont, P.J. 2000. Microtubule binding to Smads may regulate TGF beta activity. *Mol. Cell* **5**:27-34.

62. Sasaki, A., Masuda, Y., Ohta, Y., Ikeda, K., and Watanabe, K. 2001. Filamin associates with Smads and regulates transforming growth factor-beta signaling. *J. Biol. Chem.* **276**:17871-17877.

63. Batut, J., Howell, M., and Hill, C.S. 2007. Kinesin-mediated transport of Smad2 is required for signaling in response to TGF-beta ligands. *Dev. Cell.* **12**:261-274.

64. Macias-Silva, M., Abdollah, S., Hoodless, P.A., Pirone, R., Attisano, L., and Wrana, J.L. 1996. MADR2 is a substrate of the TGFbeta receptor and its phosphorylation is required for nuclear accumulation and signaling. *Cell* **87**:1215-1224.

65. Zhang, Y., Feng, X., We, R., and Derynck, R. 1996. Receptor-associated Mad homologues synergize as effectors of the TGF-beta response. *Nature* **383**:168-172.

66. Inui, M., Manfrin, A., Mamidi, A., Martello, G., Morsut, L., Soligo, S., Enzo, E., Moro, S., Polo, S., Dupont, S. et al. 2011. USP15 is a deubiquitylating enzyme for receptor-activated SMADs. *Nat. Cell Biol.* **13**:1368-1375.

67. Kavsak, P., Rasmussen, R.K., Causing, C.G., Bonni, S., Zhu, H., Thomsen, G.H., and Wrana, J.L. 2000. Smad7 binds to Smurf2 to form an E3 ubiquitin ligase that targets the TGF beta receptor for degradation. *Mol. Cell* **6**:1365-1375.

68. Ebisawa, T., Fukuchi, M., Murakami, G., Chiba, T., Tanaka, K., Imamura, T., and Miyazono, K. 2001. Smurf1 interacts with transforming growth factor-beta type I receptor through Smad7 and induces receptor degradation. *J. Biol. Chem.* **276**:12477-12480.

69. Kowanetz, M., Lonn, P., Vanlandewijck, M., Kowanetz, K., Heldin, C.H., and Moustakas, A. 2008. TGFbeta induces SIK to negatively regulate type I receptor kinase signaling. *J. Cell Biol.* **182**:655-662.

70. Yamaguchi, T., Kurisaki, A., Yamakawa, N., Minakuchi, K., and Sugino, H. 2006. FKBP12 functions as an adaptor of the Smad7-Smurf1 complex on activin type I receptor. *J. Mol. Endocrinol.* **36**:569-579.

71. Hao, X., Wang, Y., Ren, F., Zhu, S., Ren, Y., Jia, B., Li, Y.P., Shi, Y., and Chang, Z. 2011. SNX25 regulates TGF-beta signaling by enhancing the receptor degradation. *Cell. Signal.* **23**:935-946.

72. Su, Y., Zhang, L., Gao, X., Meng, F., Wen, J., Zhou, H., Meng, A., and Chen, Y.G. 2007. The evolutionally conserved activity of Dapper2 in antagonizing TGF-beta signaling. *FASEB J.* **21**:682-690.

73. Kardassis, D., Murphy, C., Fotsis, T., Moustakas, A., and Stournaras, C. 2009. Control of transforming growth factor beta signal transduction by small GTPases. *FEBS J.* **276**:2947-2965.

74. Derynck, R., and Zhang, Y.E. 2003. Smad-dependent and Smad-independent pathways in TGF-beta family signalling. *Nature* **425**:577-584.

75. Moustakas, A., and Heldin, C.H. 2005. Non-Smad TGF-beta signals. *J. Cell. Sci.* **118**:3573-3584.

76. Lee, M.K., Pardoux, C., Hall, M.C., Lee, P.S., Warburton, D., Qing, J., Smith, S.M., and Derynck, R. 2007. TGF-beta activates Erk MAP kinase signalling through direct phosphorylation of ShcA. *EMBO J.* **26**:3957-3967.

77. Yamashita, M., Fatyol, K., Jin, C., Wang, X., Liu, Z., and Zhang, Y.E. 2008. TRAF6 mediates Smad-independent activation of JNK and p38 by TGF-beta. *Mol. Cell* **31**:918-924.

78. Sorrentino, A., Thakur, N., Grimsby, S., Marcusson, A., von Bulow, V., Schuster, N., Zhang, S., Heldin, C.H., and Landstrom, M. 2008. The type I TGF-beta receptor engages TRAF6 to activate TAK1 in a receptor kinase-independent manner. *Nat. Cell Biol.* **10**:1199-1207.

79. Hong, M., Wilkes, M.C., Penheiter, S.G., Gupta, S.K., Edens, M., and Leof, E.B. 2011. Non-Smad transforming growth factor-beta signaling regulated by focal adhesion kinase binding the p85 subunit of phosphatidylinositol 3-kinase. *J. Biol. Chem.* **286**:17841-17850.

80. Bailey, J.S., Rave-Harel, N., McGillivray, S.M., Coss, D., and Mellon, P.L. 2004. Activin regulation of the follicle-stimulating hormone beta-subunit gene involves Smads and the TALE homeodomain proteins Pbx1 and Prep1. *Mol. Endocrinol.* **18**:1158-1170.

81. Naso, M., Uitto, J., and Klement, J.F. 2003. Transcriptional control of the mouse Col7a1 gene in keratinocytes: basal and transforming growth factor-beta regulated expression. *J. Invest. Dermatol.* **121**:1469-1478.

82. Zhang, Y., Feng, X.H., and Derynck, R. 1998. Smad3 and Smad4 cooperate with c-Jun/c-Fos to mediate TGF-beta-induced transcription. *Nature* **394**:909-913.

83. Yoon, S.J., Wills, A.E., Chuong, E., Gupta, R., and Baker, J.C. 2011. HEB and E2A function as SMAD/FOXH1 cofactors. *Genes Dev.* **25**:1654-1661.

84. Seoane, J., Le, H.V., Shen, L., Anderson, S.A., and Massague, J. 2004. Integration of Smad and forkhead pathways in the control of neuroepithelial and glioblastoma cell proliferation. *Cell* **117**:211-223.

85. de Caestecker, M.P., Yahata, T., Wang, D., Parks, W.T., Huang, S., Hill, C.S., Shioda, T., Roberts, A.B., and Lechleider, R.J. 2000. The Smad4 activation domain (SAD) is a proline-rich, p300-dependent transcriptional activation domain. *J. Biol. Chem.* **275**:2115-2122.

86. Weisberg, E., Winnier, G.E., Chen, X., Farnsworth, C.L., Hogan, B.L., and Whitman, M. 1998. A mouse homologue of FAST-1 transduces TGF beta superfamily signals and is expressed during early embryogenesis. *Mech. Dev.* **79**:17-27.

87. Yeo, C.Y., Chen, X., and Whitman, M. 1999. The role of FAST-1 and Smads in transcriptional regulation by activin during early Xenopus embryogenesis. *J. Biol. Chem.* **274**:26584-26590.

88. Hoodless, P.A., Tsukazaki, T., Nishimatsu, S., Attisano, L., Wrana, J.L., and Thomsen, G.H. 1999. Dominant-negative Smad2 mutants inhibit activin/Vg1 signaling and disrupt axis formation in Xenopus. *Dev. Biol.* **207**:364-379.

89. Howell, M., Inman, G.J., and Hill, C.S. 2002. A novel Xenopus Smad-interacting forkhead transcription factor (XFast-3) cooperates with XFast-1 in regulating gastrulation movements. *Development* **129**:2823-2834.

90. Germain, S., Howell, M., Esslemont, G.M., and Hill, C.S. 2000. Homeodomain and winged-helix transcription factors recruit activated Smads to distinct promoter elements via a common Smad interaction motif. *Genes Dev.* **14**:435-451.

91. Dennler, S., Itoh, S., Vivien, D., ten Dijke, P., Huet, S., and Gauthier, J.M. 1998. Direct binding of Smad3 and Smad4 to critical TGF beta-inducible elements in the promoter of human plasminogen activator inhibitor-type 1 gene. *EMBO J.* **17**:3091-3100.

92. Qin, H., Chan, M.W., Liyanarachchi, S., Balch, C., Potter, D., Souriraj, I.J., Cheng, A.S., Agosto-Perez, F.J., Nikonova, E.V., Yan, P.S. et al. 2009. An integrative ChIP-chip and gene expression profiling to model SMAD regulatory modules. *BMC Syst. Biol.* **3**:73.

93. Kim, S.J., Glick, A., Sporn, M.B., and Roberts, A.B. 1989. Characterization of the promoter region of the human transforming growth factor-beta 1 gene. *J. Biol. Chem.* **264**:402-408.

94. Weigert, C., Sauer, U., Brodbeck, K., Pfeiffer, A., Haring, H.U., and Schleicher, E.D. 2000. AP-1 proteins mediate hyperglycemia-induced activation of the human TGF-beta1 promoter in mesangial cells. *J. Am. Soc. Nephrol.* **11**:2007-2016.

95. Yue, J., and Mulder, K.M. 2000. Requirement of Ras/MAPK pathway activation by transforming growth factor beta for transforming growth factor beta 1 production in a smad-dependent pathway. *J. Biol. Chem.* **275**:35656.

96. Lee, C.G., Kang, H.R., Homer, R.J., Chupp, G., and Elias, J.A. 2006. Transgenic modeling of transforming growth factor-beta(1): role of apoptosis in fibrosis and alveolar remodeling. *Proc. Am. Thorac. Soc.* **3**:418-423.

97. Van Obberghen-Schilling, E., Roche, N.S., Flanders, K.C., Sporn, M.B., and Roberts, A.B. 1988. Transforming growth factor beta 1 positively regulates its own expression in normal and transformed cells. *J. Biol. Chem.* **263**:7741-7746.

98. Annes, J.P., Munger, J.S., and Rifkin, D.B. 2003. Making sense of latent TGFbeta activation. *J. Cell. Sci.* **116**:217-224.

99. Kim, K.K., Kugler, M.C., Wolters, P.J., Robillard, L., Galvez, M.G., Brumwell, A.N., Sheppard, D., and Chapman, H.A. 2006. Alveolar epithelial cell mesenchymal transition develops in vivo during pulmonary fibrosis and is regulated by the extracellular matrix. *Proc. Natl. Acad. Sci. U. S. A.* **103**:13180-13185.

100. Chapman, H.A. 2011. Epithelial-mesenchymal interactions in pulmonary fibrosis. *Annu. Rev. Physiol.* **73**:413-435.

101. Camara, J., and Jarai, G. 2010. Epithelial-mesenchymal transition in primary human bronchial epithelial cells is Smad-dependent and enhanced by fibronectin and TNF-alpha. *Fibrogenesis Tissue Repair* **3**:2.

102. Kolosova, I., Nethery, D., and Kern, J.A. 2011. Role of Smad2/3 and p38 MAP kinase in TGF-beta1-induced epithelial-mesenchymal transition of pulmonary epithelial cells. *J. Cell. Physiol.* **226**:1248-1254.

103. Grinnell, F. 1994. Fibroblasts, myofibroblasts, and wound contraction. *J. Cell Biol.* **124**:401-404.

104. Fukamizu, H., and Grinnell, F. 1990. Spatial organization of extracellular matrix and fibroblast activity: effects of serum, transforming growth factor beta, and fibronectin. *Exp. Cell Res.* **190**:276-282.

105. Rossi, P., Karsenty, G., Roberts, A.B., Roche, N.S., Sporn, M.B., and de Crombrugghe, B. 1988. A nuclear factor 1 binding site mediates the transcriptional activation of a type I collagen promoter by transforming growth factor-beta. *Cell* **52**:405-414.

106. Roberts, A.B., Sporn, M.B., Assoian, R.K., Smith, J.M., Roche, N.S., Wakefield, L.M., Heine, U.I., Liotta, L.A., Falanga, V., and Kehrl, J.H. 1986. Transforming growth factor type beta: rapid induction of fibrosis and angiogenesis in vivo and stimulation of collagen formation in vitro. *Proc. Natl. Acad. Sci. U. S. A.* **83**:4167-4171.

107. Kelly, M., Kolb, M., Bonniaud, P., and Gauldie, J. 2003. Re-evaluation of fibrogenic cytokines in lung fibrosis. *Curr. Pharm. Des.* **9**:39-49.

108. Khalil, N., O'Connor, R.N., Flanders, K.C., and Unruh, H. 1996. TGF-beta 1, but not TGF-beta 2 or TGF-beta 3, is differentially present in epithelial cells of advanced pulmonary fibrosis: an immunohistochemical study. *Am. J. Respir. Cell Mol. Biol.* **14**:131-138.

109. Bonniaud, P., Margetts, P.J., Ask, K., Flanders, K., Gauldie, J., and Kolb, M. 2005. TGF-beta and Smad3 signaling link inflammation to chronic fibrogenesis. *J. Immunol.* **175**:5390-5395.

110. Lee, C.G., Homer, R.J., Zhu, Z., Lanone, S., Wang, X., Koteliansky, V., Shipley, J.M., Gotwals, P., Noble, P., Chen, Q. et al. 2001. Interleukin-13 induces tissue fibrosis by selectively stimulating and activating transforming growth factor beta(1). *J. Exp. Med.* **194**:809-821.

111. Kaviratne, M., Hesse, M., Leusink, M., Cheever, A.W., Davies, S.J., McKerrow, J.H., Wakefield, L.M., Letterio, J.J., and Wynn, T.A. 2004. IL-13 activates a mechanism of tissue fibrosis that is completely TGF-beta independent. *J. Immunol.* **173**:4020-4029.

112. Fattouh, R., Midence, N.G., Arias, K., Johnson, J.R., Walker, T.D., Goncharova, S., Souza, K.P., Gregory, R.C.,Jr, Lonning, S., Gauldie, J. et al. 2008. Transforming growth factor-beta regulates house dust mite-induced allergic airway inflammation but not airway remodeling. *Am. J. Respir. Crit. Care Med.* **177**:593-603.

113. Strieter, R.M. 2008. What differentiates normal lung repair and fibrosis? Inflammation, resolution of repair, and fibrosis. *Proc. Am. Thorac. Soc.* **5**:305-310.

114. Buscemi, L., Ramonet, D., Klingberg, F., Formey, A., Smith-Clerc, J., Meister, J.J., and Hinz, B. 2011. The single-molecule mechanics of the latent TGF-beta1 complex. *Curr. Biol.* **21**:2046-2054.

115. Moeller, A., Ask, K., Warburton, D., Gauldie, J., and Kolb, M. 2008. The bleomycin animal model: a useful tool to investigate treatment options for idiopathic pulmonary fibrosis? *Int. J. Biochem. Cell Biol.* **40**:362-382.

116. Ask, K., Labiris, R., Farkas, L., Moeller, A., Froese, A., Farncombe, T., McClelland, G.B., Inman, M., Gauldie, J., and Kolb, M.R. 2008. Comparison between conventional and "clinical" assessment of experimental lung fibrosis. *J. Transl. Med.* **6**:16.

117. van der Slot, A.J., Zuurmond, A.M., van den Bogaerdt, A.J., Ulrich, M.M., Middelkoop, E., Boers, W., Karel Ronday, H., DeGroot, J., Huizinga, T.W., and Bank, R.A. 2004. Increased formation of pyridinoline cross-links due to higher telopeptide lysyl hydroxylase levels is a general fibrotic phenomenon. *Matrix Biol.* **23**:251-257.

118. Dubois, C.M., Laprise, M.H., Blanchette, F., Gentry, L.E., and Leduc, R. 1995. Processing of transforming growth factor beta 1 precursor by human furin convertase. *J. Biol. Chem.* **270**:10618-10624.

119. Gleizes, P.E., Beavis, R.C., Mazzieri, R., Shen, B., and Rifkin, D.B. 1996. Identification and characterization of an eight-cysteine repeat of the latent transforming growth factor-beta binding protein-1 that mediates bonding to the latent transforming growth factor-beta1. *J. Biol. Chem.* **271**:29891-29896.

120. Griffin, M., Casadio, R., and Bergamini, C.M. 2002. Transglutaminases: nature's biological glues. *Biochem. J.* **368**:377-396.

121. Lawrence, D.A., Pircher, R., Kryceve-Martinerie, C., and Jullien, P. 1984. Normal embryo fibroblasts release transforming growth factors in a latent form. *J. Cell. Physiol.* **121**:184-188.

122. Lyons, R.M., Gentry, L.E., Purchio, A.F., and Moses, H.L. 1990. Mechanism of activation of latent recombinant transforming growth factor beta 1 by plasmin. *J. Cell Biol.* **110**:1361-1367.

123. Lawrence, D.A., Pircher, R., and Jullien, P. 1985. Conversion of a high molecular weight latent beta-TGF from chicken embryo fibroblasts into a low molecular weight active beta-TGF under acidic conditions. *Biochem. Biophys. Res. Commun.* **133**:1026-1034.

124. Perng, D.W., Wu, Y.C., Tsai, C.C., Su, K.C., Liu, L.Y., Hsu, W.H., and Lee, Y.C. 2008. Bile acids induce CCN2 production through p38 MAP kinase activation in human bronchial epithelial cells: a factor contributing to airway fibrosis. *Respirology* **13**:983-989.

125. Tobin, R.W., Pope, C.E.,2nd, Pellegrini, C.A., Emond, M.J., Sillery, J., and Raghu, G. 1998. Increased prevalence of gastroesophageal reflux in patients with idiopathic pulmonary fibrosis. *Am. J. Respir. Crit. Care Med.* **158**:1804-1808.

126. Raghu, G., Freudenberger, T.D., Yang, S., Curtis, J.R., Spada, C., Hayes, J., Sillery, J.K., Pope, C.E.,2nd, and Pellegrini, C.A. 2006. High prevalence of abnormal acid gastro-oesophageal reflux in idiopathic pulmonary fibrosis. *Eur. Respir. J.* **27**:136-142.

127. Noth, I., Zangan, S.M., Soares, R.V., Forsythe, A., Demchuk, C., Takahashi, S.M., Patel, S.B., Strek, M.E., Krishnan, J.A., Patti, M.G. et al. 2012. Prevalence of hiatal hernia by blinded multidetector CT in patients with idiopathic pulmonary fibrosis. *Eur. Respir. J.* **39**:344-351.

128. Raghu, G. 2003. The role of gastroesophageal reflux in idiopathic pulmonary fibrosis. *Am. J. Med.* **115 Suppl 3A**:60S-64S.

129. Popper, H., Juettner, F., and Pinter, J. 1986. The gastric juice aspiration syndrome (Mendelson syndrome). Aspects of pathogenesis and treatment in the pig. *Virchows Arch. A Pathol. Anat. Histopathol.* **409**:105-117.

130. Engleman, V.W., Nickols, G.A., Ross, F.P., Horton, M.A., Griggs, D.W., Settle, S.L., Ruminski, P.G., and Teitelbaum, S.L. 1997. A peptidomimetic antagonist of the alpha(v)beta3 integrin inhibits bone resorption in vitro and prevents osteoporosis in vivo. *J. Clin. Invest.* **99**:2284-2292.

131. Li, Y.P., Chen, W., Liang, Y., Li, E., and Stashenko, P. 1999. Atp6i-deficient mice exhibit severe osteopetrosis due to loss of osteoclast-mediated extracellular acidification. *Nat. Genet.* **23**:447-451.

132. Teitelbaum, S.L. 2000. Bone resorption by osteoclasts. *Science* **289**:1504-1508.

133. Silver, I.A., Murrills, R.J., and Etherington, D.J. 1988. Microelectrode studies on the acid microenvironment beneath adherent macrophages and osteoclasts. *Exp. Cell Res.* **175**:266-276.

134. Oursler, M.J. 1994. Osteoclast synthesis and secretion and activation of latent transforming growth factor beta. *J. Bone Miner. Res.* **9**:443-452.

135. Kettle, A.J., Anderson, R.F., Hampton, M.B., and Winterbourn, C.C. 2007. Reactions of superoxide with myeloperoxidase. *Biochemistry* **46**:4888-4897.

136. Lee, I.T., and Yang, C.M. 2012. Role of NADPH oxidase/ROS in pro-inflammatory mediators-induced airway and pulmonary diseases. *Biochem. Pharmacol.*

137. Gamaley, I.A., Kirpichnikova, K.M., and Klyubin, I.V. 1994. Activation of murine macrophages by hydrogen peroxide. *Cell. Signal.* **6**:949-957.

138. Klyubin, I.V., Kirpichnikova, K.M., and Gamaley, I.A. 1996. Hydrogen peroxide-induced chemotaxis of mouse peritoneal neutrophils. *Eur. J. Cell Biol.* **70**:347-351.

139. Qi, S., den Hartog, G.J., and Bast, A. 2009. Superoxide radicals increase transforming growth factor-beta1 and collagen release from human lung fibroblasts via cellular influx through chloride channels. *Toxicol. Appl. Pharmacol.* **237**:111-118.

140. Barcellos-Hoff, M.H., Derynck, R., Tsang, M.L., and Weatherbee, J.A. 1994. Transforming growth factor-beta activation in irradiated murine mammary gland. *J. Clin. Invest.* **93**:892-899.

141. Barcellos-Hoff, M.H., and Dix, T.A. 1996. Redox-mediated activation of latent transforming growth factor-beta 1. *Mol. Endocrinol.* **10**:1077-1083.

142. Jobling, M.F., Mott, J.D., Finnegan, M.T., Jurukovski, V., Erickson, A.C., Walian, P.J., Taylor, S.E., Ledbetter, S., Lawrence, C.M., Rifkin, D.B. et al. 2006. Isoform-specific activation of latent transforming growth factor beta (LTGF-beta) by reactive oxygen species. *Radiat. Res.* **166**:839-848.

143. Flanders, K.C., Sullivan, C.D., Fujii, M., Sowers, A., Anzano, M.A., Arabshahi, A., Major, C., Deng, C., Russo, A., Mitchell, J.B. et al. 2002. Mice lacking Smad3 are protected against cutaneous injury induced by ionizing radiation. *Am. J. Pathol.* **160**:1057-1068.

144. Terasaki, Y., Ohsawa, I., Terasaki, M., Takahashi, M., Kunugi, S., Dedong, K., Urushiyama, H., Amenomori, S., Kaneko-Togashi, M., Kuwahara, N. et al. 2011. Hydrogen therapy attenuates irradiation-induced lung damage by reducing oxidative stress. *Am. J. Physiol. Lung Cell. Mol. Physiol.* **301**:L415-26.

145. Patel, R.B., Kotha, S.R., Sauers, L.A., Malireddy, S., Gurney, T.O., Gupta, N.N., Elton, T.S., Magalang, U.J., Marsh, C.B., Haley, B.E. et al. 2012. Thiol-redox antioxidants protect against lung vascular endothelial cytoskeletal alterations caused by pulmonary fibrosis inducer, bleomycin: Comparison between classical thiol protectant, N-acetyl-L-cysteine (NAC) and novel thiol antioxidant, N,N'-bis-2-mercaptoethyl isophthalamide (NBMI). *Toxicol. Mech. Methods*.

146. Suntres, Z.E. 2002. Role of antioxidants in paraquat toxicity. *Toxicology* **180**:65-77.

147. Cui, Y., Robertson, J., Maharaj, S., Waldhauser, L., Niu, J., Wang, J., Farkas, L., Kolb, M., and Gauldie, J. 2011. Oxidative stress contributes to the induction and persistence of TGF-beta1 induced pulmonary fibrosis. *Int. J. Biochem. Cell Biol.* **43**:1122-1133.

148. Teramoto, S., Fukuchi, Y., Uejima, Y., Shu, C.Y., and Orimo, H. 1995. Superoxide anion formation and glutathione metabolism of blood in patients with idiopathic pulmonary fibrosis. *Biochem. Mol. Med.* **55**:66-70.

149. Amara, N., Goven, D., Prost, F., Muloway, R., Crestani, B., and Boczkowski, J. 2010. NOX4/NADPH oxidase expression is increased in pulmonary fibroblasts from patients with idiopathic pulmonary fibrosis and mediates TGFbeta1-induced fibroblast differentiation into myofibroblasts. *Thorax* **65**:733-738.

150. Bocchino, M., Agnese, S., Fagone, E., Svegliati, S., Grieco, D., Vancheri, C., Gabrielli, A., Sanduzzi, A., and Avvedimento, E.V. 2010. Reactive oxygen species are required for maintenance and differentiation of primary lung fibroblasts in idiopathic pulmonary fibrosis. *PLoS One* **5**:e14003.

151. Waghray, M., Cui, Z., Horowitz, J.C., Subramanian, I.M., Martinez, F.J., Toews, G.B., and Thannickal, V.J. 2005. Hydrogen peroxide is a diffusible paracrine signal for the induction of epithelial cell death by activated myofibroblasts. *FASEB J.* **19**:854-856.

152. Behr, J., Demedts, M., Buhl, R., Costabel, U., Dekhuijzen, R.P., Jansen, H.M., MacNee, W., Thomeer, M., Wallaert, B., Laurent, F. et al. 2009. Lung function in idiopathic pulmonary fibrosis--extended analyses of the IFIGENIA trial. *Respir. Res.* **10**:101.

153. Hakulinen, J., Sankkila, L., Sugiyama, N., Lehti, K., and Keski-Oja, J. 2008. Secretion of active membrane type 1 matrix metalloproteinase (MMP-14) into extracellular space in microvesicular exosomes. *J. Cell. Biochem.* **105**:1211-1218.

154. Yu, Q., and Stamenkovic, I. 2000. Cell surface-localized matrix metalloproteinase-9 proteolytically activates TGF-beta and promotes tumor invasion and angiogenesis. *Genes Dev.* **14**:163-176.

155. Bauman, K.A., Wettlaufer, S.H., Okunishi, K., Vannella, K.M., Stoolman, J.S., Huang, S.K., Courey, A.J., White, E.S., Hogaboam, C.M., Simon, R.H. et al. 2010. The antifibrotic effects of plasminogen activation occur via prostaglandin E2 synthesis in humans and mice. *J. Clin. Invest.* **120**:1950-1960.

156. Nunes, I., Shapiro, R.L., and Rifkin, D.B. 1995. Characterization of latent TGF-beta activation by murine peritoneal macrophages. *J. Immunol.* **155**:1450-1459.

157. Khalil, N., Corne, S., Whitman, C., and Yacyshyn, H. 1996. Plasmin regulates the activation of cell-associated latent TGF-beta 1 secreted by rat alveolar macrophages after in vivo bleomycin injury. *Am. J. Respir. Cell Mol. Biol.* **15**:252-259.

158. Yehualaeshet, T., O'Connor, R., Green-Johnson, J., Mai, S., Silverstein, R., Murphy-Ullrich, J.E., and Khalil, N. 1999. Activation of rat alveolar macrophage-derived latent transforming growth factor beta-1 by plasmin requires interaction with thrombospondin-1 and its cell surface receptor, CD36. *Am. J. Pathol.* **155**:841-851.

159. Rowley, D.A., Becken, E.T., and Stach, R.M. 1995. Autoantibodies produced spontaneously by young 1pr mice carry transforming growth factor beta and suppress cytotoxic T lymphocyte responses. *J. Exp. Med.* **181**:1875-1880.

160. Stach, R.M., and Rowley, D.A. 1993. A first or dominant immunization. II. Induced immunoglobulin carries transforming growth factor beta and suppresses cytolytic T cell responses to unrelated alloantigens. *J. Exp. Med.* **178**:841-852.

161. Caver, T.E., O'Sullivan, F.X., Gold, L.I., and Gresham, H.D. 1996. Intracellular demonstration of active TGFbeta1 in B cells and plasma cells of autoimmune mice. IgG-bound TGFbeta1 suppresses neutrophil function and host defense against Staphylococcus aureus infection. *J. Clin. Invest.* **98**:2496-2506.

162. Kehrl, J.H., Wakefield, L.M., Roberts, A.B., Jakowlew, S., Alvarez-Mon, M., Derynck, R., Sporn, M.B., and Fauci, A.S. 1986. Production of transforming growth factor beta by human T lymphocytes and its potential role in the regulation of T cell growth. *J. Exp. Med.* **163**:1037-1050.

163. Snapper, C.M., Waegell, W., Beernink, H., and Dasch, J.R. 1993. Transforming growth factor-beta 1 is required for secretion of IgG of all subclasses by LPS-activated murine B cells in vitro. *J. Immunol.* **151**:4625-4636.

164. Assoian, R.K., Komoriya, A., Meyers, C.A., Miller, D.M., and Sporn, M.B. 1983. Transforming growth factor-beta in human platelets. Identification of a major storage site, purification, and characterization. *J. Biol. Chem.* **258**:7155-7160.

165. Assoian, R.K., and Sporn, M.B. 1986. Type beta transforming growth factor in human platelets: release during platelet degranulation and action on vascular smooth muscle cells. *J. Cell Biol.* **102**:1217-1223.

166. Goldsack, N.R., Chambers, R.C., Dabbagh, K., and Laurent, G.J. 1998. Thrombin. *Int. J. Biochem. Cell Biol.* **30**:641-646.

167. Ollendorff, V., Noguchi, T., deLapeyriere, O., and Birnbaum, D. 1994. The GARP gene encodes a new member of the family of leucine-rich repeat-containing proteins. *Cell Growth Differ.* **5**:213-219.

168. Stockis, J., Colau, D., Coulie, P.G., and Lucas, S. 2009. Membrane protein GARP is a receptor for latent TGF-beta on the surface of activated human Treg. *Eur. J. Immunol.* **39**:3315-3322.

169. Wang, R., Zhu, J., Dong, X., Shi, M., Lu, C., and Springer, T.A. 2012. GARP regulates the bioavailability and activation of TGFbeta. *Mol. Biol. Cell* **23**:1129-1139.

170. Strieter, R.M. 2002. Con: Inflammatory mechanisms are not a minor component of the pathogenesis of idiopathic pulmonary fibrosis. *Am. J. Respir. Crit. Care Med.* **165**:1206-7; discussion 1207-8.

171. Gauldie, J. 2002. Pro: Inflammatory mechanisms are a minor component of the pathogenesis of idiopathic pulmonary fibrosis. *Am. J. Respir. Crit. Care Med.* **165**:1205-1206.

172. Murphy-Ullrich, J.E., and Poczatek, M. 2000. Activation of latent TGF-beta by thrombospondin-1: mechanisms and physiology. *Cytokine Growth Factor Rev.* **11**:59-69.

173. Crawford, S.E., Stellmach, V., Murphy-Ullrich, J.E., Ribeiro, S.M., Lawler, J., Hynes, R.O., Boivin, G.P., and Bouck, N. 1998. Thrombospondin-1 is a major activator of TGF-beta1 in vivo. *Cell* **93**:1159-1170.

174. Bugge, T.H., Kombrinck, K.W., Flick, M.J., Daugherty, C.C., Danton, M.J., and Degen, J.L. 1996. Loss of fibrinogen rescues mice from the pleiotropic effects of plasminogen deficiency. *Cell* **87**:709-719.

175. Rajkumar, R., Konishi, K., Richards, T.J., Ishizawar, D.C., Wiechert, A.C., Kaminski, N., and Ahmad, F. 2010. Genomewide RNA expression profiling in lung identifies distinct signatures in idiopathic pulmonary arterial hypertension and secondary pulmonary hypertension. *Am. J. Physiol. Heart Circ. Physiol.* **298**:H1235-48.

176. Hynes, R.O. 1992. Integrins: versatility, modulation, and signaling in cell adhesion. *Cell* **69**:11-25.

177. Sheppard, D. 2000. In vivo functions of integrins: lessons from null mutations in mice. *Matrix Biol.* **19**:203-209.

178. Munger, J.S., Harpel, J.G., Giancotti, F.G., and Rifkin, D.B. 1998. Interactions between growth factors and integrins: latent forms of transforming growth factor-beta are ligands for the integrin alphavbeta1. *Mol. Biol. Cell* **9**:2627-2638.

179. Huang, X.Z., Wu, J.F., Cass, D., Erle, D.J., Corry, D., Young, S.G., Farese, R.V.,Jr, and Sheppard, D. 1996. Inactivation of the integrin beta 6 subunit gene reveals a role of epithelial integrins in regulating inflammation in the lung and skin. *J. Cell Biol.* **133**:921-928.

180. Yang, Z., Mu, Z., Dabovic, B., Jurukovski, V., Yu, D., Sung, J., Xiong, X., and Munger, J.S. 2007. Absence of integrin-mediated TGFbeta1 activation in vivo recapitulates the phenotype of TGFbeta1-null mice. *J. Cell Biol.* **176**:787-793.

181. Annes, J.P., Rifkin, D.B., and Munger, J.S. 2002. The integrin alphaVbeta6 binds and activates latent TGFbeta3. *FEBS Lett.* **511**:65-68.

182. Nakagawa, S., Pawelek, P., and Grinnell, F. 1989. Extracellular matrix organization modulates fibroblast growth and growth factor responsiveness. *Exp. Cell Res.* **182**:572-582.

183. Hinz, B., Phan, S.H., Thannickal, V.J., Galli, A., Bochaton-Piallat, M.L., and Gabbiani, G. 2007. The myofibroblast: one function, multiple origins. *Am. J. Pathol.* **170**:1807-1816.

184. Thannickal, V.J., Lee, D.Y., White, E.S., Cui, Z., Larios, J.M., Chacon, R., Horowitz, J.C., Day, R.M., and Thomas, P.E. 2003. Myofibroblast differentiation by transforming growth factor-beta1 is dependent on cell adhesion and integrin signaling via focal adhesion kinase. *J. Biol. Chem.* **278**:12384-12389.

185. Xu, M.Y., Porte, J., Knox, A.J., Weinreb, P.H., Maher, T.M., Violette, S.M., McAnulty, R.J., Sheppard, D., and Jenkins, G. 2009. Lysophosphatidic acid induces alphavbeta6 integrin-mediated TGF-beta activation via the LPA2 receptor and the small G protein G alpha(q). *Am. J. Pathol.* **174**:1264-1279.

186. Giacomini, M.M., Travis, M.A., Kudo, M., and Sheppard, D. 2012. Epithelial cells utilize cortical actin/myosin to activate latent TGF-beta through integrin alpha(v)beta(6)-dependent physical force. *Exp. Cell Res.* **318**:716-722.

187. Lindahl, G.E., Chambers, R.C., Papakrivopoulou, J., Dawson, S.J., Jacobsen, M.C., Bishop, J.E., and Laurent, G.J. 2002. Activation of fibroblast procollagen alpha 1(I) transcription by mechanical strain is transforming growth factor-beta-dependent and involves increased binding of CCAAT-binding factor (CBF/NF-Y) at the proximal promoter. *J. Biol. Chem.* **277**:6153-6161.

188. Kimura, M., Tani, K., Miyata, J., Sato, K., Hayashi, A., Otsuka, S., Urata, T., and Sone, S. 2005. The significance of cathepsins, thrombin and aminopeptidase in diffuse interstitial lung diseases. *J. Med. Invest.* **52**:93-100.

189. Specks, U., Martin, W.J.,2nd, and Rohrbach, M.S. 1990. Bronchoalveolar lavage fluid angiotensin-converting enzyme in interstitial lung diseases. *Am. Rev. Respir. Dis.* **141**:117-123.

190. Sofia, M., Mormile, M., Faraone, S., Alifano, M., Zofra, S., Romano, L., and Carratu, L. 1993. Increased endothelin-like immunoreactive material on bronchoalveolar lavage fluid from patients with bronchial asthma and patients with interstitial lung disease. *Respiration* **60**:89-95.

191. De Candia, E. 2012. Mechanisms of platelet activation by thrombin: a short history. *Thromb. Res.* **129**:250-256.

192. Jenkins, R.G., Su, X., Su, G., Scotton, C.J., Camerer, E., Laurent, G.J., Davis, G.E., Chambers, R.C., Matthay, M.A., and Sheppard, D. 2006. Ligation of protease-activated receptor 1 enhances alpha(v)beta6 integrin-dependent TGF-beta activation and promotes acute lung injury. *J. Clin. Invest.* **116**:1606-1614.

193. Mercer, P.F., Deng, X., and Chambers, R.C. 2007. Signaling pathways involved in proteinase-activated receptor1-induced proinflammatory and profibrotic mediator release following lung injury. *Ann. N. Y. Acad. Sci.* **1096**:86-88.

194. Scotton, C.J., Krupiczojc, M.A., Konigshoff, M., Mercer, P.F., Lee, Y.C., Kaminski, N., Morser, J., Post, J.M., Maher, T.M., Nicholson, A.G. et al. 2009. Increased local expression of coagulation factor X contributes to the fibrotic response in human and murine lung injury. *J. Clin. Invest.* **119**:2550-2563.

195. Levin, E.R. 1995. Endothelins. *N. Engl. J. Med.* **333**:356-363.

196. Guidry, C., and Hook, M. 1991. Endothelins produced by endothelial cells promote collagen gel contraction by fibroblasts. *J. Cell Biol.* **115**:873-880.

197. Appleton, I., Tomlinson, A., Chander, C.L., and Willoughby, D.A. 1992. Effect of endothelin-1 on croton oil-induced granulation tissue in the rat. A pharmacologic and immunohistochemical study. *Lab. Invest.* **67**:703-710.

198. Xu, S., Denton, C.P., Holmes, A., Dashwood, M.R., Abraham, D.J., and Black, C.M. 1998. Endothelins: effect on matrix biosynthesis and proliferation in normal and scleroderma fibroblasts. *J. Cardiovasc. Pharmacol.* **31 Suppl 1**:S360-3.

199. Kulasekaren, P., Scavone, C.A., Rogers, D.S., Arenberg, D.A., Thannickal, V.J., and Horowitz, J.C. 2009. Endothelin-1 and TGF-{beta} Independently Induce Fibroblast Resistance to Apoptosis via AKT Activation. *Am. J. Respir. Cell Mol. Biol.*

200. Konigshoff, M., Wilhelm, A., Jahn, A., Sedding, D., Amarie, O.V., Eul, B., Seeger, W., Fink, L., Gunther, A., Eickelberg, O. et al. 2007. The angiotensin II receptor 2 is expressed and mediates angiotensin II signaling in lung fibrosis. *Am. J. Respir. Cell Mol. Biol.* **37**:640-650.

201. Horiuchi, M., Mogi, M., and Iwai, M. 2006. Signaling crosstalk angiotensin II receptor subtypes and insulin. *Endocr. J.* **53**:1-5.

202. Numata, T., Shimizu, T., and Okada, Y. 2007. TRPM7 is a stretch- and swelling-activated cation channel involved in volume regulation in human epithelial cells. *Am. J. Physiol. Cell. Physiol.* **292**:C460-7.

203. Fischer, A.N., Fuchs, E., Mikula, M., Huber, H., Beug, H., and Mikulits, W. 2007. PDGF essentially links TGF-beta signaling to nuclear beta-catenin accumulation in hepatocellular carcinoma progression. *Oncogene* **26**:3395-3405.

204. Wei, C., Wang, X., Chen, M., Ouyang, K., Song, L.S., and Cheng, H. 2009. Calcium flickers steer cell migration. *Nature* **457**:901-905.

205. Mukherjee, S., Kolb, M.R., Duan, F., and Janssen, L.J. 2012. Transforming Growth Factor Beta Evoked Ca2+ Wave and Enhances Gene Expression in Human Pulmonary Fibroblast. *Am. J. Respir. Cell Mol. Biol.*

206. Sandbo, N., Lau, A., Kach, J., Ngam, C., Yau, D., and Dulin, N.O. 2011. Delayed stress fiber formation mediates pulmonary myofibroblast differentiation in response to TGF-beta. *Am. J. Physiol. Lung Cell. Mol. Physiol.* **301**:L656-66.

207. Bett, A.J., Haddara, W., Prevec, L., and Graham, F.L. 1994. An efficient and flexible system for construction of adenovirus vectors with insertions or deletions in early regions 1 and 3. *Proc. Natl. Acad. Sci. U. S. A.* **91**:8802-8806.

208. Abe, M., Harpel, J.G., Metz, C.N., Nunes, I., Loskutoff, D.J., and Rifkin, D.B. 1994. An assay for transforming growth factor-beta using cells transfected with a plasminogen activator inhibitor-1 promoter-luciferase construct. *Anal. Biochem.* **216**:276-284.

209. Demedts, M., Behr, J., Buhl, R., Costabel, U., Dekhuijzen, R., Jansen, H.M., MacNee, W., Thomeer, M., Wallaert, B., Laurent, F. et al. 2005. High-dose acetylcysteine in idiopathic pulmonary fibrosis. *N. Engl. J. Med.* **353**:2229-2242.

210. Mantel, P.Y., and Schmidt-Weber, C.B. 2011. Transforming growth factor-beta: recent advances on its role in immune tolerance. *Methods Mol. Biol.* **677**:303-338.

211. Masszi, A., and Kapus, A. 2011. Smaddening complexity: the role of Smad3 in epithelial-myofibroblast transition. *Cells Tissues Organs* **193**:41-52.

212. Taipale, J., Koli, K., and Keski-Oja, J. 1992. Release of transforming growth factor-beta 1 from the pericellular matrix of cultured fibroblasts and fibrosarcoma cells by plasmin and thrombin. *J. Biol. Chem.* **267**:25378-25384.

213. Chua, F., Dunsmore, S.E., Clingen, P.H., Mutsaers, S.E., Shapiro, S.D., Segal, A.W., Roes, J., and Laurent, G.J. 2007. Mice lacking neutrophil elastase are resistant to bleomycin-induced pulmonary fibrosis. *Am. J. Pathol.* **170**:65-74.

214. Tatler, A.L., Porte, J., Knox, A., Jenkins, G., and Pang, L. 2008. Tryptase activates TGFbeta in human airway smooth muscle cells via direct proteolysis. *Biochem. Biophys. Res. Commun.* **370**:239-242.

215. Taipale, J., Lohi, J., Saarinen, J., Kovanen, P.T., and Keski-Oja, J. 1995. Human mast cell chymase and leukocyte elastase release latent transforming growth factor-beta 1 from the extracellular matrix of cultured human epithelial and endothelial cells. *J. Biol. Chem.* **270**:4689-4696.

216. Karsdal, M.A., Larsen, L., Engsig, M.T., Lou, H., Ferreras, M., Lochter, A., Delaisse, J.M., and Foged, N.T. 2002. Matrix metalloproteinase-dependent activation of latent transforming growth factor-beta controls the conversion of osteoblasts into osteocytes by blocking osteoblast apoptosis. *J. Biol. Chem.* **277**:44061-44067.

217. Aluwihare, P., Mu, Z., Zhao, Z., Yu, D., Weinreb, P.H., Horan, G.S., Violette, S.M., and Munger, J.S. 2009. Mice that lack activity of alphavbeta6- and alphavbeta8-integrins reproduce the abnormalities of Tgfb1- and Tgfb3-null mice. *J. Cell. Sci.* **122**:227-232.

218. Cabrera-Benitez, N.E., Parotto, M., Post, M., Han, B., Spieth, P.M., Cheng, W.E., Valladares, F., Villar, J., Liu, M., Sato, M. et al. 2012. Mechanical stress induces lung fibrosis by epithelial-mesenchymal transition. *Crit. Care Med.* **40**:510-517.

219. Villar, J., Cabrera, N.E., Valladares, F., Casula, M., Flores, C., Blanch, L., Quilez, M.E., Santana-Rodriguez, N., Kacmarek, R.M., and Slutsky, A.S. 2011. Activation of the Wnt/beta-catenin signaling pathway by mechanical ventilation is associated with ventilator-induced pulmonary fibrosis in healthy lungs. *PLoS One* **6**:e23914.

220. Sakamoto, S., Homma, S., Mun, M., Fujii, T., Kurosaki, A., and Yoshimura, K. 2011. Acute exacerbation of idiopathic interstitial pneumonia following lung surgery in 3 of 68 consecutive patients: a retrospective study. *Intern. Med.* **50**:77-85.

221. Watanabe, A., Kawaharada, N., and Higami, T. 2011. Postoperative Acute Exacerbation of IPF after Lung Resection for Primary Lung Cancer. *Pulm. Med.* **2011**:960316.

222. Pociask, D.A., Sime, P.J., and Brody, A.R. 2004. Asbestos-derived reactive oxygen species activate TGF-beta1. *Lab. Invest.* **84**:1013-1023.

223. Keeley, E.C., Mehrad, B., and Strieter, R.M. 2009. The role of circulating mesenchymal progenitor cells (fibrocytes) in the pathogenesis of fibrotic disorders. *Thromb. Haemost.* **101**:613-618.

224. Schmidt, M., Sun, G., Stacey, M.A., Mori, L., and Mattoli, S. 2003. Identification of circulating fibrocytes as precursors of bronchial myofibroblasts in asthma. *J. Immunol.* **171**:380-389.

225. Phillips, R.J., Burdick, M.D., Hong, K., Lutz, M.A., Murray, L.A., Xue, Y.Y., Belperio, J.A., Keane, M.P., and Strieter, R.M. 2004. Circulating fibrocytes traffic to the lungs in response to CXCL12 and mediate fibrosis. *J. Clin. Invest.* **114**:438-446.

226. Chauhan, H., Abraham, A., Phillips, J.R., Pringle, J.H., Walker, R.A., and Jones, J.L. 2003. There is more than one kind of myofibroblast: analysis of CD34 expression in benign, in situ, and invasive breast lesions. *J. Clin. Pathol.* **56**:271-276.

227. Bucala, R., Spiegel, L.A., Chesney, J., Hogan, M., and Cerami, A. 1994. Circulating fibrocytes define a new leukocyte subpopulation that mediates tissue repair. *Mol. Med.* **1**:71-81.

228. Abe, R., Donnelly, S.C., Peng, T., Bucala, R., and Metz, C.N. 2001. Peripheral blood fibrocytes: differentiation pathway and migration to wound sites. *J. Immunol.* **166**:7556-7562.

229. Gomperts, B.N., and Strieter, R.M. 2007. Fibrocytes in lung disease. *J. Leukoc. Biol.* **82**:449-456.

230. Bellini, A., and Mattoli, S. 2007. The role of the fibrocyte, a bone marrow-derived mesenchymal progenitor, in reactive and reparative fibroses. *Lab. Invest.* **87**:858-870.

231. Vinader, V., and Afarinkia, K. 2012. A beginner's guide to chemokines. *Future Med. Chem.* **4**:845-852.

232. LaPar, D.J., Burdick, M.D., Emaminia, A., Harris, D.A., Strieter, B.A., Liu, L., Robbins, M., Kron, I.L., Strieter, R.M., and Lau, C.L. 2011. Circulating fibrocytes correlate with bronchiolitis obliterans syndrome development after lung transplantation: a novel clinical biomarker. *Ann. Thorac. Surg.* **92**:470-7; discussion 477.

233. Moeller, A., Gilpin, S.E., Ask, K., Cox, G., Cook, D., Gauldie, J., Margetts, P.J., Farkas, L., Dobranowski, J., Boylan, C. et al. 2009. Circulating fibrocytes are an indicator of poor prognosis in idiopathic pulmonary fibrosis. *Am. J. Respir. Crit. Care Med.* **179**:588-594.

234. Fujiwara, A., Kobayashi, H., Masuya, M., Maruyama, M., Nakamura, S., Ibata, H., Fujimoto, H., Ohnishi, M., Urawa, M., Naito, M. et al. 2012. Correlation between circulating fibrocytes, and activity and progression of interstitial lung diseases. *Respirology* **17**:693-698.

235. Andersson-Sjoland, A., de Alba, C.G., Nihlberg, K., Becerril, C., Ramirez, R., Pardo, A., Westergren-Thorsson, G., and Selman, M. 2008. Fibrocytes are a potential source of lung fibroblasts in idiopathic pulmonary fibrosis. *Int. J. Biochem. Cell Biol.* **40**:2129-2140.

236. Veeraraghavan, S., Latsi, P.I., Wells, A.U., Pantelidis, P., Nicholson, A.G., Colby, T.V., Haslam, P.L., Renzoni, E.A., and du Bois, R.M. 2003. BAL findings in idiopathic nonspecific interstitial pneumonia and usual interstitial pneumonia. *Eur. Respir. J.* **22**:239-244.

237. Kohno, N., Kyoizumi, S., Awaya, Y., Fukuhara, H., Yamakido, M., and Akiyama, M. 1989. New serum indicator of interstitial pneumonitis activity. Sialylated carbohydrate antigen KL-6. *Chest* **96**:68-73.

238. Snijdewint, F.G., von Mensdorff-Pouilly, S., Karuntu-Wanamarta, A.H., Verstraeten, A.A., Livingston, P.O., Hilgers, J., and Kenemans, P. 2001. Antibody-dependent cell-mediated cytotoxicity can be induced by MUC1 peptide vaccination of breast cancer patients. *Int. J. Cancer* **93**:97-106.

239. Hiraga, Y., Tanaka, S., Haruma, K., Yoshihara, M., Sumii, K., Kajiyama, G., Shimamoto, F., and Kohno, N. 1998. Immunoreactive MUC1 expression at the deepest invasive portion correlates with prognosis of colorectal cancer. *Oncology* **55**:307-319.

240. Inoue, Y., Nishimura, K., Shiode, M., Akutsu, H., Hamada, H., Fujioka, S., Fujino, S., Yokoyama, A., Kohno, N., and Hiwada, K. 1995. Evaluation of serum KL-6 levels in patients with pulmonary tuberculosis. *Tuber. Lung Dis.* **76**:230-233.

241. Hirasawa, Y., Kohno, N., Yokoyama, A., Kondo, K., Hiwada, K., and Miyake, M. 2000. Natural autoantibody to MUC1 is a prognostic indicator for non-small cell lung cancer. *Am. J. Respir. Crit. Care Med.* **161**:589-594.

242. Yokoyama, A., Kohno, N., Hamada, H., Sakatani, M., Ueda, E., Kondo, K., Hirasawa, Y., and Hiwada, K. 1998. Circulating KL-6 predicts the outcome of rapidly progressive idiopathic pulmonary fibrosis. *Am. J. Respir. Crit. Care Med.* **158**:1680-1684.

243. Takahashi, H., Fujishima, T., Koba, H., Murakami, S., Kurokawa, K., Shibuya, Y., Shiratori, M., Kuroki, Y., and Abe, S. 2000. Serum surfactant proteins A and D as prognostic factors in idiopathic pulmonary fibrosis and their relationship to disease extent. *Am. J. Respir. Crit. Care Med.* **162**:1109-1114.

244. Greene, K.E., King, T.E.,Jr, Kuroki, Y., Bucher-Bartelson, B., Hunninghake, G.W., Newman, L.S., Nagae, H., and Mason, R.J. 2002. Serum surfactant proteins-A and -D as biomarkers in idiopathic pulmonary fibrosis. *Eur. Respir. J.* **19**:439-446.

245. Kinder, B.W., Brown, K.K., McCormack, F.X., Ix, J.H., Kervitsky, A., Schwarz, M.I., and King, T.E.,Jr. 2009. Serum surfactant protein-A is a strong predictor of early mortality in idiopathic pulmonary fibrosis. *Chest* **135**:1557-1563.

246. Thomeer, M., Grutters, J.C., Wuyts, W.A., Willems, S., and Demedts, M.G. 2010. Clinical use of biomarkers of survival in pulmonary fibrosis. *Respir. Res.* **11**:89.

247. Prasse, A., Probst, C., Bargagli, E., Zissel, G., Toews, G.B., Flaherty, K.R., Olschewski, M., Rottoli, P., and Muller-Quernheim, J. 2009. Serum CC-chemokine ligand 18 concentration predicts outcome in idiopathic pulmonary fibrosis. *Am. J. Respir. Crit. Care Med.* **179**:717-723.

248. Schutyser, E., Richmond, A., and Van Damme, J. 2005. Involvement of CC chemokine ligand 18 (CCL18) in normal and pathological processes. *J. Leukoc. Biol.* **78**:14-26.

249. Prasse, A., Pechkovsky, D.V., Toews, G.B., Jungraithmayr, W., Kollert, F., Goldmann, T., Vollmer, E., Muller-Quernheim, J., and Zissel, G. 2006. A vicious circle of alveolar

macrophages and fibroblasts perpetuates pulmonary fibrosis via CCL18. *Am. J. Respir. Crit. Care Med.* **173**:781-792.

250. Anonymous 1999. The diagnosis, assessment and treatment of diffuse parenchymal lung disease in adults. Introduction. *Thorax* **54 Suppl 1**:S1-14.

251. Martinez, F.J., Safrin, S., Weycker, D., Starko, K.M., Bradford, W.Z., King, T.E.,Jr, Flaherty, K.R., Schwartz, D.A., Noble, P.W., Raghu, G. et al. 2005. The clinical course of patients with idiopathic pulmonary fibrosis. *Ann. Intern. Med.* **142**:963-967.

252. Raghu, G., Brown, K.K., Bradford, W.Z., Starko, K., Noble, P.W., Schwartz, D.A., King, T.E.,Jr, and Idiopathic Pulmonary Fibrosis Study Group. 2004. A placebo-controlled trial of interferon gamma-1b in patients with idiopathic pulmonary fibrosis. *N. Engl. J. Med.* **350**:125-133.

253. du Bois, R.M., Weycker, D., Albera, C., Bradford, W.Z., Costabel, U., Kartashov, A., King, T.E.,Jr, Lancaster, L., Noble, P.W., Sahn, S.A. et al. 2011. Forced vital capacity in patients with idiopathic pulmonary fibrosis: test properties and minimal clinically important difference. *Am. J. Respir. Crit. Care Med.* **184**:1382-1389.

254. du Bois, R.M., Weycker, D., Albera, C., Bradford, W.Z., Costabel, U., Kartashov, A., Lancaster, L., Noble, P.W., Sahn, S.A., Szwarcberg, J. et al. 2011. Six-minute-walk test in idiopathic pulmonary fibrosis: test validation and minimal clinically important difference. *Am. J. Respir. Crit. Care Med.* **183**:1231-1237.

255. Flaherty, K.R., Mumford, J.A., Murray, S., Kazerooni, E.A., Gross, B.H., Colby, T.V., Travis, W.D., Flint, A., Toews, G.B., Lynch, J.P.,3rd et al. 2003. Prognostic implications of physiologic and radiographic changes in idiopathic interstitial pneumonia. *Am. J. Respir. Crit. Care Med.* **168**:543-548.

256. Fragiadaki, M., Ikeda, T., Witherden, A., Mason, R.M., Abraham, D., and Bou-Gharios, G. 2011. High doses of TGF-beta potently suppress type I collagen via the transcription factor CUX1. *Mol. Biol. Cell* **22**:1836-1844.

257. Hunninghake, G.W., Lynch, D.A., Galvin, J.R., Gross, B.H., Muller, N., Schwartz, D.A., King, T.E.,Jr, Lynch, J.P.,3rd, Hegele, R., Waldron, J. et al. 2003. Radiologic findings are strongly associated with a pathologic diagnosis of usual interstitial pneumonia. *Chest* **124**:1215-1223.

258. Hunninghake, G.W., Zimmerman, M.B., Schwartz, D.A., King, T.E.,Jr, Lynch, J., Hegele, R., Waldron, J., Colby, T., Muller, N., Lynch, D. et al. 2001. Utility of a lung biopsy for the diagnosis of idiopathic pulmonary fibrosis. *Am. J. Respir. Crit. Care Med.* **164**:193-196.

259. Raghu, G., Mageto, Y.N., Lockhart, D., Schmidt, R.A., Wood, D.E., and Godwin, J.D. 1999. The accuracy of the clinical diagnosis of new-onset idiopathic pulmonary fibrosis and other interstitial lung disease: A prospective study. *Chest* **116**:1168-1174.

260. Lettieri, C.J., Veerappan, G.R., Helman, D.L., Mulligan, C.R., and Shorr, A.F. 2005. Outcomes and safety of surgical lung biopsy for interstitial lung disease. *Chest* **127**:1600-1605.

261. Ohno, Y., Koyama, H., Yoshikawa, T., Nishio, M., Matsumoto, S., Iwasawa, T., and Sugimura, K. 2011. Pulmonary magnetic resonance imaging for airway diseases. *J. Thorac. Imaging* **26**:301-316.

262. Braker, W., Mossman, A.L., and Matheson Company, i. 1980. *Matheson gas data book.* 6th edition. Matheson. Lyndhurst, NJ. 711pp.

263. Markstaller, K., Kauczor, H.U., Puderbach, M., Mayer, E., Viallon, M., Gast, K., Weiler, N., Thelen, M., and Eberle, B. 2002. 3He-MRI-based vs. conventional determination of lung volumes in patients after unilateral lung transplantation: a new approach to regional spirometry. *Acta Anaesthesiol. Scand.* **46**:845-852.

264. Win, T., Lambrou, T., Hutton, B.F., Kayani, I., Screaton, N.J., Porter, J.C., Maher, T.M., Endozo, R., Shortman, R.I., Lukey, P. et al. 2012. 18F-Fluorodeoxyglucose positron emission tomography pulmonary imaging in idiopathic pulmonary fibrosis is reproducible: implications for future clinical trials. *Eur. J. Nucl. Med. Mol. Imaging* **39**:521-528.

265. Groves, A.M., Win, T., Screaton, N.J., Berovic, M., Endozo, R., Booth, H., Kayani, I., Menezes, L.J., Dickson, J.C., and Ell, P.J. 2009. Idiopathic pulmonary fibrosis and diffuse parenchymal lung disease: implications from initial experience with 18F-FDG PET/CT. *J. Nucl. Med.* **50**:538-545.

266. Azad, B., Ashique, R., Labiris, R., and Chirakal, R. 2012. Temperature effects on the stereospecificity of nucleophilic fluorination: formation of trans-[18F]-4-fluoro-L-

proline during the synthesis of cis-[18F]-4-fluoro-L-proline. *Journal of Labelled Compounds and Radiopharmaceuticals* **55**:23-28.

267. Labiris, R., Ask, K., Kolb, M., and Farncombe, T. 2006. Pulmonary disease models with lung imaging outcome measures: Making the black box more transparent. *Respiratory Drug Delivery* **1**:191-204.

268. Wallace, W.E., Gupta, N.C., Hubbs, A.F., Mazza, S.M., Bishop, H.A., Keane, M.J., Battelli, L.A., Ma, J., and Schleiff, P. 2002. Cis-4-[(18)F]fluoro-L-proline PET imaging of pulmonary fibrosis in a rabbit model. *J. Nucl. Med.* **43**:413-420.

269. Jones, H.A., Hamacher, K., Clark, J.C., Schofield, J.B., Krausz, T., Haslett, C., and Boobis, A.R. 2005. Positron emission tomography in the quantification of cellular and biochemical responses to intrapulmonary particulates. *Toxicol. Appl. Pharmacol.* **207**:230-236.

270. Leung, K. 2004. 125I-Single-chain antibody B5 targeting a pancreatic beta-cell surface antigen. In *Molecular Imaging and Contrast Agent Database (MICAD).* . Bethesda (MD).

271. Poselt, E., Schmidtke, C., Fischer, S., Peldschus, K., Salamon, J., Kloust, H., Tran, H., Pietsch, A., Heine, M., Adam, G. et al. 2012. Tailor-made quantum dot and iron oxide based contrast agents for in vitro and in vivo tumor imaging. *ACS Nano* **6**:3346-3355.

272. Jain, S., Hirst, D.G., and O'Sullivan, J.M. 2012. Gold nanoparticles as novel agents for cancer therapy. *Br. J. Radiol.* **85**:101-113.

273. Ismail, T.F., Prasad, S.K., and Pennell, D.J. 2012. Prognostic importance of late gadolinium enhancement cardiovascular magnetic resonance in cardiomyopathy. *Heart* **98**:438-442.

274. Kitajima, K., Maeda, T., Watanabe, S., Ueno, Y., and Sugimura, K. 2012. Recent topics related to nephrogenic systemic fibrosis associated with gadolinium-based contrast agents. *Int. J. Urol.*

275. Thabut, G., Mal, H., Castier, Y., Groussard, O., Brugiere, O., Marrash-Chahla, R., Leseche, G., and Fournier, M. 2003. Survival benefit of lung transplantation for patients with idiopathic pulmonary fibrosis. *J. Thorac. Cardiovasc. Surg.* **126**:469-475.

276. Khalil, N., and O'Connor, R. 2004. Idiopathic pulmonary fibrosis: current understanding of the pathogenesis and the status of treatment. *CMAJ* **171**:153-160.

277. Hilberg, O., Simonsen, U., du Bois, R., and Bendstrup, E. 2012. Pirfenidone: significant treatment effects in idiopathic pulmonary fibrosis. *Clin. Respir. J.* **6**:131-143.

278. Ashcroft, T., Simpson, J.M., and Timbrell, V. 1988. Simple method of estimating severity of pulmonary fibrosis on a numerical scale. *J. Clin. Pathol.* **41**:467-470.

279. WOESSNER, J.F.,Jr. 1961. The determination of hydroxyproline in tissue and protein samples containing small proportions of this imino acid. *Arch. Biochem. Biophys.* **93**:440-447.

280. SALAZAR, E., and KNOWLES, J.H. 1964. An Analysis of Pressure-Volume Characteristics of the Lungs. *J. Appl. Physiol.* **19**:97-104.

281. Izbicki, G., Segel, M.J., Christensen, T.G., Conner, M.W., and Breuer, R. 2002. Time course of bleomycin-induced lung fibrosis. *Int. J. Exp. Pathol.* **83**:111-119.

282. Maina, J.N., Jimoh, S.A., and Hosie, M. 2010. Implicit mechanistic role of the collagen, smooth muscle, and elastic tissue components in strengthening the air and blood capillaries of the avian lung. *J. Anat.* **217**:597-608.

283. Souza-Fernandes, A.B., Pelosi, P., and Rocco, P.R. 2006. Bench-to-bedside review: the role of glycosaminoglycans in respiratory disease. *Crit. Care* **10**:237.

284. Buckley, C.D., Rainger, G.E., Bradfield, P.F., Nash, G.B., and Simmons, D.L. 1998. Cell adhesion: more than just glue (review). *Mol. Membr. Biol.* **15**:167-176.

285. Campo, G.M., Avenoso, A., D'Ascola, A., Prestipino, V., Scuruchi, M., Nastasi, G., Calatroni, A., and Campo, S. 2012. Inhibition of hyaluronan synthesis reduced inflammatory response in mouse synovial fibroblasts subjected to collagen-induced arthritis. *Arch. Biochem. Biophys.* **518**:42-52.

286. Laurent, G.J. 1982. Rates of collagen synthesis in lung, skin and muscle obtained in vivo by a simplified method using [3H]proline. *Biochem. J.* **206**:535-544.

287. McAnulty, R.J., and Laurent, G.J. 1987. Collagen synthesis and degradation in vivo. Evidence for rapid rates of collagen turnover with extensive degradation of newly synthesized collagen in tissues of the adult rat. *Coll. Relat. Res.* **7**:93-104.

288. Kelley, J., Stirewalt, W.S., and Chrin, L. 1984. Protein synthesis in rat lung. Measurements in vivo based on leucyl-tRNA and rapidly turning-over procollagen I. *Biochem. J.* **222**:77-83.

289. Last, J.A., and Reiser, K.M. 1989. Biosynthesis of collagen crosslinks. III. In vivo labeling and stability of lung collagen in rats with bleomycin-induced pulmonary fibrosis. *Am. J. Respir. Cell Mol. Biol.* **1**:111-117.

290. Reiser, K.M., Tryka, A.F., Lindenschmidt, R.C., Last, J.A., and Witschi, H.R. 1986. Changes in collagen cross-linking in bleomycin-induced pulmonary fibrosis. *J. Biochem. Toxicol.* **1**:83-91.

291. Koslowski, R., Seidel, D., Kuhlisch, E., and Knoch, K.P. 2003. Evidence for the involvement of TGF-beta and PDGF in the regulation of prolyl 4-hydroxylase and lysyloxidase in cultured rat lung fibroblasts. *Exp. Toxicol. Pathol.* **55**:257-264.

292. Sroga, G.E., and Vashishth, D. 2011. UPLC methodology for identification and quantitation of naturally fluorescent crosslinks in proteins: a study of bone collagen. *J. Chromatogr. B. Analyt Technol. Biomed. Life. Sci.* **879**:379-385.

293. Kagan, H.M., and Li, W. 2003. Lysyl oxidase: properties, specificity, and biological roles inside and outside of the cell. *J. Cell. Biochem.* **88**:660-672.

294. Hanson, D.A., and Eyre, D.R. 1996. Molecular site specificity of pyridinoline and pyrrole cross-links in type I collagen of human bone. *J. Biol. Chem.* **271**:26508-26516.

295. Takaluoma, K., Lantto, J., and Myllyharju, J. 2007. Lysyl hydroxylase 2 is a specific telopeptide hydroxylase, while all three isoenzymes hydroxylate collagenous sequences. *Matrix Biol.* **26**:396-403.

296. van der Slot, A.J., van Dura, E.A., de Wit, E.C., De Groot, J., Huizinga, T.W., Bank, R.A., and Zuurmond, A.M. 2005. Elevated formation of pyridinoline cross-links by profibrotic cytokines is associated with enhanced lysyl hydroxylase 2b levels. *Biochim. Biophys. Acta* **1741**:95-102.

297. Last, J.A., King, T.E.,Jr, Nerlich, A.G., and Reiser, K.M. 1990. Collagen cross-linking in adult patients with acute and chronic fibrotic lung disease. Molecular markers for fibrotic collagen. *Am. Rev. Respir. Dis.* **141**:307-313.

298. Gerriets, J.E., Reiser, K.M., and Last, J.A. 1996. Lung collagen cross-links in rats with experimentally induced pulmonary fibrosis. *Biochim. Biophys. Acta* **1316**:121-131.

299. van der Slot, A.J., Zuurmond, A.M., Bardoel, A.F., Wijmenga, C., Pruijs, H.E., Sillence, D.O., Brinckmann, J., Abraham, D.J., Black, C.M., Verzijl, N. et al. 2003. Identification of PLOD2 as telopeptide lysyl hydroxylase, an important enzyme in fibrosis. *J. Biol. Chem.* **278**:40967-40972.

300. Last, J.A., Gerriets, J.E., Armstrong, L.C., Gelzleichter, T.R., and Reiser, K.M. 1990. Hydroxylation of collagen by lungs of rats administered bleomycin. *Am. J. Respir. Cell Mol. Biol.* **2**:543-548.

301. Eyre, D. 1987. Collagen cross-linking amino acids. *Methods Enzymol.* **144**:115-139.

302. Eyre, D.R., and Glimcher, M.J. 1973. Collagen cross-linking. Isolation of cross-linked peptides from collagen of chicken bone. *Biochem. J.* **135**:393-403.

303. Eyre, D.R., Weis, M.A., and Wu, J.J. 2010. Maturation of collagen Ketoimine cross-links by an alternative mechanism to pyridinoline formation in cartilage. *J. Biol. Chem.* **285**:16675-16682.

304. Light, N., and Bailey, A.J. 1985. Collagen cross-links: location of pyridinoline in type I collagen. *FEBS Lett.* **182**:503-508.

305. Ricard-Blum, S., Bresson-Hadni, S., Vuitton, D.A., Ville, G., and Grimaud, J.A. 1992. Hydroxypyridinium collagen cross-links in human liver fibrosis: study of alveolar echinococcosis. *Hepatology* **15**:599-602.

306. Stone, P.J., Korn, J.H., North, H., Lally, E.V., Miller, L.C., Tucker, L.B., Strongwater, S., Snider, G.L., and Franzblau, C. 1995. Cross-linked elastin and collagen degradation products in the urine of patients with scleroderma. *Arthritis Rheum.* **38**:517-524.

307. Stone, P.J., Gottlieb, D.J., O'Connor, G.T., Ciccolella, D.E., Breuer, R., Bryan-Rhadfi, J., Shaw, H.A., Franzblau, C., and Snider, G.L. 1995. Elastin and collagen degradation

products in urine of smokers with and without chronic obstructive pulmonary disease. *Am. J. Respir. Crit. Care Med.* **151**:952-959.

308. Brinckmann, J., Notbohm, H., Tronnier, M., Acil, Y., Fietzek, P.P., Schmeller, W., Muller, P.K., and Batge, B. 1999. Overhydroxylation of lysyl residues is the initial step for altered collagen cross-links and fibril architecture in fibrotic skin. *J. Invest. Dermatol.* **113**:617-621.

309. van der Slot-Verhoeven, A.J., van Dura, E.A., Attema, J., Blauw, B., Degroot, J., Huizinga, T.W., Zuurmond, A.M., and Bank, R.A. 2005. The type of collagen cross-link determines the reversibility of experimental skin fibrosis. *Biochim. Biophys. Acta* **1740**:60-67.

310. Cantin, A.M., Boileau, R., and Begin, R. 1988. Increased procollagen III aminoterminal peptide-related antigens and fibroblast growth signals in the lungs of patients with idiopathic pulmonary fibrosis. *Am. Rev. Respir. Dis.* **137**:572-578.

311. Whittaker, P., Kloner, R.A., Boughner, D.R., and Pickering, J.G. 1994. Quantitative assessment of myocardial collagen with picrosirius red staining and circularly polarized light. *Basic Res. Cardiol.* **89**:397-410.

312. Milman, N., Kristensen, M.S., and Bentsen, K. 1995. Hyaluronan and procollagen type III aminoterminal peptide in serum and bronchoalveolar lavage fluid from patients with pulmonary fibrosis. *APMIS* **103**:749-754.

313. Allanore, Y., Borderie, D., Lemarechal, H., Cherruau, B., Ekindjian, O.G., and Kahan, A. 2003. Correlation of serum collagen I carboxyterminal telopeptide concentrations with cutaneous and pulmonary involvement in systemic sclerosis. *J. Rheumatol.* **30**:68-73.

314. Istok, R., Czirjak, L., Lukac, J., Stancikova, M., and Rovensky, J. 2001. Increased urinary pyridinoline cross-link compounds of collagen in patients with systemic sclerosis and Raynaud's phenomenon. *Rheumatology (Oxford)* **40**:140-146.

315. Lichy, A., Macek, J., and Adam, M. 1991. Determination of hydroxylysylpyridinoline in tissues and urine by high-performance liquid chromatography. *J. Chromatogr.* **563**:153-157.

316. Black, D., Duncan, A., and Robins, S.P. 1988. Quantitative analysis of the pyridinium crosslinks of collagen in urine using ion-paired reversed-phase high-performance liquid chromatography. *Anal. Biochem.* **169**:197-203.

317. James, I.T., Perrett, D., and Thompson, P.W. 1990. Rapid assay for hard tissue collagen cross-links using isocratic ion-pair reversed-phase liquid chromatography. *J. Chromatogr.* **525**:43-57.

318. Kollerup, G., Thamsborg, G., Bhatia, H., and Sorensen, O.H. 1992. Quantitation of urinary hydroxypyridinium cross-links from collagen by high-performance liquid chromatography. *Scand. J. Clin. Lab. Invest.* **52**:657-662.

319. Yoshimura, Y., Ohnishi, K., Hamamura, M., Oda, T., and Sohda, T. 1993. Automated high-performance liquid chromatographic determination of hydroxylysylpyridinoline and lysylpyridinoline in urine using a column-switching method. *J. Chromatogr.* **613**:43-49.

320. James, I., Crowley, C., and Perrett, D. 1993. Assay of pyridinium crosslinks in serum using narrow-bore ion-paired reversed-phase high-performance liquid chromatography. *J. Chromatogr.* **612**:41-48.

321. Abbiati, G., Rigoldi, M., Frignani, S., Colombo, L., and Mussini, E. 1994. Determination of pyridinium crosslinks in plasma and serum by high-performance liquid chromatography. *J. Chromatogr. B. Biomed. Appl.* **656**:303-310.

322. Kakinuma, M., Watanabe, Y., Hori, Y., Oh-I, T., and Tsuboi, R. 2005. Quantification of hydroxyproline in small amounts of skin tissue using isocratic high performance liquid chromatography with NBD-F as fluorogenic reagent. *J. Chromatogr. B. Analyt Technol. Biomed. Life. Sci.* **824**:161-165.

323. Sinigaglia, L., Varenna, M., Binelli, L., Beltrametti, P., Zucchi, F., Arrigoni, M., Frignani, S., and Abbiati, G. 1997. Serum levels of pyridinium crosslinks in postmenopausal women and in Paget's disease of bone. *Calcif. Tissue Int.* **61**:279-284.

324. Barber, M., Bordoli, R.S., Elliott, G.J., Fujimoto, D., and Scott, J.E. 1982. The structure(s) of pyridinoline(s). *Biochem. Biophys. Res. Commun.* **109**:1041-1046.

325. Schwartz, M.A. 2010. Integrins and extracellular matrix in mechanotransduction. *Cold Spring Harb Perspect. Biol.* **2**:a005066.

326. Antonov, A.S., Antonova, G.N., Munn, D.H., Mivechi, N., Lucas, R., Catravas, J.D., and Verin, A.D. 2011. alphaVbeta3 integrin regulates macrophage inflammatory responses via PI3 kinase/Akt-dependent NF-kappaB activation. *J. Cell. Physiol.* **226**:469-476.

327. Tomasek, J.J., Vaughan, M.B., Kropp, B.P., Gabbiani, G., Martin, M.D., Haaksma, C.J., and Hinz, B. 2006. Contraction of myofibroblasts in granulation tissue is dependent on Rho/Rho kinase/myosin light chain phosphatase activity. *Wound Repair Regen.* **14**:313-320.

328. Thannickal, V.J., and Fanburg, B.L. 1995. Activation of an H2O2-generating NADH oxidase in human lung fibroblasts by transforming growth factor beta 1. *J. Biol. Chem.* **270**:30334-30338.

329. Redente, E.F., Jacobsen, K.M., Solomon, J.J., Lara, A.R., Faubel, S., Keith, R.C., Henson, P.M., Downey, G.P., and Riches, D.W. 2011. Age and sex dimorphisms contribute to the severity of bleomycin-induced lung injury and fibrosis. *Am. J. Physiol. Lung Cell. Mol. Physiol.* **301**:L510-8.

330. Xu, J., Gonzalez, E.T., Iyer, S.S., Mac, V., Mora, A.L., Sutliff, R.L., Reed, A., Brigham, K.L., Kelly, P., and Rojas, M. 2009. Use of senescence-accelerated mouse model in bleomycin-induced lung injury suggests that bone marrow-derived cells can alter the outcome of lung injury in aged mice. *J. Gerontol. A Biol. Sci. Med. Sci.* **64**:731-739.

10.0 Appendix: Records of Permission to Present Published Data

1. Orphanet Journal of Rare Diseases, 2008, (3) p8. Adapted a CT scan image of IPF lungs for illustrative purposes.

   This journal is open access and free.

2. Growth Factors, 2011, (29) p196-202. Adapted figure for TGFβ biology and intracellular signaling.

   INFORMA HEALTHCARE LICENSE

   TERMS AND CONDITIONS

   Nov 27, 2012

   This is a License Agreement between Aaron Froese ("You") and Informa Healthcare ("Informa Healthcare") provided by Copyright Clearance Center ("CCC"). The license consists of your order details, the terms and conditions provided by Informa Healthcare, and the payment terms and conditions.

   License Number: 3037150182801

   License date: Nov 27, 2012

   Licensed content publisher: Informa Healthcare. Licensed content publication: Growth Factors. Licensed content title: TGF-β signaling in fibrosis. Licensed content author: Anna Biernacka, Marcin Dobaczewski, Nikolaos G. Frangogiannis. Licensed content date: Oct 1, 2011. Volume number: 29. Issue number: 5. Start Page: 196. End Page: 202

3. Respiratory Drug Delivery 2006, (1), p191-204. Adapted Figure 4 from this article as an illustration of metabolic PET scanning images.

   RDD Online <info@rddonline.com> Mon, Nov 26, 2012 at 4:56 PM

   Hello Aaron

   Many thanks for your email and interest in Respiratory Drug Delivery.

   Of course we will grant permission for you to reproduce Figure 4 from the article

   Pulmonary Disease Models with Lung Imaging Outcome Measures: Making the Black Box More Transparent Renee Labiris, Kjetil Ask, Martin Kolb, Troy Farncombe. Respiratory Drug Delivery 2006 (2006), Vol 1, pp 191-204.

   Please indicate that this is reproduced with permission from Respiratory Drug Delivery / Virginia Commonwealth University. Good luck with your thesis!

   Virginia Biotechnology Research Center

   800 East Leigh Street, Suite 206-10 Richmond, VA 23219 Phone: (804) 827-1490 Fax: (804) 828-8277 Email: info@rddonline.com

4. Journal of Translational Medicine 2008, (6) p16. Comparison between conventional and "clinical" assessment of experimental lung fibrosis.

   jtransmed <jtransmed@biomedcentral.com> Wed, Nov 28, 2012 at 9:23 AM

   To: Aaron Froese <aaron.froese@gmail.com>

   Dear Dr. Froese,

   Thank you for your email. As the submitting authors of open access journals such as the Journal of Translational Medicine retain copyright of their published articles, you are free to reproduce and/ or redistribute a part or the whole of your article.

   We hope the above has helped and if you have further concerns, please do not hesitate to let us know.

   Kind regards, Casy Javier

   Journal Editorial OfficeBioMed Central

5. Use of Flexivent Rodent Ventilator Image.

Adelle Keys [SCIREQ] <Adelle.Keys@scireq.com> Mon, Dec 3, 2012 at 1:54 PM

To: Aaron Froese <aaron.froese@gmail.com>

Dear Mr. Froese,

Thank you for your interest in the flexiVent.

I have consulted with the President of SCIREQ and he has approved your request to include images of the flexiVent in your thesis. May we have a copy of your thesis or at least the abstract? We are always interested to note different practical applications of our products.

Good luck with your dissertation.

Best regards,

Adelle

Adelle Keys, BSc | Application Specialist

T. 514.286.1429 ext. 139 F. 514.286.1627

SCIREQ Scientific Respiratory Equipment Inc.

www.scireq.com